

Review

Recent Advances in New-Generation Electrolytes for Sodium-Ion Batteries

Hatice Aylin Karahan Toprakci ^{1,2,*} and Ozan Toprakci ^{1,2,*} ¹ Department of Polymer Materials Engineering, Yalova University, 77100 Yalova, Turkey² Institute of Graduate Studies, Yalova University, 77100 Yalova, Turkey

* Correspondence: aylin.toprakci@yalova.edu.tr (H.A.K.T.); ozan.toprakci@yalova.edu.tr (O.T.)

Abstract: Sodium-ion batteries (SIBs) are one of the recent trends in energy storage systems due to their promising properties, the high abundance of sodium in the Earth's crust, and their low cost. However, the commercialization process of SIBs is in the early stages of development because of some challenges related to electrodes and electrolytes. Electrolytes are vital components of secondary batteries because they determine anode/cathode performance; energy density; operating conditions (electrochemical stability window, open circuit voltage, current rate, etc.); cyclic properties; electrochemical, thermal, mechanical, and dimensional stability; safety level; and the service life of the system. The performance of the battery is based on the structural, morphological, electrical, and electrochemical properties of the electrolytes. In this review, electrolytes used for SIBs are classified according to their state and material, including liquid, quasi-solid, solid, and hybrid, and recent advances in electrolyte research have been presented by considering their contributions and limitations. Additionally, future trends and recent cutting-edge research are highlighted.

Keywords: solid electrolytes; sodium-ion batteries; quasi-solid electrolytes; liquid electrolytes; hybrid electrolytes



Citation: Karahan Toprakci, H.A.; Toprakci, O. Recent Advances in New-Generation Electrolytes for Sodium-Ion Batteries. *Energies* **2023**, *16*, 3169. <https://doi.org/10.3390/en16073169>

Academic Editor:
Massimo Guarnieri

Received: 7 March 2023

Revised: 26 March 2023

Accepted: 29 March 2023

Published: 31 March 2023



Copyright: © 2023 by the authors. Licensee MDPI, Basel, Switzerland. This article is an open access article distributed under the terms and conditions of the Creative Commons Attribution (CC BY) license (<https://creativecommons.org/licenses/by/4.0/>).

1. Introduction

One of the most important problems in the world is solving how to increase the rate of clean energy production. This is of importance not only due to limited oil reserves but also to combat global warming. Solutions and precautions, such as reducing oil consumption, disseminating of clean and renewable energy systems, and the widespread use of electric vehicles, will be helpful in solving a significant part of the problem. Since oil sources are limited, renewable energy sources are gaining importance in the long term; however, the use of clean, renewable energy sources at high efficiency is very important in terms of increasing life quality and solving ecological problems. In other words, energy needs to be stored in an efficient way by high-performance, stable, and reliable systems. Lithium-ion batteries (LIBs) have been widely used for energy storage since the 1990s in many applications from cell phones to electric vehicles. LIBs are preferred because of their lightweight structure, high energy density, low/zero memory effect, and longer cycle life; however, the relatively low abundance and the high production cost of lithium (Li) are the main problems for the future. The price of Li carbonate increased more than four times in the last five years. Day by day, lithium resources are being depleted and new potential battery systems, which are made from cheaper, non-toxic, and more abundant materials, are being developed. At this point, has sodium become an important alternative. Sodium-ion batteries (SIBs), being one of the most popular alternative secondary battery systems, use sodium instead of lithium. Sodium (Na) is a soft alkali metal with a silvery-white metallic luster, an atomic number of 11, and a density of 0.97 g cm^{-3} . Na metal is highly reactive and can easily react with water and air, meaning that various sodium compounds can be found in nature. Sodium is one of the most abundant elements in the Earth's crust (sixth most abundant element,

~2.8%) and the most abundant alkali metal. It has been used for many years, both in metal and compound forms, in agriculture and food, and in the textile, medical, and metallurgy industries. Recently, sodium has also become a promising material in the secondary battery industry, mainly because of its low price and some physical and promising electrochemical properties. It is known that lightness is of great importance to the battery industry, and sodium is the second lightest alkali metal in the periodic table, with a theoretical specific capacity of 1166 mAh g^{-1} , a theoretical volumetric capacity of 1131 mAh cm^{-3} , and an electrical potential of -2.714 V . Although these values are relatively lower than lithium, sodium is more abundant and affordable than lithium, and it is preferred for conditions in which cost is more important than energy density, including in stationary applications such as solar and wind [1–14].

SIBs work as a standard secondary battery. As shown in Figure 1, an SIB consists of an anode (negative electrode), a cathode (positive electrode), a separator, and an electrolyte medium. When the battery is charged/discharged, sodium ions deintercalate from the positive electrode/negative electrode and intercalate into the negative electrode/positive electrode. Electron flow between the electrodes throughout the charging and discharging cycles enables the conversion and storage of electrochemical energy within the battery. This process is driven through electrolytes. An electrolyte can be defined as a medium that consists of positively and negatively charged ions in various forms, including liquid, gel, quasi-solid, solid, or hybrid. As given in Figure 1, liquid electrolytes are in the liquid phase, and they have high ionic conductivity. On the other hand, they have safety issues, including flammability and leakage. Quasi-solid electrolytes are a combination of liquid and polymer solid electrolytes. Since they are in gel form, they are safer than liquid electrolytes. Additionally, mechanical stability leads to the suppression of dendrite growth. However, they have low ionic conductivity compared to liquid electrolytes and show low performance at low temperatures. Solid electrolytes are the other common type of electrolytes. They have high mechanical properties with nonflammable safe structures, but they have relatively lower ionic conductivity compared to liquid electrolytes. Based on these facts, one of the recent trends in electrolyte research has involved hybrid electrolytes that consist of at least two different electrolyte materials, including liquid, quasi-solid, and/or solid electrolytes. By using various forms of electrolytes, the performance of SIBs has been reported to increase [8–10].

The basic function of an electrolyte is to provide ion transfer between electrodes during charging and discharging (sodiation/desodiation). Since ion transfer directly affects power density, the performance of the SIB can be tuned by using various types of electrolytes. The ionic conductivity, ion transference number, electrical conductivity, electrochemical stability window, thermal stability, electrochemical stability, inertness, and mechanical properties of the electrolyte, as well as the properties related to the electrolyte/electrode contact region, including interfacial resistance and solid/cathode electrolyte interface formation, are significant points to be considered [8–10].

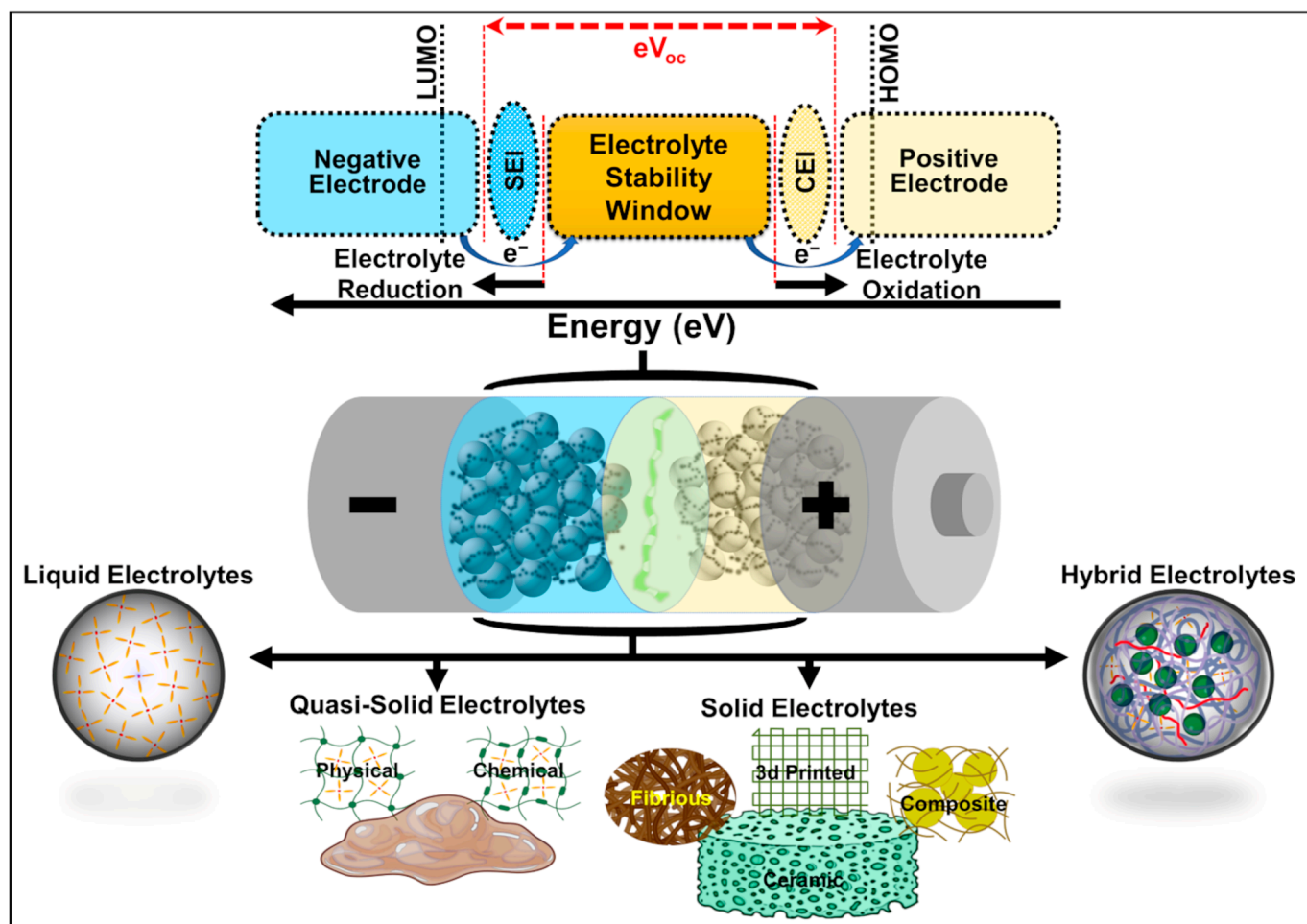


Figure 1. Classification of electrolytes used in SIBs and corresponding energy diagram of the electrolyte interface with positive and negative electrodes. Reproduced with the permission of reference [15].

Ionic conductivity is the flow of electrons caused by ions. Ionic conductivity is a vital requirement for the electrolyte medium. The contents of the electrolyte (solvents, ionic species, and additives), the ratio of the components (concentration), temperature, viscosity, molecular scale interactions such as solvent–ion and ion–ion interactions, the dynamic/static ionic radius, and the diffusion behavior of the ion have been reported to be significant for ionic conductivity [10,16,17]. In the case of low ionic conductivity, Na^+ transfer will be slower, charging/discharging time increases, and the power density of the cell decreases. However, ionic conductivity is not enough, and a high ion transference number is also required for high power density. The ion transference number is the portion of the electric current caused by the ion compared to the total electric current passing between the electrodes. The ion transference number is an indication of ions' contribution to conductivity. High values are desired for fast-charging high-power batteries with satisfied rate capability values. In addition, ionic conductivity, electrolyte viscosity, the phase behavior of the electrolyte, concentration polarization, and coordination structure of the ion should also be considered, since they are of critical significance to the mechanism of ion transport from anode to cathode [10,18–21]. On the other hand, electrical conductivity of the electrolyte is expected to be as low as possible to prevent short circuits [9,10]. Interfacial resistance between the electrode and electrolyte is another factor that is an indication of interfacial compatibility in terms of the electrochemical performance of the cell. The interface is the region that acts as a boundary or interconnection between two different phases. Higher interfacial resistance is mostly caused by insufficient contact, and it minimizes the ion transfer and slows the charging/discharging processes, which leads to lower power density.

High interfacial resistance is an important and challenging problem, especially for solid electrolytes and their derivatives [22,23]. In addition, the electrochemical stability window (ESW) of an electrolyte should be considered, since it is critical in terms of open circuit voltage (V_{oc}) and battery life. The ESW of the electrolyte is calculated from its oxidation and reduction potentials. These values are related to the highest occupied molecular orbital (HOMO) and lowest unoccupied molecular orbital (LUMO) values. It is known that the energy gap between these values can be given as the level of conductivity, which should be more than the difference between the anode (V_A) and cathode (V_C) electrochemical potentials. In addition, as given in Figure 1, HOMO should be lower than V_C and LUMO should be higher than V_A [8–10,24]. Although the above-mentioned properties are significant for an electrolyte system, their impacts are mostly dependent on the passive films formed on electrodes. The passive films can form during initial charging/discharging cycles between the electrolyte/electrode interfaces on the anode and cathode, which are referred to as the solid electrolyte interface (SEI) and the cathode electrolyte interphase (CEI), respectively. Since these layers modify the electrolyte/electrode interface, their morphology (thickness, porosity, etc.), chemical/electrochemical structure, reactivity, and stability directly affect cyclic properties, side reactions, safety, power density, and the life of the battery. If the ESW of the electrolyte is in the range of electrochemical potential of the anode and cathode, the reduction and decomposition of the electrolyte occur, leading to the growth of products and deposition of a passive SEI layer on the anode during the initial charging cycle of the cell. The SEI layer is an electrical insulator and ionic conductive layer. Although it reduces ion transfer, an electrical insulator structure is advantageous in terms of preventing further undesired reactions that lead to electrolyte decomposition. Similarly to SEIs, CEIs are formed on the cathode because of the oxidation of electrolytes. To control properties, the SEI/CEI layer's compatibility of the electrolyte with both electrodes must be considered [10,25–28]. Since the electrolyte has an interface with all components and electrified interfaces, it should also be chemically inert to electrodes, the separator, the binder, current collectors, and casing elements to keep the chemical integrity of the cell. Nonflammability is another expectation. It should show good thermal and electrochemical stability under a wide temperature range. The electrochemical stability of an electrolyte is related to the interfacial charge transport between electrodes and electrolyte. The stability of this process is significant for cyclic behavior and energy density throughout the life cycle of the battery [8–10,13]. Electrolytes, such as polymer gels, quasi-solid state, solid state, and hybrids, obtained from these processes should have good mechanical properties to withstand battery fabrication and electrochemical cycling processes. During charging/discharging cycles, positive and negative electrodes experience volume changes that can create internal stress and might affect the mechanical integrity of the electrolyte. Low cost, sustainability, ease of synthesis, and the incorporation into the cell are important for the industrial scalability of the electrolytes [8–10,13].

Various electrolytes are used for SIBs. They can be classified as liquid, quasi-solid, solid, and hybrid electrodes. The aim of this study is to review the latest state of all types of electrolytes used in SIBs, their advantages, and their challenges.

2. Liquid Electrolytes

Liquid electrolytes (LEs) are the common systems used for SIBs that are solutions or mixtures of salts dissolved in an aqueous or nonaqueous solvent or an ionic liquid. The liquid electrolytes consist of positively and negatively charged ions. Since they can freely move in the liquid phase, the ionic conductivity of LEs is relatively higher compared to other types of electrolytes. LEs generally have a wide temperature range with low viscosity. Since LEs do not have a definite form, separators are required to prevent the short circuit between the anode and cathode. Due to the bad wettability of polyolefin-based separators, relatively thick glass fiber membranes are generally used in SIBs with liquid electrolytes, and this results in a decrement in both volumetric and gravimetric energy densities. This issue can be overcome by dip coating polyolefin separators with ceramic

particles. LEs used in SIBs can be classified into non-aqueous (organic) liquid electrolytes, ionic liquids, and aqueous electrolytes. Out of these types, organic LEs have serious safety problems, including leakage, flammability, and explosion. There are many factors that affect the ionic conductivity of LEs, including the type and ratio of the salts, solvents, ion–solvent interaction, the solubility of salt, ion–ion interaction, the side reaction rate, SEI/CEI formation, temperature, aging, the dielectric constant, and the viscosity of the electrolyte [29–33]. Figure 2a. shows five different kinetic barriers during the intercalation of Na^+ into the negative electrode. These kinetic energy barriers critically increase at high charge rates or low temperatures. From the first step to the fourth step, each is primarily related to electrolyte composition. For example, a solvent with a high dielectric constant can easily dissolve Na salts and improve Na^+ diffusion kinetics in the bulk electrolyte.

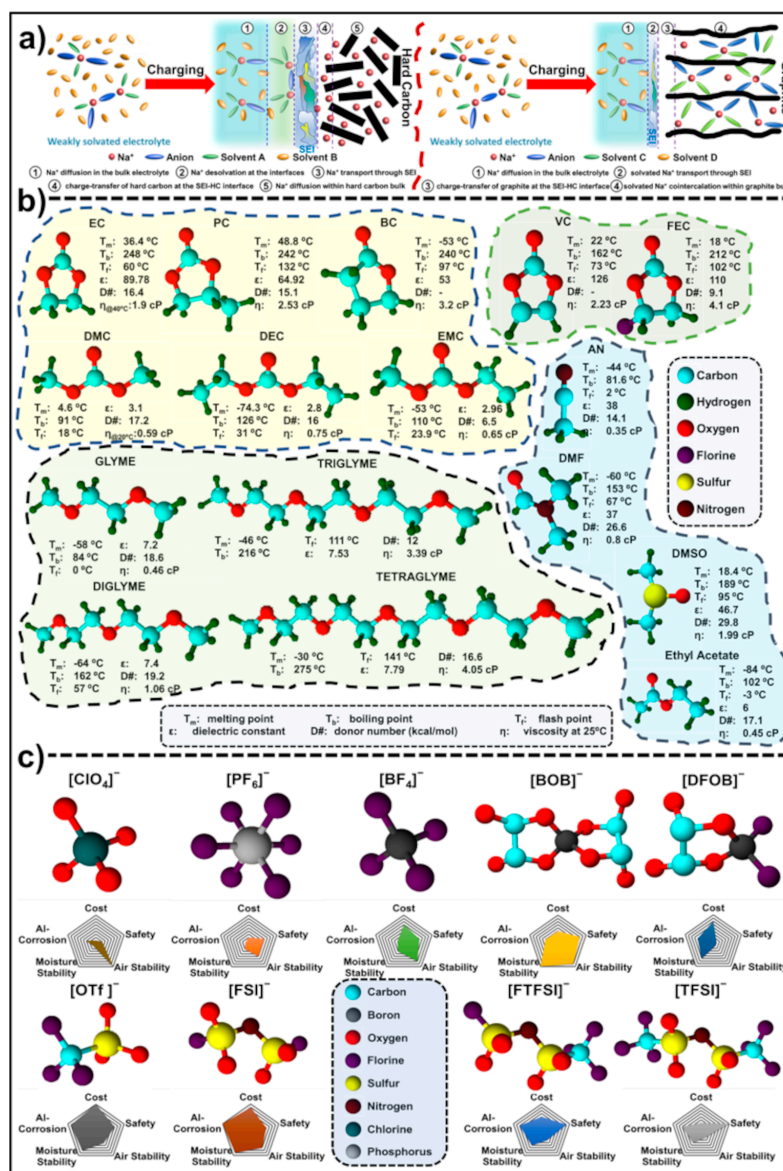


Figure 2. (a) Schematic illustrations of the electrolyte solution structures and the process of Na^+ intercalation into hard carbon and solvated Na^+ cointercalation into graphite layer during charging. Reproduced with the permission of references [34,35]. (b) Common organic electrolyte solvents used in SIBs and their physical and chemical properties. Reproduced with the permission of references [36,37]. (c) Common Na salts and ionic liquids used in SIBs. Reproduced with the permission of references [36,37].

Furthermore, a solvent with a low donor number shows a lower kinetic energy barrier for Na^+ desolvation at the interfaces. If the viscosity of the solvent is low, the ionic conductivity of the electrolyte will be high. This means that all these properties should be taken into consideration before the formulation of electrolytes. The physical and chemical properties of common solvents used in SIB electrolytes are shown in Figure 2b.

2.1. Non-Aqueous Electrolytes

Non-aqueous electrolytes are water-free organic solvents. In the literature, organic solvents used in LEs for SIBs are similar to solvents used in LEs for LIBs. Non-aqueous LEs for SIBs are currently classified into two types: ester- and ether-based electrolytes [28].

Common Na salts used in LEs for SIBs are sodium perchlorate (NaClO_4), sodium hexafluorophosphate (NaPF_6), sodium tetrafluoroborate (NaBF_4), sodium-difluoro(oxalato) borate (NaDFOB , $\text{C}_2\text{O}_4\text{BF}_2\text{Na}$), sodium bis(trifluoromethane sulfonyl)imide (NaTFSI , $\text{NaC}_2\text{F}_6\text{NS}_2\text{O}_4$), sodium fluoro sulfonyl-(trifluoromethane sulfonyl)imide (NaFTFSI , $\text{NaCF}_4\text{NS}_2\text{O}_4$), sodium bis(fluoro sulfonyl)imide (NaFSI , $\text{NaS}_2\text{O}_4\text{NF}_2$), sodium trifluoromethane sulfonate (NaOTf , NaSO_3CF_3), and CF_3COONa . Among these salts, NaPF_6 -based electrolytes show higher conductivity due to the lower polarization of the $(\text{PF}_6)^-$ anions, which improves salt solubility and ionic mobility. In general, as the concentration of sodium salt increases, the conductivity of the electrolyte using a common ester solvent increases gradually to its maximum and then begins to decrease due to the reduction of the number of free ions. The concentration of salts in LEs should, thus, be well-balanced to obtain ideal viscosity and ionic conductivity values [8]. Figure 2c shows different salts used in electrolytes for SIBs. Among these salts, NaTFSI , NaFTFSI , NaBOB , and NaFSI are good choices for high-performance electrolytes in sodium-ion batteries, due to their good air and moisture stability and good thermal stability. However, the choice of sodium salt may also depend on other factors, such as cost, availability, and compatibility with other components of the electrolyte [38].

SEI/CEI formation is one of the challenges posed by liquid electrolytes. They form on the surface of the negative/positive electrode, due to the self-reduction reactions of the ester-based electrolytes and the anion/cation of sodium salt during cycling, and affect the electrochemical performance of SIBs. As in LIBs, the size and morphology of an SEI directly affects the performance of the system. While a thin and uniform SEI can be advantageous in terms of improving the cycling stability and uniform Na^+ deposition on the surface of the electrode, a thicker SEI with a heterogeneous morphology may lead to problems such as higher polarization and slow ion migration. In order to stabilize an SEI, some additives can be used in the SIBs [39]. Fluoroethylene carbonate (FEC) and vinylene carbonate (VC) are common additives used for SIBs. A typical additive solvent affects the ionic conductivity of an electrolyte with its viscosity and its dielectric constant; the former determines ionic mobility and the latter governs salt dissociation. In general, solvents with a high dielectric constant can show good dissociation of Na salts, but also show high viscosity. For this reason, binary or ternary additive solvent systems are used to balance the ionic conductivity of LEs (Figure 2b) [40].

2.1.1. Ester-Based Electrolytes

Ethylene carbonate (EC), propylene carbonate (PC), butylene carbonate (BC), diethyl carbonate (DEC), dimethyl carbonate (DMC), ethyl methyl carbonate (EMC), and their mixtures are the most used ester-based solvents for SIBs [29]. Figure 3 shows the effect of ester-based and ether-based electrolytes on SEI formation on certain negative electrodes for SIBs. Komaba et al. studied the effects of carbonate esters on the SEI of hard carbon (HC) anodes and cycling performance. They found that the electrochemical performance and cycle life of electrolyte solutions was $\text{PC} > \text{EC} > \text{BC}$ solution containing 1 M NaClO_4 at 25 mA g^{-1} . They have also studied binary solvents and found cyclic performances as $\text{EC}:\text{DEC} > \text{EC}:\text{EMC} > \text{EC}:\text{DMC}$ solution containing 1 M NaClO_4 at 25 mA g^{-1} . They have also discovered that adding 2% VC resulted in a negative effect on the Na insertion into

the HC electrodes [41]. On the other hand, Maça and Etacheri demonstrated that a 3% VC additive in 1 M NaClO₄/PC electrolyte had excellent pseudocapacitive Na-ion diffusion on the SEI of the TiO₂ anode. After 750 cycles, a TiO₂ nanosheet anode in a Na-ion half cell configuration retained around 90% of its initial capacity and almost 100% Coulombic efficiency. Na-ion half cells containing VC-free electrolyte solution retained only 16% of their initial capacity while maintaining 98% Coulombic efficiency [41].

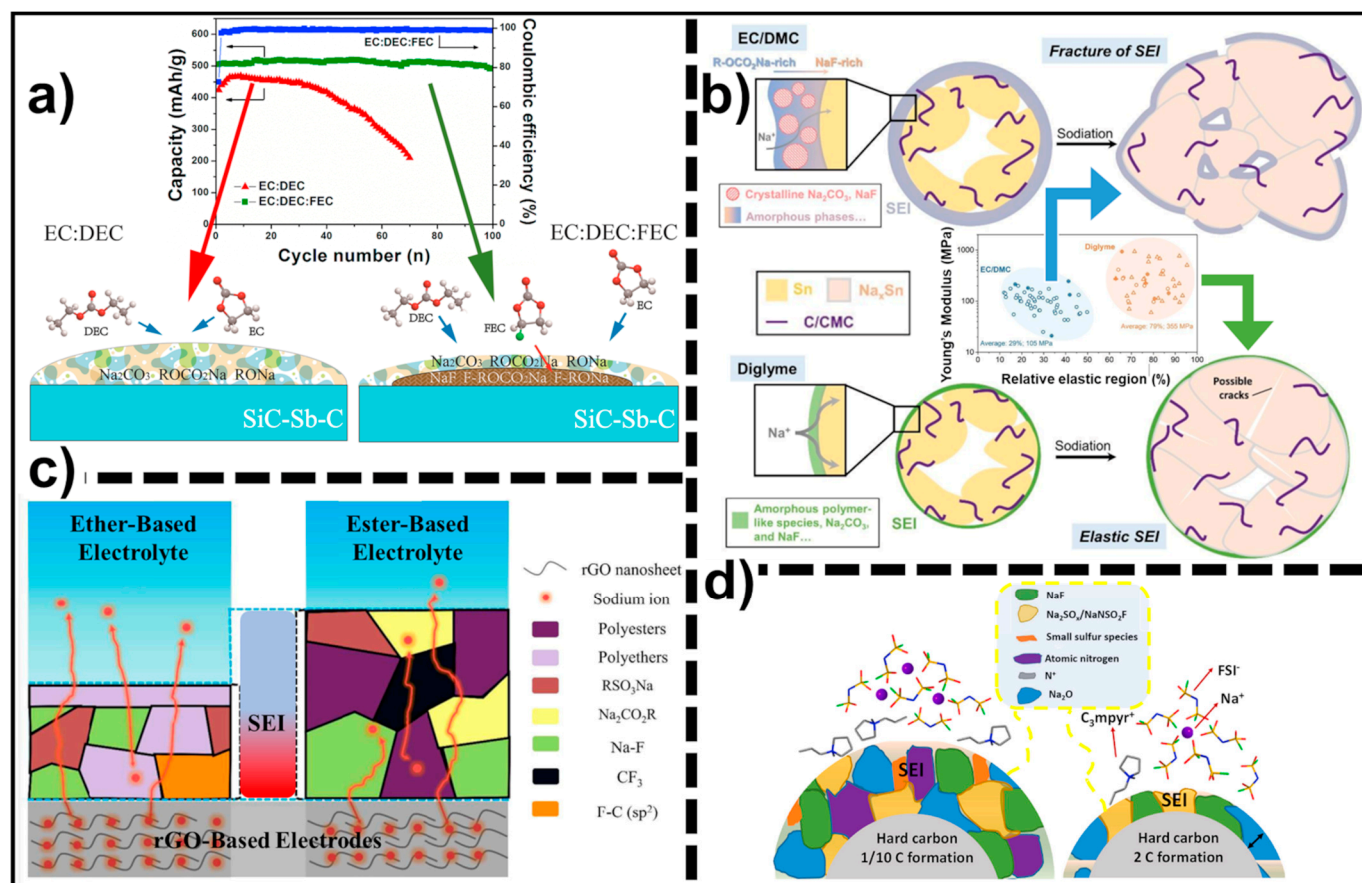


Figure 3. Effects of additives and solvents of liquid electrolytes on SEI formation. (a) Cycling performance of SiC-Sb-C electrode at a cycling rate of 100 mA g⁻¹ in FEC-free and FEC-containing electrolytes and corresponding film-forming mechanism on electrodes. Reproduced with the permission of reference [42]. (b) Illustration of chemical compositions, structures, and the mechanical response to the volume expansion of SEIs on Sn anodes in different liquid electrolytes. Reproduced with the permission of reference [43]. (c) Schematic representation of SEI components on rGO anodes in different liquid electrolytes. Reproduced with the permission of reference [44]. (d) Illustration of different components of SEI on hard carbon anodes under different formation conditions. Reproduced with the permission of reference [45].

Hou et al. demonstrated the effects of anions in the solvated shell on Na storage kinetics and the SEI evolution process. In contrast to Ponrouch et al. [41] and Dugas et al. [46], they showed that PF₆⁻ anions and a 1% FEC additive formed a thin, compact, and protective SEI with layered morphology. They have also produced a 5 Ah pouch-cell including Na₃V₂(PO₄)₃-HC in 1 M NaPF₆/EC:DEC (1% FEC) electrolyte with superior cycling stability and a retention of 85.6% at 1 C after 800 cycles [47]. In another study, Lu et al. investigated the effect of FEC additives on Sb-based composite anodes for SIBs. Due to the formation of a double-layer SEI film on the electrode surface, the addition of 5% FEC to 1 M NaClO₄/EC:DEC electrolyte improved the cycling stability of the Sb-based anode (Figure 3a) [42]. Eshetu et al. carried out comprehensive research about the effects

of various Na salts and solvent mixtures on Al current collector stability, and reactivity with HC and SEI formation. They found that various salt anions in EC:DEC revealed that the trend in Al dissolution and/or anion decomposition increased in the order of $\text{NaPF}_6 < \text{NaClO}_4 < \text{NaTFSI} < \text{NaFTFSI} < \text{NaFSI}$. The reactivity of solvent mixtures on HC decreased in the order of $\text{EC:DMC} > \text{EC:DEC} > \text{EC:PC}$ for a fixed Na salt. For a fixed solvent mixture, the reactivity on HC decreased in the following order: $\text{NaClO}_4 > \text{NaFTFSI} > \text{NaPF}_6 > \text{NaTFSI} > \text{NaFSI}$ [48,49]. Similarly, Sun et al. compared different salts, NaDFOB, NaPF_6 , and NaClO_4 , in EC:DEC:DMC (2:1:1) for FeF_3/C nanofiber cathodes for SIBs. In terms of cyclic stability, FeF_3 cells based on NaDFOB showed better performance than NaPF_6 - and NaClO_4 -based ones. They also observed that ternary solvents (EC:DEC:DMC) showed more stable electrochemical performance compared to binary solvents (EC:DEC and EC:DMC) due to the formation of a thin and protective CEI film on the cathode [50]. Tao et al. prepared MoS_2 -porous carbon composite anode half cells in 1 M $\text{NaClO}_4/\text{EC:DEC}$ with 5% FEC. The cyclic test demonstrated very good stability (310.74 mAh g^{-1} after 1000 cycles with an 86.26% retentive capacity at 1.0 A g^{-1}) [51].

2.1.2. Ether-Based Electrolytes

Monoglyme, diglyme, triglyme, and tetraglyme are the most used ether-based solvents in SIBs. Although ether-based electrolytes have higher HOMO levels (around -0.21 eV), their LUMO levels are also much higher than carbonate-based electrolytes, which makes them promising solvents for SIB electrolytes. Additionally, they have shown better electrochemical performance than carbonate-based electrolytes, as reported in many studies, especially when coupled with graphite-based negative electrodes (Figure 2a,b) [36,37]. In general, ether-based electrolytes offer highly reversible solvent cointercalation reactions, as well as the formation of a thin and stable SEI for SIBs due to their stable solvation structure [32]. Liu et al. prepared a full cell composed of a carbomethoxy-modified insoluble quinone-based disodium salt/CNTs composite anode and P2-type— $\text{Na}_{0.67}\text{Mn}_{0.75}\text{Li}_{0.25}\text{O}_2$ cathode in 1 M $\text{NaPF}_6/\text{dimethoxy ether}$ (DME or glyme) electrolyte. The full cell showed a capacity of around 125 mAh g^{-1} at 0.2 C and capacity retention of around 25% at the end of 1000 cycles at 2 C [52].

In 2017, Zhang et al. published work on the performance of electrolytes consisting of diglyme and EC:DEC with 1 M NaOTf for Na^+/rGO half cells operating at room temperature. They found that the concentration of polymer species in rGO electrodes cycled in diglyme is lower in the exteriors and significantly lower in the interior of the SEI compared to rGO electrodes cycled in EC:DEC. With an initial Coulombic efficiency of 74.6%, an rGO electrode cycled in an ether-based solvent provided significantly better electrochemical performance compared to an rGO electrode cycled in ester-based solvents due to the formation of a thinner and denser layer of solvent decomposition products in the exteriors of SEI (Figure 3c) [44]. In another study, Yang et al. synthesized mesoporous hollow TiO_2 nanospheres as the anode for SIBs and active material showed better electrochemical performance (110 mAh g^{-1} after 1000 cycles at 1 A g^{-1}) in an ether-based electrolyte than in an ester-based one for sodium-ion storage [53]. Nacimiento et al. used 1 M NaPF_6 in diglyme electrolyte for a fully graphitized carbon nanofibers (CNF)/ $\text{Na}_3\text{V}_2(\text{PO}_4)_3$ full cell. The battery's average discharge voltage was around 2.2 V, and had a discharge capacity of 96 mA h g^{-1} with a Coulombic efficiency of 87%. They found that fiber breakage opened new pathways for sodium to enter the interlayer due to strains and swelling during sodium insertion [54]. Wang et al. compared different ether-based electrolytes for $\text{Na}/\text{Na}_3\text{V}_2(\text{PO}_4)_3$ full cells. They prepared 1 M NaBF_4 electrolyte solution in tetrahydrofuran (THF), 1,2-dimethoxyethane (DME), diethylene glycol dimethyl ether (diglyme), triethylene glycol monomethyl ether (triglyme), and tetraethylene glycol dimethyl ether (tetraglyme). According to their solubility analysis, 1 M NaBF_4/THF and 1 M NaBF_4/DME showed no solubility and 1 M $\text{NaBF}_4/\text{diglyme}$ showed partial solubility. 1 M $\text{NaBF}_4/\text{tetraglyme}$ and 1 M $\text{NaBF}_4/\text{triglyme}$ were completely dissolved. In terms of electrochemical performance, 0.5 M $\text{NaBF}_4/\text{diglyme}$ electrolyte showed the best result [55]. In another study, 1 M $\text{NaBF}_4/\text{diglyme}$ white-turbid electrolyte solution outperformed 1 M

NaBF₄/EC:DMC electrolyte in terms of Coulombic efficiencies, rate capabilities, and cyclic stability due to high elasticity and high ionic conductivity of the SEI (Figure 3b) [43].

Another significant route to improve charging/discharging kinetics is removing some steps during cation intercalation. This phenomenon can be achieved by using novel electrolyte/electrode couples, as well as a narrower working potential window. For instance, Zhang et al. showed the pseudocapacitive behavior of solvated-ion cointercalation into a MoS₂ anode in a novel electrolyte system (1 M LiTFSI in glyme: tetraglyme, 3:1 by volume). By using a 1–3 V working window, desolvation of lithium ions and lithium diffusion through SEI steps were eliminated (Figure 2c) [56]. These approaches are critically important to improving the energy and power densities of SIBs. Kim et al. quantitatively analyzed the cointercalation of solvated Na ions in graphite for the first time. They found that glyme-based electrolytes are suitable choices for graphitic carbons [57]. In another study, their group also analyzed the sodium storage behavior of natural graphite by using ether-based electrolytes. Different ether-based electrolytes, including 1 M NaPF₆ in glyme, diglyme, and tetraglyme, were used. It was observed that the plateau potential for sodium storage increased from 0.6 to 0.78 V as the molecular size increased. Furthermore, electrolyte decomposition was suppressed by using ether-based solvents, and a negligible thin SEI film formed on the graphite surface. Due to solvated sodium ion cointercalation and partial pseudocapacitive behavior, a natural graphite anode with a large particle size showed a high capacity of 150 mAh g⁻¹ at 500 mA g⁻¹ after 2500 cycles [34]. Recently, Song et al. studied the optimization of an electric double layer of a CuS anode by dissolving Cu⁺ from a Cu current collector into the electrode. They assembled a half cell with a surface-tailored CuS anode in NaOTf/diglyme electrolyte. The half cell showed excellent specific capacity, which was 402.8 mAh g⁻¹ at 2 C after 7000 cycles with almost 100% capacity retention. They proposed that NaOTf/diglyme electrolyte created an ultrathin, stable, and CuF₂-rich SEI on the CuS surface [58].

2.2. Ionic Liquids

Ionic liquids (ILs) can be defined as room- or ambient-temperature molten salts with good ionic conductivities. They also offer important characteristics such as nonflammability and negligible vapor pressure, which are of great importance for the safety of SIBs. ILs can be used in both positive [59,60] or negative active material synthesis [51,61] and many examples of the applications of ILs in SIBs are given in Table 1.

Table 1. Liquid electrolytes used in SIBs.

	Cathode	Anode	Solvent	Na Salt	Molarity	Additive	Ref.
Non-aqueous Electrolytes	NaNi _{0.5} Mn _{0.5} O ₂	HC	PC	NaClO ₄	1	VC	[41]
	Na ₃ V ₂ (PO ₄) ₃	HC	EC:DEC	NaPF ₆	1	FEC	[47]
	Na	SiC-Sb-C	EC:DEC	NaClO ₄	1	FEC	[42]
	Na	TiO ₂	PC	NaClO ₄	1	VC	[62]
	Na	MoS ₂ /C	EC:DEC	NaClO ₄	1	FEC	[63]
	Na _{0.67} Mn _{0.75} Li _{0.25} O ₂	CNT/Na-IL	DME	NaPF ₆	1		[52]
	Na	rGO	Diglyme	NaOTf	1		[44]
	Na	TiO ₂	Tetraglyme	NaOTf	1		[53]
	Na ₃ V ₂ (PO ₄) ₃	CNF	Diglyme	NaPF ₆	1		[54]
Na ₃ V ₂ (PO ₄) ₃	Na	Diglyme	NaBF ₄	0.5		[55]	
Ionic Liquids	Na	Red P	MPPFSA	NaFSI	0.25		[64]
	Na _{0.67} Mn _{0.67} Ni _{0.23} Mg _{0.10} O ₂	Na	Pyr _{1.4} FSI	NaFSI	1		[65]
	FeF ₃ /C NFs	Na	Pyr _{1.3} FSI	NaFSI	1		[66]
	Na	HC	C ₃ mpyrFSI	NaFSI	0.5		[45]

Table 1. Cont.

	Cathode	Anode	Solvent	Na Salt	Molarity	Additive	Ref.
Aqueous	Na ₂ MnFe(CN) ₆	NaTi ₂ (PO ₄) ₃	H ₂ O	NaTFSI	30	EMImTFSI	[67]
	PBA	AC	H ₂ O	NaClO ₄	1	GO	[68]
	Na ₃ V _{1.3} Fe _{0.5} W _{0.2} (PO ₄) ₃	NaTi ₂ (PO ₄) ₃	H ₂ O	Na ₂ SO ₄	1		[69]
	Na ₂ VTi(PO ₄) ₃	Na ₂ VTi(PO ₄) ₃	H ₂ O	CF ₃ COONa	26		[70]

Santamaria et al. produced half cells including P2-Na_{0.67}Mn_{0.67}Ni_{0.23}Mg_{0.1}O₂ cathodes contacting with 1 M NaFSI in N-butyl-N-methylpyrrolidinium bis(fluoro sulfonyl)imide, Pyr_{1,4}FSI electrolyte. Half cells using ionic liquid electrolytes showed better electrochemical performance than those using 1 M NaFSI/PC electrolyte in terms of cyclic performance, high-rate performance, and energy density [65]. Sun et al. showed that FeF₃/C nanofibers performed significantly better in a variety of ionic liquid (IL) electrolytes at both room temperature and elevated temperatures compared to ester-based electrolytes. In their study, they used different ILs including N-propyl-N-methylpyrrolidinium bis(fluoro sulfonyl)imide (Pyr_{1,3}FSI), 1-butyl-1-methylpyrrolidinium bis(fluoro sulfonyl)imide (Pyr_{1,4}FSI), and 1-ethyl-3-methylimidazolium bis-(fluoro sulfonyl)imide (EMImFSI). Among these electrolytes, electrochemical cycling stabilities could be given as Pyr_{1,4}FSI > EMImFSI > Pyr_{1,3}FSI at room temperature. At elevated temperatures, Pyr_{1,3}FSI-based electrolyte showed better performance than Pyr_{1,4}FSI-based electrolyte [66]. Dahbi et al. investigated the Na storage performance of red phosphorus (P) in N-methyl-N-propylpyridinium bisfluoro sulfonyl amide (MPPFSA) ionic liquid electrolyte at 25 °C. Red P anodes showed a high reversible capacity (1480 mAh g⁻¹ at 125 mA g⁻¹) and a capacity retention of 93% over 80 cycles in NaFSI/MPPFSA electrolyte without additives [64]. Sun et al. investigated interfacial characteristics of mesoporous carbon (CMK) anodes in SIBs in contact with highly concentrated (3.8 M) NaFSI/N-methyl-N-propylpyrrolidinium bis(fluoro sulfonyl)imide (C₃mpyrFSI). They found that an inorganic SEI on the CMK electrode with high ionic conductivity was produced because of the contribution of anion breakdown species in ILs. With a high reversible capacity of 320 mAh g⁻¹ at 0.5 A g⁻¹, the Na/CMK cell in the IL electrolyte had exceptional cycling stability up to 3500 cycles [71]. In another study, Sun et al. analyzed the interaction between the SEI on HC anodes and the formation procedure. They found that 0.5 M NaFSI/C₃mpyrFSI electrolytes reduced formation time by 38 times due to the absence of reduced S and N species in the SEI after high-rate formation (Figure 3d) [45]. Recently, Fiates et al. conducted molecular dynamics (MD) simulations and density functional theory (DFT) calculations of imidazolium and branched and bulky ammonium-based cations coupled with a weakly coordinated fluoroalkoxyaluminate [Al(OHfip)₄]⁻ anion. They found that anion size and charge distribution affect the Na⁺ transport mechanism and that the selection of a suitable cation is of great importance to Na⁺ mobility and electrolyte stability. According to their MD results, bulky ammonium cations and imidazolium-based cations have been found to have a beneficial effect on Na⁺ mobility, making them attractive candidates for enhancing Na⁺ dynamics [72]. In sum, ILs are promising organic electrolyte substitutes due to their superior thermal stability, large electrochemical window, and low flammability. On the other hand, their high cost and high viscosity due to strong Coulombic interactions between cations and anions are the main bottleneck in their applications as electrolytes for SIBs. ILs can form a protective and ionically conductive CEI layer on the cathode, which reduces side reactions that commonly cause gassing and excessive CEI growth in organic electrolytes, especially at high temperatures.

2.3. Aqueous Electrolytes

Aqueous sodium-ion batteries (ASIBs) are potential alternative energy storage systems due to their environmentally friendly nature and high safety. The stability of aqueous batteries' performance depends on the compatibility of their electrode and electrolyte. Poor cycle stability is still a problem for aqueous SIBs due to the narrow ESW of water and

causes significant electrode erosion (or parasitic side reactions) during cycling. In addition, water has a relatively high freezing point, and this limits the practical usage of aqueous electrolytes under extreme conditions. To address these problems, several approaches have been developed, such as using highly concentrated electrolytes, solvent mixtures, additives, etc. Recently, Yang et al. comprehensively reviewed electrolytes and electrode materials for ASIBs; the authors recommend this study to readers who want to obtain detailed information on this subject [73]. Kühnel et al. carried out research on NaFSI-based aqueous electrolytes for ASIBs. They found that NaFSI had an extremely high solubility at room temperature (up to $\sim 37 \text{ mol L}^{-1}$) with a wide electrochemical stability window of 2.6 V [74]. Reber et al. comprehensively analyzed 11 different sodium salts according to their anions for water-in-salt type electrolytes. According to their results, the anion's nature has a significant impact on solution structure and performance in aqueous high-voltage batteries at high salt concentrations. They concluded that anions for water-in-salt electrolytes should be cheap, chaotropic, resistant to hydrolysis, resistant to oxidation, soluble enough to reach critical salt concentrations, and be involved in the formation of anion-derived SEIs [67]. Nakamoto et al. prepared an inexpensive water-in-salt electrolyte by dissolving the maximum amount of sodium trifluoroacetate (CF_3COONa , 26 mol kg^{-1}) in water, and this composition gave a broad electrochemical stability window of 3.1 V. They also found that the electrolyte created a robust fluoride layer formed on the $\text{Na}_2\text{VTi}(\text{PO}_4)_3$ anode and the symmetric full cell gave a capacity of around 30 mAh g^{-1} at 2 mA cm^{-2} with good cycling behavior [70].

During the test of a carbon-coated $\text{Na}_3\text{V}_{1.3}\text{Fe}_{0.5}\text{W}_{0.2}(\text{PO}_4)_3$ cathode and a $\text{NaTi}_2(\text{PO}_4)_3$ anode in 1 M $\text{Na}_2\text{SO}_4/\text{H}_2\text{O}$ full cell prepared by Yang et al., a high capacity of 64 mAh g^{-1} at 1 A g^{-1} and 95% capacity retention after 50 cycles were discovered to be possible with full cells [69]. Bi et al. produced a full cell with a Prussian blue analogue (PBA) cathode and an activated carbon (AC) anode in 1 M $\text{NaClO}_4/\text{graphene oxide (GO)}$ in water electrolyte. After 17,000 cycles, SIBs in the low-concentration aqueous electrolyte could maintain a capacity of 65.5 mAh g^{-1} at 2 A g^{-1} with 65.1% capacity retention. GO addition into electrolyte acted similarly to a selective membrane, which could prevent the structural degradation and Fe^{+3} mass transfer between the cathode and anode. Reduced side reactions and the dissolution of the PBA cathode in the electrolyte were achieved by the numerous hydrophilic functional groups in the GO nanosheets' interactions with a variety of free water molecules [68]. Zhu et al. prepared a full cell including an activated carbon (nitrogen and sulfur-doped porous carbon) cathode and a polyimide anode in contact with $(\text{NaClO}_4)_{1.7}(\text{H}_2\text{O})_{5.5}(\text{formamide})_{5.81}$ electrolyte ($\text{H}_2\text{O}:\text{FA}$ volume ratio of 3:7). In their study, FA was used as a nonflammable cosolvent to lower the freezing point of electrolyte up to $-50 \text{ }^\circ\text{C}$. They concluded that the reconstructed hydrogen bond network between carbonyl, amino, and hydroxyl groups in the hybrid solution was responsible for the antifreeze mechanism. At $-50 \text{ }^\circ\text{C}$, the full cell showed around 80 mAh g^{-1} capacity at 4 C after 8000 cycles [60]. Similarly, Reber et al. used a hybrid aqueous electrolyte by mixing 1-ethyl-3-methylimidazolium bis(trifluoromethylsulfonyl)imide (EMImTFSI) ionic liquid with water to improve the solubility of NaTFSI by up to 30 mol kg^{-1} . A full cell composed of a $\text{Na}_2\text{Mn}[\text{Fe}(\text{CN})_6]$ cathode and a $\text{NaTi}_2(\text{PO}_4)_3$ anode contacting with a gel-like hybrid aqueous electrolyte ($80 \text{ mol NaTFSI}_{0.375}\text{EMImTFSI}_{0.625}$) showed a 77 Wh kg^{-1} energy density at 1 C with a Coulombic efficiency of $>99.5\%$ after 300 cycles [67]. Recently, Ge et al., produced an aqueous potassium ion battery by using a surface engineered PBA cathode paired with a 3,4,9,10-perylenetetracarboxylic diimide anode in 21 M $\text{KOTf}/0.2 \text{ M FeOTf}$ in water. The full cell showed excellent cycling performance and an energy density as high as 92 Wh kg^{-1} with 82.5% capacity retention after 6500 cycles at 1.5 A g^{-1} [75]. In another study, Ge et al. used an electrolyte composed of 2 M $\text{Zn}(\text{OTf})_2/\text{EMImOTf}$ in water for aqueous Zn batteries. By using novel salt and ionic salts, a very thin, stable, and zinc fluoride/zinc sulfide-rich interface was produced due to the decomposition of OTf^- [76]. To improve the electrochemical performance of SIBs, these novel approaches should be adapted to aqueous or non-aqueous SIBs.

3. Quasi-Solid Electrolytes

Quasi-solid-state electrolytes are a type of electrolyte material that is intermediate between solid-state and liquid-state electrolytes. They are called “quasi” solid-state electrolytes because they have some characteristics of both solid and liquid electrolytes. Quasi-solid-state electrolytes are typically composed of a solid polymer matrix that is filled with a liquid electrolyte. The solid polymer matrix provides mechanical stability and helps to prevent the liquid electrolyte from leaking or evaporating. The liquid electrolyte provides the ionic conductivity necessary for the material to act as an electrolyte. Quasi-solid-state electrolytes have several advantages over traditional liquid electrolytes, including increased mechanical stability, improved safety, and improved processing characteristics, because they are composed of low-cost and scalable polymeric materials. Mechanical properties of QSEs can be improved by chemical crosslinking of the polymer matrix, by in situ polymerization, or by reinforcement with fibrous mesh [77].

The segmental motion of polymer chains provides sodium-ion conduction in polymer-based electrolytes (Figure 4a). For this reason, polymers used in polymer electrolytes should have a low glass transition temperature (T_g) and low crystallinity. In polymer electrolytes, polymer should be able to couple with sodium ions, as well as dissolve sodium salt, for improved conductivity. Polar groups on the chain backbone or side chains (-O-, -S-, -NH-, -CN-, -Cl-, -SO₃-, etc.) are efficient building blocks for dissolving sodium salts. Although polyethylene oxide (PEO) is used in polymer-based electrolytes in many studies for SIBs, polymers such as poly(vinylidene fluoride) (PVDF) [78], poly(vinylidene fluoride-co-hexafluoro-propylene) (P(VdF-HFP)) [79], polyacrylonitrile (PAN) [80], polyvinyl chloride (PVC) [81], polyvinylene carbonate (PVN) [82], and polymethyl methacrylate (PMMA) [83] can also be used for a polymer matrix.

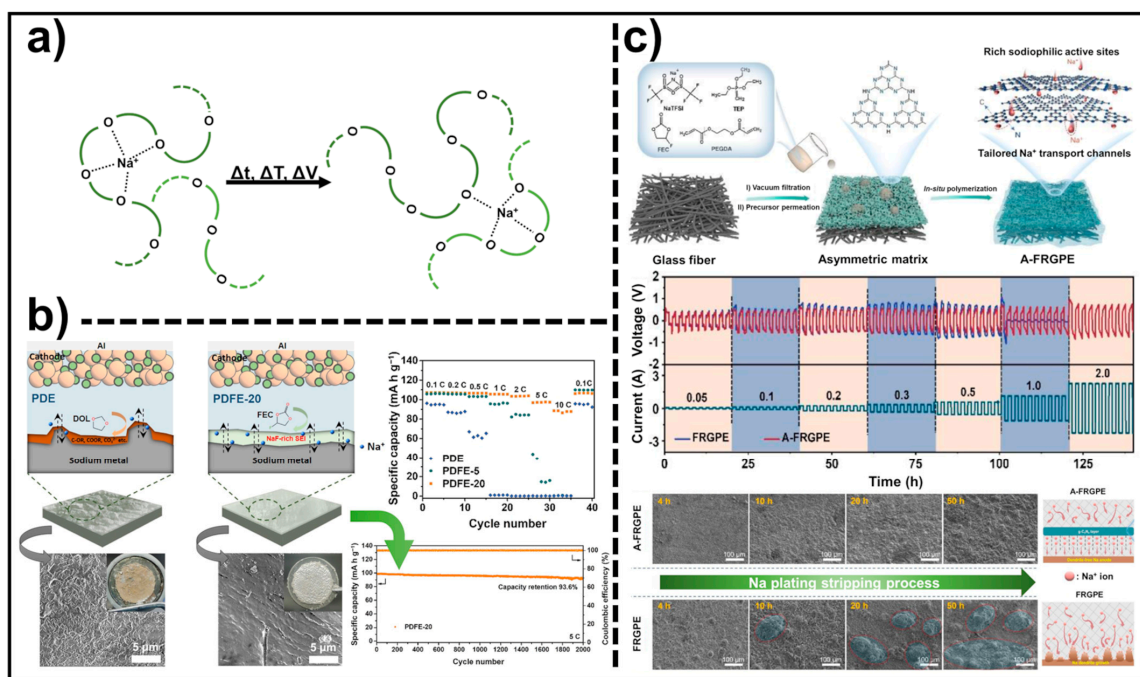


Figure 4. (a) Schematic diagram of sodium-ion conduction mechanism of PEO-based electrolyte. Reproduced with the permission of reference [84]. (b) A schematic view of stable SEI formation by FEC additive and corresponding C-rate and long-term cyclic performances. Reproduced with the permission of reference [85]. (c) Schematic representation of A-FRGPE preparation process, Na plating/stripping tests at different current densities, and corresponding SEM images of the Na metal anodes in symmetric cells with Na deposition mechanism. Reproduced with the permission of reference [86].

Colo et al. developed a PEO-based crosslinked polymer electrolyte (XPE) composed of NaClO_4 :PC:PEO (5:50:45 by weight) with a high ionic conductivity of $>1 \text{ mS cm}^{-1}$ at room temperature and a high ESW of $>4.7 \text{ V}$ by light-induced free-radical polymerization. TiO_2 /XPE/Na cell showed a high capacity of 250 mAh g^{-1} at 0.1 mA cm^{-2} and a capacity retention of $>60\%$ at 0.5 mA cm^{-2} after 1000 cycles [87].

Parveen et al. reported a P(VdF-HFP)-based gel electrolyte plasticized with NaClO_4 :triglyme (0.3:1 by mol) with a high ionic conductivity of 2.54 mS cm^{-1} and a wide ESW of $\sim 4.7 \text{ V}$ [88]. Zhao et al. fabricated a gel polymer electrolyte by simply soaking a P(VdF-HFP) membrane into 1 M NaClO_4 /PC:FEC (95:5 by volume) liquid electrolyte for 24 h with a high ionic conductivity of 0.42 mS cm^{-1} . The full cell, including a $\text{Na}_3\text{V}_2(\text{PO}_4)_2\text{O}_2\text{F}$ cathode and an HC anode from cotton cloth, in a P(VdF-HFP)-based gel electrolyte showed a high capacity of 78.1 mAh g^{-1} at 10 C with $>90\%$ capacity retention after 500 cycles [77]. In another study, Zhao et al. produced a full cell including a $\text{Na}_3\text{V}_2(\text{PO}_4)_2\text{O}_2\text{F}/\text{C}$ cloth cathode and a flexible carbon cloth anode in the same gel electrolyte from their previous research. The flexible full cell showed outstanding cyclic performance with 0.0114% capacity decay per cycle over 2000 cycles at 5 C and a high capacity of 71.4 mAh g^{-1} at 10 C [89].

To improve the mechanical properties of P(VdF-HFP)-based gel polymer electrolytes, inert nonwoven fabrics can be incorporated into the gel structure. For example, a porous composite gel polymer electrolyte using a P(VdF-HFP) membrane reinforced with polypropylene (PP) nonwoven in 1 M NaClO_4 /EC:DMC:EMC (1:1:1 by weight) was reported to possess a high ionic conductivity of 0.82 mS cm^{-1} at room temperature, as well as a wide electrochemical stability window of 4.8 V [90]. A similar study was carried out by Zheng et al. [91]. In their study, the PVDF-HFP membrane reinforced by PP nonwoven in 1 M NaClO_4 /EC:DEC:FEC (95:95:10 by weight) also showed a high ionic conductivity of 1.38 mS cm^{-1} at room temperature.

Another approach to improve the mechanical properties, electrochemical performance, and ionic conductivity of gel polymer electrolytes is to produce composite gel polymer electrolytes (CGPEs) by mixing or crosslinking inorganic and organic materials [92]. Zhao et al. prepared a PVDF-HFP/ SnO_2 /1-(4-cyanophenyl)guanidine composite membrane by solution casting followed by immersion in liquid electrolyte (1 M NaClO_4 /EC:DMC:FEC, 90:90:20 by volume) with 0.232 mS cm^{-1} at 70°C . SnO_2 loading improved the electrolyte uptake behavior of gel electrolytes and 8 wt.% SnO_2 -loaded CGPE showed the highest electrolyte uptake of 206%. On the other hand, the introduction of 1-(4-cyanophenyl)guanidine into the structure created Na^+ -transport channels by establishing a ligand with a strong metal-ligand bond [93]. In another study, hydroxyapatite (HAP, $\text{Ca}_{10}(\text{PO}_4)_6(\text{OH})_2$) was introduced into a PVDF-HFP/poly(butyl methacrylate) (PBMA) blend to improve the safety and the life time of the battery. An HAP/PVDF-HFP/PBMA composite membrane was prepared by solution casting and drying routes. Due to the high porosity (64%) and low tortuosity of membranes, a high liquid electrolyte (1 M NaClO_4 /EC:PC) uptake of $\sim 350\%$ was observed. In addition, HAP/PVDF-HFP/PBMA-based CGPEs showed a high ionic conductivity of 1.086 mS cm^{-1} at room temperature and a wide ESW up to 4.9 V [94]. Similarly, Wang et al. introduced different amounts of Na^+ -conducting inorganic $\text{Na}_3\text{Zr}_2\text{Si}_2\text{PO}_{12}$ nanoparticles into PVDF-HFP/PMMA/thermoplastic polyurethane (TPU) polymer blends by facile solution mixing. CGPEs were prepared by immersing PVDF-HFP/PMMA/TPU- $\text{Na}_3\text{Zr}_2\text{Si}_2\text{PO}_{12}$ composites in the liquid electrolyte (1 M NaClO_4 /EC:DMC) for 12 h. An amount of 4 wt.% $\text{Na}_3\text{Zr}_2\text{Si}_2\text{PO}_{12}$ containing CGPEs showed a high ionic conductivity of 2.83 mS cm^{-1} at room temperature with a wide ESW of 5.16 V and high porosity (28.71%) [83].

Lai et al. fabricated a PVDF-HFP/ β - Al_2O_3 composite membrane by using a silane coupling agent (3-aminopropyl-trimethoxysilane). They produced CGPEs by immersing PVDF-HFP/ β - Al_2O_3 membranes with different amounts of Na^+ -conducting β - Al_2O_3 in the liquid electrolyte (1 M NaPF_6 /PC:FEC, 95:5 by volume) for 3 h. A total of 60% β - Al_2O_3 containing CGPEs demonstrated the highest ionic conductivity of 1.37 mS cm^{-1} at 20°C

with an ESW up to 4.52 V and good flame retardancy. A $\text{Na}_3\text{V}_2(\text{PO}_4)_3/\text{Na}$ full cell in 60% $\beta\text{-Al}_2\text{O}_3$ containing CGPEs showed an initial discharge capacity of 93.6 mAh g^{-1} with 92.2% capacity retention at 3 C after 1000 cycles [95]. Another approach to improve electrolyte uptake is making ionogel electrolytes. Ionogel electrolytes are nanoscale, two-phase materials composed of an ionic liquid contained within an organic or inorganic matrix. Although ionogels are a new class of quasi-solid electrolytes, their use in SIBs is becoming common. In a recent study, DeBlock et al. synthesized ionogel electrolytes for $\text{Na}_3(\text{VO})_2(\text{PO}_4)_2\text{F@rGO}/\text{Na}$ cells. They encapsulated NaBF_4 :tetraglyme (1:4 by mol) liquid electrolyte into a PVDF-HFP/ SiO_2 polymer composite matrix by a sol-gel route. Ionogel electrolyte showed a high ionic conductivity of 0.9 mS cm^{-1} at room temperature with a wide ESW of $>4 \text{ V}$. $\text{Na}_3(\text{VO})_2(\text{PO}_4)_2\text{F@rGO}/\text{Na}$ full cells including ionogel electrolyte showed more than 100 mAh g^{-1} capacity at 1 C ($\sim 165 \text{ Wh kg}^{-1}$ energy density) [79].

Gel polymer electrolytes are less capable of wetting electrodes than liquid electrolytes. This increases charge transfer resistance between the electrode and electrolyte. To reduce charge transfer resistance between electrodes and electrolytes, electrolytes can be synthesized on the surface of electrodes by in situ polymerization. Ma et al. synthesized poly(1,3-dioxolane)-based quasi-solid electrolytes by in situ polymerization for sodium metal batteries. Anode/cathode interfaces were conformally coated by gel electrolyte and this eliminated geometrical gaps and decreased charge transfer resistance with the aid of in situ polymerization. FEC greatly enhanced ionic transport while acting as a plasticizer to prevent crystallization during polymerization. In addition, FEC increased the mechanical uniformity of the electrolyte–electrode interfaces during battery cycling while creating a stable SEI at the anode that was rich in NaF. (Figure 4b) [85].

The safety of SIBs is an important consideration in their design and use. Thermal runaway, short circuits, and the use of flammable liquid electrolytes are the major safety concerns for SIBs. Glass fiber-based nonwovens are the most used separators for SIBs. Among quasi-solid-state electrolytes, glass fiber-based electrolytes offer some advantages such as high safety, high thermal stability, and excellent mechanical performance. For example, Yang et al. developed an asymmetric flame-retardant gel polymer electrolyte (A-FRGPE) with a high ionic conductivity of 2 mS cm^{-1} at room temperature and a wide ESW of 5.63 V vs. Na^+/Na . As shown in Figure 4c, during the stripping/plating process, the sodiophilic porous $\text{g-C}_3\text{N}_4$ layer in A-FRGPE improved Na^+ migration kinetics and Na^+ deposition to form a stable and dendrite-free SEI. They also produced a $\text{Na}_3\text{V}_2(\text{PO}_4)_3/\text{A-FRGPE}/\text{Na}$ full cell, which showed a high initial capacity of 120 mAh g^{-1} at 1 C with 96.1% capacity retention after 1100 cycles [86]. In another study, Chen et al. prepared poly(ethylene glycol methyl ether methacrylate) (PEGMA)-based electrolytes on glass fiber by using in situ thermal curing. They used nonflammable triethyl phosphate as a plasticizer to improve flame retardancy and ionic conductivity, and the PEGMA-based electrolyte had a relatively high ionic conductivity of 0.91 mS cm^{-1} with a wide ESW of 4.8 V at room temperature [96]. Similarly, Zheng et al. synthesized a PMMA- and poly(trifluoroethyl methacrylate) (PFEMA)-based gel polymer electrolyte crosslinked with a series of methyl phosphonate containing monomers with varying flexible PEO chain lengths by in situ radical thermal polymerization. Optimized electrolytes showed a high ionic conductivity of $>1.4 \text{ mS cm}^{-1}$ with a wide ESW of $>5 \text{ V}$ at room temperature. According to their electrochemical performance results, a $\text{Na}_3\text{V}_2(\text{PO}_4)_3/\text{glass fiber supported copolymer gel electrolyte}/\text{Na}$ full cell showed a 90.7 mA h^{-1} capacity with an 85.6% capacity retention rate after 5000 cycles at 2 C [97].

Due to sustainability and environmental concerns, electrolytes are increasingly requiring biodegradable and environmentally friendly polymers, such as PVA, polylactic acid (PLA), polycaprolactone (PCL), and polysaccharides, including cellulose, cellulose derivatives, etc. Among these polymers, PCL is an important candidate for gel polymer electrolytes due to its low glass transition temperature ($-60 \text{ }^\circ\text{C}$) and melting point ($\sim 60 \text{ }^\circ\text{C}$). Sehwat et al. reported a gel electrolyte containing varying amounts of immobilized liquid electrolyte (1 M NaOTf/EC:PC 1:1 by volume) in the PCL polymer host structure.

A total of 80 wt.% liquid electrolyte containing a PCL-based gel electrolyte showed a high ionic conductivity of $\sim 1.3 \text{ mS cm}^{-1}$ at room temperature with a wide ESW of $\sim 4.3 \text{ V}$ [98]. Liu et al. reported bacterial cellulose-based gel polymer electrolytes (BCGE) for SIBs containing a $\text{Na}_{3.5}\text{Mn}_{0.5}\text{V}_{1.5}(\text{PO}_4)_3\text{@C}$ cathode and a Na anode. They prepared gel polymer electrolytes by simply immersing liquid electrolytes (1 M $\text{NaClO}_4/\text{EC}:\text{DEC}:\text{FEC}$, 95:95:10 by volume) into a commercial bacterial cellulose film. BCGE demonstrated a high ionic conductivity of 0.632 mS cm^{-1} at 20°C with an ESW up to $\sim 4.5 \text{ V}$, as well as better mechanical properties (such as higher tensile stress and strain) than commercial polyolefin-based membranes. A $\text{Na}_{3.5}\text{Mn}_{0.5}\text{V}_{1.5}(\text{PO}_4)_3\text{@C}/\text{BCGE}/\text{Na}$ full cell showed a high initial discharge capacity of 104.4 mAh g^{-1} at 2 C with 90.6% capacity retention after 1250 cycles [99]. In another study, Mittal et al. produced nanocellulose-based gel polymer electrolytes for $\text{Na}_2\text{Fe}_2(\text{SO}_4)_3/\text{Na}$ full cells. They fabricated gel electrolytes by encapsulating liquid electrolytes (1 M $\text{NaClO}_4/\text{EC}:\text{PC}$, 1:1 by volume) in cellulose nanocrystals (CNC)/cellulose nanofibers (CNF) cryogels. Due to the interconnected highly porous nanocellulose structure, nanocellulose-based gel polymer electrolytes showed a large amount of liquid electrolyte uptake (up to 4441%). CNC/CNF (50:50 by weight)-based electrolytes showed a high ionic conductivity of 2.32 mS cm^{-1} at room temperature with a wide ESW up to 4.7 V vs. Na/Na^+ [100]. Similarly, Chen et al. reported hydroxypropyl methylcellulose (HPMC)-based gel electrolytes with a high ionic conductivity of 3.3 mS cm^{-1} at room temperature, a high electrolyte uptake capacity ($\sim 1796\%$), and a wide ESW of 4.72 V vs. Na/Na^+ . They prepared gel polymer electrolytes by introducing different liquid electrolytes (1 M $\text{NaClO}_4/\text{DMC}:\text{PC}$, 1 M $\text{NaClO}_4/\text{DMC}$, and 1 M NaClO_4/PC) into HPMC-coated nonwoven fabrics and electrolyte uptake values for these mixtures were at 1796%, 252%, and 1432%, respectively. According to their post-mortem FTIR analysis, they proposed that PC was grafted on HPMC, the distance between HPMC polymer chains increased, and the hydrodynamic volume of polymer chains increased. They also emphasized that DMC in a binary solvent system acted similarly to a plasticizer and synergistic improvement was observed for polymer swelling based on electrolyte uptake [101]. Various quasi-solid-state electrolytes used in SIBs and their ionic conductivity values under certain temperatures can be seen in Table 2.

Table 2. Quasi-solid-state electrolytes used in SIBs.

Electrolyte Content	IC (mS cm^{-1})	T ($^\circ\text{C}$)	Ref.
PEO/ NaClO_4/PC	>1	25	[87]
PVDF-HFP/ $\text{NaClO}_4/\text{triglyme}$	2.54	25	[88]
PVDF-HFP/ $\text{NaClO}_4/\text{PC}:\text{FEC}$	0.42		[77]
PVDF-HFP/ $\text{PP}/\text{NaClO}_4/\text{EC}:\text{DMC}:\text{EMC}$	0.82	25	[90]
PVDF-HFP/ $\text{PP}/\text{NaClO}_4/\text{EC}:\text{DEC}:\text{FEC}$	1.38	25	[91]
PVDF-HFP/ $\text{SnO}_2/1\text{-}(4\text{-cyanophenyl})\text{guanidine}/\text{NaClO}_4/\text{EC}:\text{DMC}:\text{FEC}$	0.232	70	[93]
PVDF-HFP/ $\text{PMMA}/\text{TPU}-\text{Na}_3\text{Zr}_2\text{Si}_2\text{PO}_{12}, \text{NaClO}_4/\text{EC}:\text{DMC}$	2.83	25	[83]
PVDF-HFP/ $\text{SiO}_2/\text{NaBF}_4/\text{tetraglyme}$	0.9	25	[79]
PEGMA/glass fiber/triethyl phosphate	0.91	25	[96]
PCL/ $\text{NaOTf}/\text{EC}:\text{PC}$	~ 1.3	25	[98]
BCGE/ $\text{NaClO}_4/\text{EC}:\text{DEC}:\text{FEC}$	0.632	20	[99]
CNC/CNF/ $\text{NaClO}_4/\text{EC}:\text{PC}$	2.32	25	[100]
HPMC/ NaClO_4/PC	3.3	25	[101]

IC: Ionic conductivity; T: temperature.

4. Solid Electrolytes

Solid-state electrolytes (SE) are solid ionic conductors used for secondary batteries. They are an important alternative as a substitute for liquid and quasi-solid electrolytes. As mentioned above, liquid electrolytes have some drawbacks, such as flammability and explosion risk. This risk is more serious in the case of SIBs because of their high reactivity under oxygen and moisture exposure. A solid electrolyte is located between the anode and the cathode, instead of between a liquid electrolyte and the separator. In addition to ion

transfer, solid electrolytes function as separators to prevent direct contact and short circuits between positive and negative electrodes. Since no liquid phase is found, there is no leakage, flammability, or explosion risk, nor are there ionic conductivity problems caused by liquid viscosity, ion–solvent and ion–ion interactions, the side-reaction rate, or SEI/CEI formation. Higher thermal, dimensional, and mechanical stability, a wide ESW, and compatibility of SEs with the anode and cathode lead to higher electrochemical stability and energy density. The use of high-voltage cathodes and Na metal anodes is also made possible by the incorporation of SEs, which further boosts the energy density of all-solid-state batteries. In addition to these, the all solid-state three-component cell structure is advantageous in terms of battery packaging; however, its development is severely constrained by the high interface resistance and dendritic growth between sodium and solid electrolytes, particularly at high current densities. Additionally, low ionic conductivity at ambient temperatures can be given as another drawback of solid electrolytes. All solid-state (ASS) batteries function as liquid electrolyte-containing batteries. During charging/discharging, Na-ions move from the cathode/anode through an ionic conductive solid electrolyte into the anode/cathode, and electron flow occurs through an external circuit [10,102,103]. SEs can be classified as either inorganic solid electrolytes (ISE) or polymer solid electrolytes (PSE).

4.1. Inorganic Solid Electrolytes

ISEs are electrolytes with high thermal and mechanical stability and moderate ionic conductivity at room temperature. Since ISEs are single-ion conductors, they do not suffer from concentration polarization. Additionally, their brittle nature and high elastic modulus make them important alternatives for rigid batteries that could adapt to a wide range of conditions. Furthermore, high mechanical properties can prevent dendrite formation to some level. Since dendrite formation is greatly influenced by the interface resistance, relative density, and electronic conductivity of the electrolytes, the limited chemical/electrochemical stability of SEs may lead to unavoidable side reactions that result in high interfacial impedance. Na- β / β'' -alumina, NAtrium Super Ionic CONductor (NASICON), and sulfide-based electrolytes are the most common subclasses of inorganic SEs [104,105].

The most promising material class for Na-ion batteries is NASICONs ($\text{Na}_{1+x}\text{M}_2\text{Si}_x\text{P}_{3-x}\text{O}_{12}$ ($0 \leq x \leq 3$, M = metals or mixture of metals)), which was firstly developed by Goodenough and Hong in 1976 [106]. Since NASICONs cover more than half of the ISEs in the literature, this review outlines recent developments in this area. NASICONs are oxides that stand out due to their ionic conductivity ($>1 \text{ mS cm}^{-1}$); high dimensional, thermal, and chemical/electrochemical stability; and good chemical/electrochemical compatibility with electrode materials. Additionally, they show high air and moisture stability. However, NASICONs have a few drawbacks, including high interfacial resistance and slow ion transfer between NASICON and cathode. As shown in the literature, various factors have a direct effect on the ionic conductivity and the charge transfer properties of NASICONs, such as the structure of the 3D conduction network, density, the stoichiometric ratio of the components, Na^+ concentration, $\text{Na}^+\text{-Na}^+$ Coulombic repulsion, Si/P ratio, phase purity, crystallite type (rhombohedral and monoclinic), crystallite size, distortions in the structure, lattice parameters, unit cell volume, bottleneck size for ion transfer, grain size, and grain boundary properties (interface between grains, ion migration barriers, secondary phases, diffusion-assisting defects in the secondary phase, microstructural features, etc.). Since the synthesis of NASICONs generally takes place at elevated temperatures, Na and P volatilization can yield the formation of the ZrO_2 phase between the grains that is known to prevent ion conduction. Excess Na and P into the precursors were reported to be effective in solving this problem. A precursor structure was also reported to be a significant property of NASICONs. Because of these, recent efforts have mostly focused on designing and developing NASICON-based materials that improve the ion conductivity, and the reduced electrolyte/electrode interface that can function at room temperature, by increasing the Na

concentration in the structure, density, and bottleneck size of the structure, and reducing the grain boundary resistance eliminating/minimizing the secondary phases [105,107–113].

As shown in Figure 5, numerous studies have been performed to design and develop NASICON-type electrolytes with improved performance, primarily via structural modification (addition or substitution of dopants) [108] and grain boundary modification [114]. Some modifications were also performed to obtain NASICON structures with better performance at low temperatures with simpler processes such as ultrafast sintering [115] and high energy ball-milling [116]. Other approaches are also conducted, such as interfacial compatibility modifications [117].

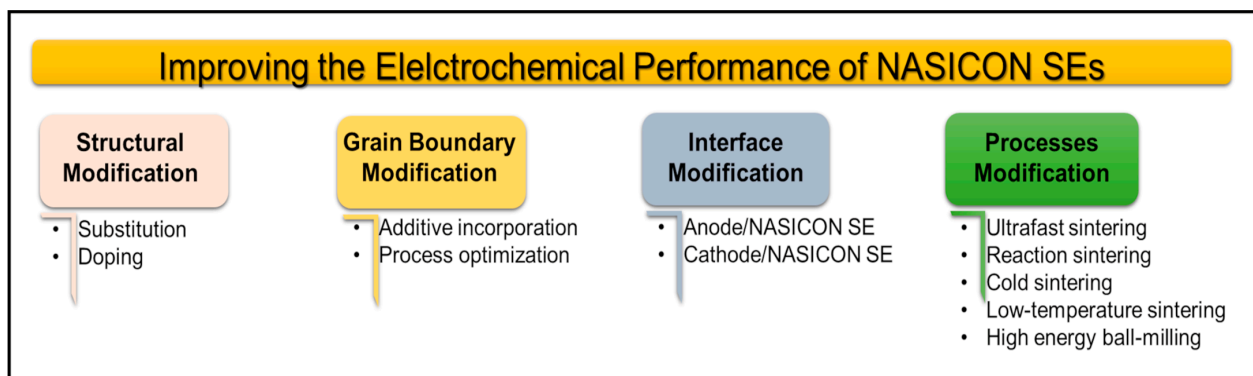


Figure 5. Recent studies for improving the electrochemical performance of NASICON SEs.

4.1.1. Structural Modification

Structural modification of NASICON is performed by the chemical synthesis process by addition or substitution of dopants. In the literature on NASICON, both doping and substitution are commonly used terminology. Generally, in chemical substitution, the chemical structure of the material is modified by the incorporation of new elements on certain atomic positions and changing the ratio of components. In substitution studies of NASICON, iso/heterovalent structures used at various ratios and properties, including unit cell properties, a 3D conductive network, a bottleneck structure, density, Si/P ratio, Na⁺ concentration, ion transfer rate, and ionic conductivity, were reported to change. On the other side, in doping, the element is added to the precursor mixture in relatively small amounts. Although the structure does not have to necessarily change, as in substitution, change is observed in certain properties of the final product. It should also be highlighted that different impurities with different phase structures can form because of dopant concentration and structure, and differences in ionic radius and charge. Due to these differences, dopants can precipitate and incorporate into the secondary phases that are found between grain boundaries. Since the amount of the elements incorporated into the structure is relatively lower than the amount in other components, the two processes can be described as the addition or substitution of dopants. In these reactions, the ratio of the material was reported to be significant in terms of the phase transition from monoclinic to rhombohedral, and the decomposition of the main phase into different phases. Furthermore, chemical composition, content, and morphology of the secondary phase(s) were reported to affect Si/P ratio, the activation energy for ion transfer, and total ionic conductivity [108,118].

Divalent [108,109,118–120], trivalent [109,120,121], tetravalent, and pentavalent dopants [122,123] were reported in the literature for the structural modification. The addition or substitution of divalent ions is one of the first approaches for the structural modification of NASICONs because of their similar ionic radius to Zr⁴⁺. Mg²⁺ [108], Ni²⁺ [108,120], Ca²⁺ [119], Zn²⁺ [120,122], Co²⁺ [120], and Cu²⁺ [124] were the divalent ions used to increase the performance of the electrolytes. Samiee et al. used Mg²⁺ and Ni²⁺ divalent dopants to modify the ionic conductivity of Na_{1+x}Zr₂Si_xP_{3-x}O₁₂ and to observe the dopant effect on solubility, segregation, secondary phase formation, and ionic

conductivity by experimental and computational approaches. As reported in the study, Mg^{2+} was found to show limited solubility and heterogenous distribution in NASICON at all concentrations and preferably dissolved in Si-poor secondary phases around grain boundaries. Ni^{2+} also showed heterogeneous distribution in NASICON. The highest ionic conductivity was 2.05 mS cm^{-1} at 0.128% Mg doping. An increase in Mg content led to a decrease in ionic conductivity caused by the formation of a Na_3PO_4 -based secondary phase. Parallel with that result, grain boundary conductivity showed maxima with minimum activation energy at 0.128% Mg and decreases at higher concentrations. Total ionic conductivities of Mg and Ni-doped electrolytes were reported as 2.7 mS cm^{-1} and 2.1 mS cm^{-1} , respectively [108]. In another study, Ca^{2+} substitution was carried out to synthesize $\text{Na}_{3+2x}\text{Zr}_{2-x}\text{Ca}_x\text{Si}_2\text{PO}_{12}$. The x value varied between 0 and 0.25. Ca^{2+} was reported to be partially substituted for Zr^{4+} and sodium-ion conductivity was $1.67 \times 10^{-3} \text{ S cm}^{-1}$ at the doping value of 5 at% [119]. Zhang et al. used Mg^{2+} for the modification of the structure, and $\text{Na}_{3+2x}\text{Zr}_{2-x}\text{Mg}_x\text{Si}_2\text{PO}_{12}$ ($x = 0, 0.05, 0.10, 0.15, 0.20$) was synthesized. The ionic conductivity at $x = 0.25$ was reported to be the highest among other samples, with a value of 3.54 mS cm^{-1} at room temperature. This high performance was reported to be caused by the precipitation of Mg in the grain boundary. The substitution of Mg was not observed and, in the ionic conductor phase, NaMgPO_4 was also formed during the synthesis [118]. Yang et al. modified $\text{Na}_3\text{Zr}_2\text{Si}_2\text{PO}_{12}$ with Zn. $\text{Na}_{3.2+2x}\text{Zr}_{2-x}\text{Zn}_x\text{Si}_{2.2}\text{P}_{0.8}\text{O}_{12}$ was synthesized with a ratio of $x = 0-0.15$. The ionic conductivity was determined as $5.27 \times 10^{-3} \text{ S cm}^{-1}$ for $x = 0.1$. This high ionic conductivity was reported to be caused by increasing the size of bottlenecks in the conducting network because of the substitution of Zr^{4+} by Zn^{2+} . This was one of the highest ionic conductivity values reported recently [125]. In a recent study by Luo et al., Co, Fe, and Ni, were used at different ratios of $x = 0.1, 0.2, \text{ and } 0.3$, respectively, for the structural modification of NASICON. In this work, both ionic and electronic conductivity were investigated. An amount of 0.1 Co-NASICON had the highest electronic conductivity of $5.03 \times 10^{-3} \text{ mS cm}^{-1}$. An increase in the Co ratio led to a decrease in electronic conductivity that was attributed to a higher impurity ratio. The highest ionic conductivity was obtained as 0.558 mS cm^{-1} for a Ni doped sample for $x = 0.1$ [126].

In addition to divalent ions, trivalent ions were also reported in the literature, including La^{3+} [127,128], Yb^{3+} [113], Sc^{3+} [113,129,130] Pr^{3+} , Lu^{3+} , Eu^{3+} [121], and Nd^{3+} [128]. In these studies, the main intention was to increase the channel size for Na^+ transport by using ions with a higher ionic radius and Coulombic repulsion between Na ions to increase the density and produce more interstitial Na^+ . Zhang et al. synthesized $\text{Na}_{3+x}\text{Zr}_{2-x}\text{La}_x\text{Si}_2\text{PO}_{12}$ by using different ratios of La^{3+} ($x = 0.05-0.40$). Although the aim of the study was to substitute the Zr^{4+} site for La^{3+} , full substitution was not achieved. In addition to the NASICON phase, based on the x value, the formation of other phases was observed, such as $\text{Na}_3\text{La}(\text{PO}_4)_2$, La_2O_3 , and LaPO_4 . These phases were reported to modify the Na^+ ion concentration, relative density, and grain boundary structure, all of which led to an increase in the total conductivity of the electrolyte system. The total ionic conductivity was reported to be affected by x and the highest ionic conductivity, 3.4 mS cm^{-1} , was observed at $x = 0.30$. It was also noted that the increase in bulk conductivity was relatively lower than the increase in the conductivity of the grain boundary and a consistent increase was observed between density and total conductivity [127]. Wang et al. used Pr^{3+} , Eu^{3+} , and Lu^{3+} to enhance the bottleneck size and ionic conductivity and decrease the electronic conductivity and dendrite formation by considering a higher ionic radius and lower electronegativity of dopants compared to Zr. The ionic conductivity of the $\text{Na}_{3+x}\text{Zr}_{2-x}\text{Pr}_x\text{Si}_2\text{PO}_{12}$ samples were reported as 0.497, 1.27, and 0.966 mS cm^{-1} for $x = 0.1, 0.3, \text{ and } 0.4$, respectively. $\text{Na}_{3+x}\text{Zr}_{2-x}\text{Eu}_x\text{Si}_2\text{PO}_{12}$ samples showed an ionic conductivity of 0.403, 0.659, 1.08, and 0.562 mS cm^{-1} when $x = 0.1, 0.2, 0.3, \text{ and } 0.4$ respectively. The ionic conductivity performances for Lu^{3+} doped samples were 0.37, 0.527, 0.831, and 0.684 mS cm^{-1} for $x = 0.1, 0.2, 0.3, \text{ and } 0.4$, respectively. As reported in the study, Lu^{3+} doped samples showed smaller grain sizes that led to increased surface area and higher grain boundary

impedance. $\text{Na}_{3.3}\text{Zr}_{1.7}\text{Pr}_{0.3}\text{Si}_2\text{PO}_{12}$, $\text{Na}_{3.4}\text{Zr}_{1.6}\text{Eu}_{0.3}\text{Si}_2\text{PO}_{12}$, and $\text{Na}_{3.3}\text{Zr}_{1.7}\text{Lu}_{0.3}\text{Si}_2\text{PO}_{12}$ were reported to have relative density values of 94.2%, 94.5%, and 92.3%, respectively. Because of its high density and lack of a ZrO_2 phase, Pr^{3+} $x = 0.3$ had the highest grain boundary conductivity [121].

Although there are not as many studies on them compared to those on divalent or trivalent ion doping, tetravalent and pentavalent dopants [105] are also reported in the literature. Chen et al. used Nb^{5+} , Ti^{4+} , Y^{3+} , and Zn^{2+} ions to investigate the effects of the valence state of dopants on the performance of $\text{Na}_3\text{Zr}_2\text{Si}_2\text{PO}_{12}$. For this aim $\text{Na}_3\text{Zr}_{2-x}\text{Nb}_{0.8x}\text{Si}_2\text{PO}_{12}$, $\text{Na}_3\text{Zr}_{2-x}\text{Ti}_x\text{Si}_2\text{PO}_{12}$, $\text{Na}_3\text{Zr}_{2-x}\text{Y}_x\text{Si}_2\text{PO}_{12-0.5x}$, and $\text{Na}_3\text{Zr}_{2-x}\text{Zn}_x\text{Si}_2\text{PO}_{12-x}$ solid electrodes were prepared with $x = 0.1-0.4$. The bulk conductivity of the NASICONs was reported to be $\text{Zn}^{2+} > \text{Y}^{3+} > \text{Ti}^{4+} > \text{Nb}^{5+}$. While divalent and trivalent dopants showed an increase, tetravalent dopants showed stable performance. On the other hand, pentavalent dopants showed a decrease because of a relatively higher activation energy. The highest total ionic conductivity and the bulk conductivity of $\text{Na}_3\text{Zr}_{1.8}\text{Zn}_{0.2}\text{Si}_2\text{PO}_{11.8}$ were determined as 1.44 and 3.41 mS cm^{-1} , respectively. As concluded in the studies, the bulk ionic conductivity increased parallel with the decrement in the valence state of the dopant due to less electrostatic interactions and high Na^+ transfer performance [122]. However, it should also be underlined that one of the highest ionic conductivity values was reported by doping NASICON with a pentavalent Nb^{5+} ion. $\text{Na}_{3.4-x}\text{Zr}_{2-x}\text{Nb}_x\text{Si}_{2.4}\text{P}_{0.6}\text{O}_{12}$ was synthesized and $x = 0.1-0.4$. The highest ionic conductivity was reported for $x = 0.1$ as 5.51 mS cm^{-1} . That high value was probably caused by the process: unlike in solid-state synthesis, solution-based and double-step calcination/sintering processes led to the formation of a highly conducting phase with low grain boundary and bulk impedance [123].

In addition to doping single ions, co-doping was also reported in the literature. Co-doping is an alternative method for structural modification and two different ions were used to tune the properties of NASICON. Pal et al. modified $\text{Na}_3\text{Zr}_2\text{Si}_2\text{PO}_{12}$ by using Sc^{3+} and Yb^{3+} , and $\text{Na}_{3.33}\text{Zr}_{1.67}\text{Sc}_{0.33}\text{Si}_2\text{PO}_{12}$ and $\text{Na}_{3.33}\text{Zr}_{1.67}\text{Sc}_{0.29}\text{Yb}_{0.04}\text{Si}_2\text{PO}_{12}$ were synthesized. In this work, co-doping and the effects of precursor crystal structure on the properties of electrolytes were investigated. Two different zirconia precursors were used as the cubic (c)-phase and the monolithic (m)-phase. NASICON was synthesized by m-phase and Sc^{3+} doped and $\text{Sc}^{3+}/\text{Yb}^{3+}$ co-doped samples were synthesized by c-phase to prevent the formation of the secondary impurity phase m-ZrO. While NASICON was observed to have a little amount of m-ZrO² phase, doped and co-doped samples showed pure phase without ZrO² impurity. In this way, it was shown that c-ZrO₂ was effective in preventing secondary phase formation. Although Sc^{3+} has a higher ionic size compared to Zr^{4+} , construction was observed after Sc^{3+} substitution. Additionally, co-doped samples showed lower density compared to the Sc^{3+} doped sample. This was assumed to be caused by the larger ionic size of Yb. Na^+ conductivities of the samples were 0.61, 0.96, and 1.62 mS cm^{-1} for the NASICON, Sc^{3+} doped, and $\text{Sc}^{3+}/\text{Yb}^{3+}$ co-doped samples, respectively [113].

Thirupathi and Omar used Sc^{3+} and Ce^{4+} as co-dopants for NASICON-type $\text{Na}_3\text{Zr}_2\text{Si}_2\text{PO}_{12}$. The Sc^{3+} ratio was 16.5 mol% and the Ce^{4+} ratio varied between 0 and 5 mol%. While m-ZrO₂ was used for $\text{Na}_3\text{Zr}_2\text{Si}_2\text{PO}_{12}$ synthesis, c-ZrO₂ was used for co-doping. A m-ZrO₂ secondary phase was observed for the bare samples, but did not exist in co-doped samples. At higher Ce^{4+} rates of more than 1 mol%, different secondary phases occurred, which was due to the low solubility of Ce^{4+} in NASICON. While NASICON had an ionic conductivity of 0.61 mS cm^{-1} , the sample that had 16.5 mol% Sc^{3+} substitution led to an ionic conductivity of 0.96 mS cm^{-1} . An amount of 1 mol% Ce^{4+} substitution for Zr^{4+} led to the increase in ionic conductivity to 2.44 mS cm^{-1} at 25 °C, which was assumed to be caused by an increase in bottleneck triangular passage [131]. Ran et al. studied the performance of $\text{Sc}^{3+}/\text{Ge}^{4+}$ co-dopants on the NASICON electrolytes. The contribution of each dopant was reported to be slightly different. While Sc^{3+} was used to tune the stabilization of the rhombohedral phase and increase the Na^+ concentration at room temperature, Ge^{4+} was used to lower the phase transition range from monoclinic to rhombohedral. Samples showed a higher density after doping. While NASICON had an ionic conductivity value

of 0.39 mS cm^{-1} , co-doped samples with $x = 0.1, 0.125, 0.15$ had values of 1.61, 4.64, and 1.89 mS cm^{-1} at 30°C , respectively. The increase was reported to be based on an increased ratio of the rhombohedral phase. The decrease in conductivity was attributed to irregular crack formation at a high dopant ratio. Cracks were reported to prevent ion transfer [132].

4.1.2. Grain Boundary Modification

Grain boundary modification is another way to increase the electrochemical performance of NASICONs. Grains consist of crystallites with a preferred orientation. Since grains have different orientations, they are separated into regions by boundaries. A grain boundary can be described as the interface between neighboring crystallites due to the polycrystalline structure of a material. Since the properties of the material are different between the grain and in the boundary, grain boundaries can be accepted as planar defects. They function as the pathways for ion transfer between the grains, and their properties are critical in terms of electrochemical performance. Since they show high resistance to ion flow compared to bulk material, they have a direct effect on conductivity. The presence of impurities and secondary phases in the grain boundary can affect the chemical reactivity and may lead to side reactions, such as the formation of a passivation layer or the decomposition of the solid electrolyte. In the case of an optimum grain boundary, defects including vacancies, dislocations, and pores will not coexist, and electrochemical stability is increased. Grain boundary size, morphology, density, and ionic conductivity are affected by the type and ratio of the precursors, the synthesis method, the sintering conditions, grain size, the existence of secondary phases, impurities, the presence and concentration of additives [114], and so on. Since there are various factors that govern the grain boundary, careful control of grain boundary composition, structure, and morphology is critical in terms of improving cell performance. Strategies including controlling the grain boundary composition, structure, and morphology by using additives can be a feasible way of increasing the electrochemical performance. The additives known as sintering aids are the most common materials used for the modification of grain boundary properties, the density of the materials, and process conditions such as sintering temperature. Sintering aids/additives can promote densification during sintering by facilitating the formation of liquid phases and reducing the sintering temperature, controlling grain size and morphology, and improving ionic conductivity and the stability of the material by preventing the formation of undesirable phases. In other words, additives play an important role in tuning the properties of NASICON solid electrolytes, and their careful selection and optimization can lead to improved processing and higher performance in solid-state batteries [114]. $\text{Na}_2\text{B}_4\text{O}_7$ [133], Na_3BO_3 [134], NaF [135], antimony–tin oxide [136], $(\text{ZnO})_2-(\text{B}_2\text{O}_3)_3$ [137], and MgF_2 [138] have been used to modify the properties of the grain boundary.

Miao et al. used Bi_2O_3 to modify the grain boundary and ionic conductivity of $\text{Na}_{3.1}\text{Y}_{0.1}\text{Zr}_{1.9}\text{Si}_2\text{PO}_{12}$ and to prevent ZrO_2 formation. The amount of Bi_2O_3 was between 0 and 2 wt.%. The highest ionic conductivity was obtained at 1 wt.% Bi_2O_3 concentration with a value of 1.21 mS cm^{-1} and an ESW of 4.8 V. These outcomes were attributed to the transformation of porous morphology into a denser, more crystalline, and connected grain network with a uniform particle distribution after the addition of Bi_2O_3 . The main reason behind the morphology change was given as the low melting point of the additive and its liquid phase at high temperatures. Additionally, it was underlined that an excess amount of additive might deteriorate the morphology, density, and ionic conductivity due to the evaporation [114]. Oh et al. used different amounts (2.5–7.5 wt.%) of Na_2SiO_3 additive to modify the properties of $\text{Na}_3\text{Zr}_2\text{Si}_2\text{PO}_{12}$. The highest ionic conductivity, 1.45 mS cm^{-1} , was observed for the sample with 5 wt.% Na_2SiO_3 additive. Grain boundary conductivity was also improved due to the higher density. As shown by XRD results, Na_2SiO_3 led to a change in stoichiometry that resulted in a higher bottleneck size and lower activation energy. This process is of significance not only because of its contribution to ionic conductivity but also for its relatively lower process temperature [139]. Noi et al. modified the grain boundary and bulk properties of $\text{Na}_3\text{Zr}_2\text{Si}_2\text{PO}_{12}$ by using Na_3BO_3 (0–9.1 wt.%)

with a liquid-phase sintering process. An optimum amount of Na_3BO_3 was reported to be effective in terms of decreasing the sintering temperature, preventing impurities, lowering the activation energy, increasing ionic conductivity, and improving the grain boundary properties with a uniform and bonded grain network. An amount of 4.8 wt.% Na_3BO_3 was found as the best concentration for the highest ionic conductivity (1 mS cm^{-1}) [134]. In a recent study, Zhou et al. used MgF_2 additive (0–3 wt.%) to observe the change in the bulk ionic and grain boundary conductivity of NASICON ($\text{Na}_{3.4}\text{Zr}_2\text{Si}_{2.4}\text{P}_{0.6}\text{O}_{12}$). As reported in the study, average grain size and density were reported to increase, and a rhombohedral crystal structure was obtained with no obvious structural modification. The bulk and grain boundary conductivity values of NASICON were determined as 2.58 and 1.99 mS cm^{-1} , respectively. In the case of 1 wt.% MgF_2 additive, these values were 3.3 and 5.28 mS cm^{-1} , respectively with a total ionic conductivity of 2.03 mS cm^{-1} . However, at higher concentrations of MgF_2 , an excess amount of material led to the formation of impurities and a decrease in ionic conductivity. Optimized MgF_2 concentration resulted in an increase in not only grain size but also grain boundary conductivity, which is critical for the performance of the electrolytes [138].

4.1.3. Modification of Interface Properties

The modification of interface properties has been studied in recent years [30]. As shown in the previous sections, the first aim was to increase the ionic conductivity and electrochemical performance of the NASICONs by the substitution of dopants or the incorporation of additives. Although these are necessary for obtaining stable, high-performance solid electrolytes, electrode/electrolyte interface properties must be considered in terms of energy storage applications. The interface is the point or region where two different phases interact. For all solid-state batteries (ASSBs), the electrode/electrolyte interface is the point/region on which ion transfer occurs, so its properties are of vital importance. Interfacial compatibility is an indication of how two systems function together and how compatible they are. Solid electrodes indicate how electrodes and electrolytes work together, without alteration, by surface interaction alone. Unlike for liquid electrolytes, for SEs, total electrolyte contact is limited and occurs only from the electrode surfaces, and proper contact is required for efficient ion transfer. In the case of poor contact between the electrode and the electrolyte, the interface functions as a barrier. High interfacial impedance, polarization, and poor rate capacity can occur, all of which can lead to a shorter battery life. Since NASICONs are ceramics and consist of grains with polycrystalline structures, each grain has a different size and hardness, and different surface properties that can also lead to discontinuity in the morphology and in many properties from charge carrier concentration to interfacial resistance. Even if they are well packed and/or the surface is polished, there might be topological differences at the nano- or micro-scale. This difference leads to the formation of a rough surface, insufficient contact, and low ion transfer. In addition, anodes, cathodes, and electrolytes have different chemical and morphological structures, and ion transfer between different phases might be challenging without good interfacial compatibility. Another point that should be considered is the homogeneous ion deposition at the interface of the electrode/electrolyte. Inhomogeneous ion deposition at the interface during electrochemical cycling can lead to dendrite formation and growth that is critical for the electrochemical, thermal, and dimensional stability and the safety of the battery. Therefore, sufficient contact, good electrochemical compatibility, and high ionic conductivity should be considered for the evaluation of the interface [30,118,140].

As mentioned above, poor physical contact is the most serious problem for NASICON/cathode interfaces. This leads to high interfacial resistance, low ion transfer, and chemical and electrochemical instability throughout the interfaces. Solutions for this poor contact can be performed by modifying the NASICON/cathode interface. Some of these modifications include wetting other types of electrolytes [118,119,132,141,142], mixing the cathode with electrolyte, the deposition of the cathode on the electrolyte [143], the preparation of layered NASICONs with unique morphology and chemical composition [119], a

polymeric layer coating [125], the impregnation of molten Na or other additives [119], and sputtering the thin platinum layer on NASICON electrolyte [117].

One of the easiest ways of increasing compatibility between two phases can be carried out by the addition of another ion conductive phase that helps to increase the ion transfer between the cathode and a SE. The incorporation of LEs [121,132,141] or ILs [127] can be a direct way of reducing the interfacial resistance between two interfaces by wetting. Another approach is the coating of the SE surface. Yang et al. synthesized a $\text{Na}_{3.4}\text{Zr}_{1.9}\text{Zn}_{0.1}\text{Si}_{2.2}\text{P}_{0.8}\text{O}_{12}$ solid electrolyte with an ionic conductivity of 5.27 mS cm^{-1} . To tune the interfacial resistance between the cathode and a NASICON-SE, an air-stable polydopamine (PDA) layer with a thickness of 34 nm was coated on the SE pellet by in situ polymerization. Since PDA has adhesive properties, it leads to the formation of a homogeneous nano indentation layer on the SE. This morphology was reported to be useful not only because it increased the SE/cathode physical contact but also because it compensated for the volumetric changes during charging/discharging. $\text{FeS}_2/\text{PDA-Na}_{3.4}\text{Zr}_{1.9}\text{Zn}_{0.1}\text{Si}_{2.2}\text{P}_{0.8}\text{O}_{12}/\text{Na}$ cells showed an enhanced cycling performance of 236.5 mAh g^{-1} (100 cycles, 0.1 C rate) and 133.1 mAh g^{-1} (300 cycles, 0.5 C) [125]. Kehne et al. used the pulsed laser deposition (PLD) method to grow a Na_xCoO_2 thin film cathode layer on the NASICON electrolyte. With $\text{Na}_x\text{CoO}_2/\text{Nasicon}/\text{Na}$, the cell had a specific capacity of 160 mAh g^{-1} at 6 C. The thickness of the cathode was $780 \text{ nm} \pm 40 \text{ nm}$ [143]. Additionally, special structures can be prepared for increased interaction. Lu et al. developed trilayer monolithic NASICON-based electrolytes, as shown in Figure 6a. Porous top and bottom layers were impregnated with SnCl_4 solution to coat the porous surface with SnO_2 particles. After the SnO_2 synthesis sample was infiltrated by the molten sodium metal to fill the pores in the electrode, the interfacial resistance was decreased and the compatibility of the SE with the electrodes was increased. The resistance of the cell was more than $10,000 \Omega \text{ cm}^2$. After the modification, it was decreased to $175 \Omega \text{ cm}^2$ by a 3D trilayer monolithic morphology that had increased surface area and better electrode contact compared to the bare electrode. A $\text{Na}_3\text{V}_2(\text{PO}_4)_3/\text{SE}/\text{Na}$ cell was prepared, and the cathode was wetted by the polymer electrolyte solution. The capacity of the cell was 94.9 mAh g^{-1} (1 C, 450 cycles) and 80.5 mAh g^{-1} at 4 C under RT conditions [119]. Zhang et al. synthesized $\text{Na}_{3.3}\text{Zr}_{1.85}\text{Mg}_{0.15}\text{Si}_2\text{PO}_{12}$ (NZSPMg0.15) that showed an ionic conductivity of around 3.54 mS cm^{-1} at 25°C . To achieve higher ionic conductivity, IL was added to the cathode and carbon nanotubes (CNTs) were incorporated to the anode by melt mixing. In the study, NASICON was coated on PE separators and a full cell showed a discharge capacity of 2.42 Ah at 1 C [101].

Na metal anodes and NASICON SEs have been widely studied as promising components in all-solid-state batteries because of their high theoretical specific capacity of 1166 mAh g^{-1} , and their negative electrical potential of $\sim 2.714 \text{ V vs. Na/Na}^+$. However, some of the major challenges involving them are the formation of a solid electrolyte interphase layer and dendrites, which can cause problems such as an increase in interfacial resistance and volumetric expansion, and a decline in Coulombic efficiency, cycling stability, and ionic conductivity. As previously mentioned, the greatest challenge is insufficient contact. This challenge can be solved with modifications to the NASICON/anode interface. Such modifications can be performed by uniaxial compression [144], wetting by liquid electrolytes, melting Na metal during cell preparation, mixing with electrically conductive fillers such as CNTs [118,142], coating the NASICON surface [142], and forming a multifunctional porous heterogeneous interface layer on the electrode [102]. Uchida et al. reported lower interfacial resistance following compression molding under 30 MPa up to $14 \Omega \text{ cm}^2$ (RT), mainly because of improved interfacial contact [144]. Sampatkumar et al. performed Au sputter coating on both sides of a $\text{Na}_3\text{Zr}_2\text{Si}_2\text{PO}_{12}$ electrolyte to increase the interaction between a Na metal anode and SE. The interfacial charge transfer resistance between the Na metal and the SE changed from $2708 \Omega \text{ cm}^2$ to $146 \Omega \text{ cm}^2$ after Au coating, which was caused by a Au/Na alloy formed while molten Na was poured on the SE. Additionally, increased wetting and physical contact between the two phases led to stable Na ion transfer and homogeneous Na stripping/plating with relatively lower polarization,

both of which suppressed dendrite growth (Figure 6b). To analyze the cell performance of a Au-coated SE, a cell was prepared by using a NA metal anode, an NFP cathode, a polymeric separator, and an LE. The aim of using the separator and the LE was to lower the cathode/SE interfacial resistance. The cell was (Na/Au-NZSP/LE-PP-NFP). The discharge capacity of the cell was determined around 90, 60, and 40 mAhg⁻¹ under current densities of 50, 100, and 150 $\mu\text{Ah cm}^{-2}$, respectively [142].

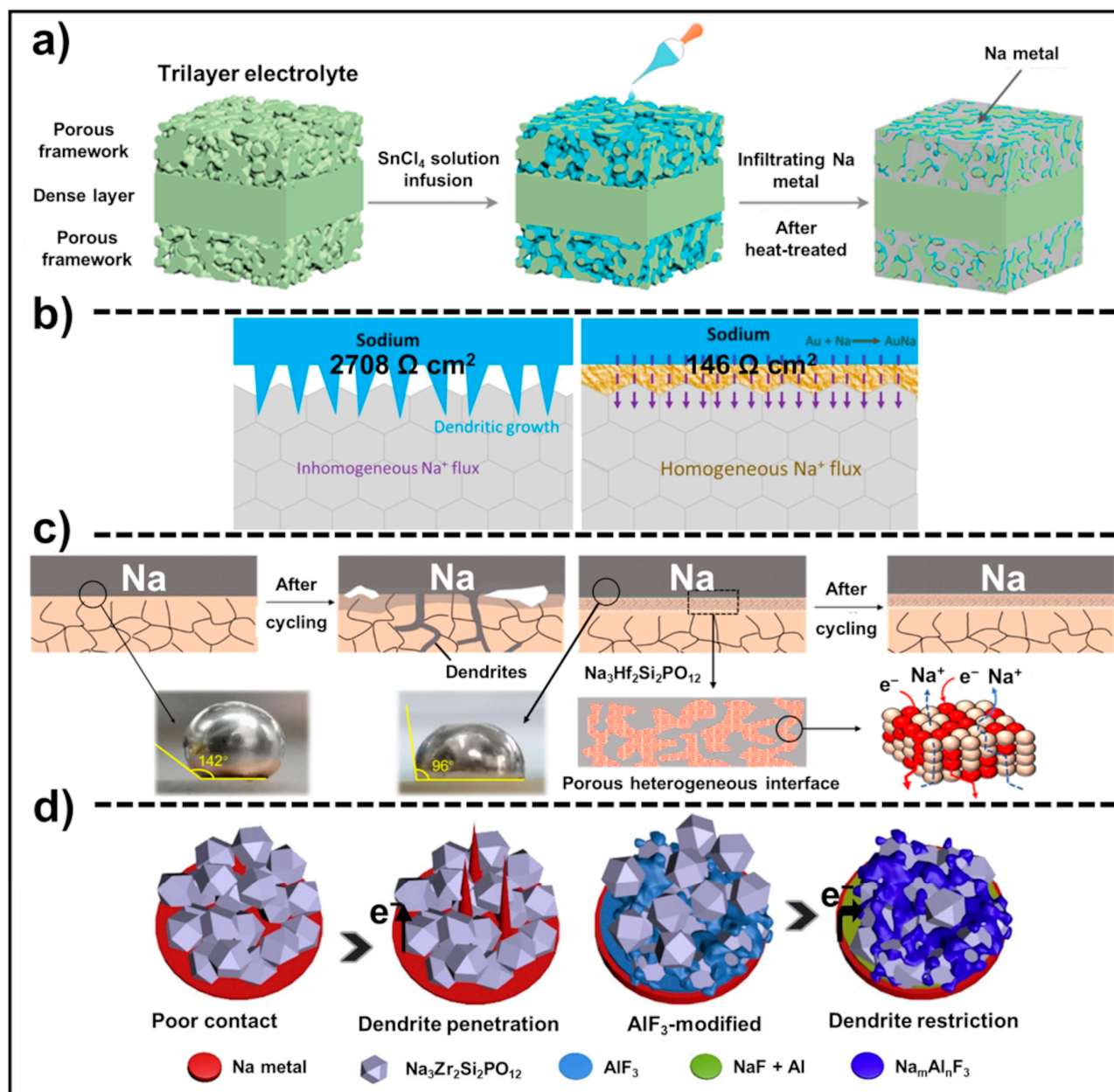


Figure 6. (a) Illustration of trilayer NZSP solid-state electrolyte production route. Reproduced with the permission of reference [119]. (b) Schematic illustration of improving the wettability of electrolyte and areal conductance by Au coating. Reproduced with the permission of reference [142]. (c) Cycling illustration of the $\text{Na}_3\text{Hf}_2\text{Si}_2\text{PO}_{12}$ solid electrolyte with/without a porous heterogeneous interface and corresponding wettability behavior against molten Na. Reproduced with the permission of reference [102]. (d) Schematic representation of dendrite formation during the cycling process and its restriction by AlF_3 coating. Reproduced with the permission of reference [145].

Cai et al. synthesized a NASICON type electrolyte, $\text{Na}_3\text{Hf}_2\text{Si}_2\text{PO}_{12}$, and the surface of the electrolyte was modified to obtain a multifunctional porous heterogeneous interface of $\text{NiO}/\text{Na}_3\text{Hf}_2\text{Si}_2\text{PO}_{12}$ (PHI@NHSP) with a thickness of 6 μm and a porosity of ~45%. The Na/PHI@NHSP/ $\text{Na}_3\text{V}_2(\text{PO}_4)_3$ full cell showed discharge capacities of 100.5, 100.3, 99.2, 98.7, and 95.8 mAh g^{-1} at 0.5, 1, 1.5, 2, and 3 C, respectively. This was attributed to the homogeneous dispersion of NiO and its positive effects on electron transport and interfacial conductance. Additionally, a higher, and more homogeneous, space charge distribution was obtained at the interface. It was also shown that PHI@NHSP showed a lower contact angle with molten Na and better wettability compared to NHSP electrolytes (Figure 6c) [102]. Similarly, Miao et al., coated a NASICON surface with AlF_3 to form a buffer layer to prevent the Na dendrite growth. Na/SSE interfacial physical contact was shown to increase significantly, resulting in higher critical current density with low dendrite growth (Figure 6d) [145].

4.1.4. Process Modification

The process modification of NASICON has gained importance not only by increasing material performance but also by reducing production costs. It is known that a high sintering temperature is required for increasing the density of the material, which leads to high energy consumption. Additionally, at high temperatures, sodium and phosphorus evaporation and secondary phase formation can take place, and, in this case, an excess amount of precursors is required, which also increases the raw material cost. Ultrafast sintering [115], reaction sintering [146], cold sintering [147], low-temperature sintering [148,149], and high-energy ball milling [116] are recent efforts in the process modification of NASICON SEs. Ultrafast high-temperature sintering (UHS), specifically, increases the performance of the NASICON SEs. The process aims to decrease the processing time, energy consumption, and decomposition or volatilization of the elements. Jiang et al. synthesized $\text{Na}_3\text{Zr}_2\text{Si}_2\text{PO}_{12}$ using this method. The pellets were placed between carbon felts, which were used as the Joule heating unit. In this method, UHS led to increased density and material performance in 1 min. The ionic conductivity was determined as 0.262 mS cm^{-1} with 0.28 eV activation energy. The cells were prepared by $\text{Na}_3\text{V}_2(\text{PO}_4)_3$ (NVP)/Na metal electrodes and showed capacities of 86.3, 83.0, and 72.5 mAh g^{-1} at 0.2, 1, and 5 C, respectively. The UHS approach is of vital importance in terms of obtaining high-performance material with cost reduction [115]. Another approach was reaction sintering, which is advantageous for obtaining the NASICON phase with high density and almost no impurities. In this process, phase formation and densification are carried out around the eutectic temperature. Jung et al. synthesized NASICON SEs by reaction sintering using rare-earth elements. As reported in the study, densification and secondary phase formation can be controlled by the optimization of the sintering temperature by considering the precursor properties. The highest ionic conductivity was reported as 1.017 mS cm^{-1} at RT [146]. Cold sintering is another process used for NASICON SE synthesis at relatively low temperatures compared to traditional sintering. In this process, a sintering aid is used to wet the powder under high pressure. Additionally, the temperature is higher than the boiling temperature of the sintering aid. Grady et al. modified the cold sintering process by using NaOH as the sintering aid mixed with NASICON powder, compressing it in a die, and increasing the temperature. As reported in the study, a sintering temperature of 375 °C resulted in satisfactory ionic conductivity and density. The grain boundary conductivity was reported to be above 0.1 mS cm^{-1} . This process is of significance when traditional sintering processes are considered that require long processing times and temperatures around 1000–1200 °C [147].

High-energy ball milling (HEBM) is another process that can be used to increase the sintering efficiency by dispersing the precursors or ceramic powders before thermal processes. Shindrov et al. used HEBM for the activation of the NASICON precursors before annealing at 1200 °C. Subsequently, NASICON powder was further processed by HEBM and samples were sintered one more time at 1050–1200 °C under 10 MPa pressure. As shown, ball milling is an extra process adapted to the traditional sintering process to

increase the homogeneity of the material. As reported in the study, 10 min of HEBM led to the synthesis (1150 °C, 1 h) of NASICON with density and ionic conductivity of 3.14 g cm^{-3} and 2.12 mS cm^{-1} , respectively [116].

4.2. Polymer Solid Electrolytes

Another group of materials that are used as solid electrolytes is polymers. Polymers are promising materials for solid electrolytes because of their easy processing, flexibility, good mechanical properties, blendability with other components, good surface interaction with the electrodes, air stability, feasibility for continuous/roll-to-roll processes and modifications, and so on. On the other hand, they have some drawbacks, such as low ionic conductivity and electrochemical stability [31,84,103,150]. Polymer solid electrolytes (PSEs) can be prepared by using promising polymers, including PEO [151–154], PVDF derivatives [154,155], cellulose, and derivations [156]. As given in the literature, various factors have effects on the ionic conductivity and electrochemical properties of polymer electrolytes, including polymer type, the molecular weight of the polymer, the morphology of the polymer amorphous/crystalline ratio, crystalline type, linearity, glass transition temperature (T_g), the chemical structure of the polymer, the number and ratio of polar groups in the polymer chain, the interaction between ion and polymer, the dielectric constant of the polymer, electrolyte thickness, surface properties, mechanical properties, temperature, heating–cooling cycles, type of the salt, anion size of the salt, and so on. In all of these, the degree of crystallinity and ion–polymer interaction is somehow critical. In the case of strong ion–polymer interaction, ion flow can be hindered, and ionic conductivity decreases [31,150–152,157].

The most common architecture for PSEs is given in Figure 7a–c. Polymers can be used in various architectures, such as bare polymers, particle/wire filled polymer composites, aligned filler containing polymer composites, and 3D scaffolds. Recently, research has evolved to use the design of functional molecules/polymers [151,157] or the preparation of polymer composites/blends [151–153,158,159] to increase the electrochemical performance of the electrolytes and meet the requirements for ASSBs. The fillers can be classified as active or inert fillers based on their structure. While active fillers have Na^+ in their structure, inert fillers are Na-free structures [154]. In addition to filler type, filler concentration, filler morphology, filler size, and filler orientation have a huge impact on the ionic conductivity of PSEs (Figure 7a) [29,160]. PEO is one of the most common polymer types used for solid electrolytes because of its flexibility caused by a low glass-transition temperature ($-60 \text{ }^\circ\text{C}$); relatively low cost; good mechanical processes; its ability to dissolve Na salts, form complexes, and coordinate with salt ions due to their chemical structure that consists of heteroatoms (O); and good electrochemical stability [84,103,150,157]. Boshchin and Johanson prepared SEs from PEO and NaFSI/NaTFSI by considering ether oxygen to sodium (O:Na) molar ratios ($n = 6, 9, 20$), and investigated the effects of morphological differences on the electrochemical performance of the electrolytes. As reported in the study, concentration and type of the salt were found significant for the aggregate formation and ionic conductivity of the system. While, at high concentrations, and regardless of the anion type, ionic conductivity was in the same range, at lower concentrations, anion type was found to be important. The basic reason for this was the size of the anion and its effect on crystallization. While a larger anion size, TFSI, was reported to prevent crystallization; a smaller anion size, FSI, was found to increase the crystallinity. The highest ionic conductivity was achieved for NaTFSI(PEO)₉ at $4.5 \times 10^{-3} \text{ mS cm}^{-1}$ [152]. In a similar study, NaFSI was used with the O:Na ratio of 20 for PEO-based SEs, and samples were prepared by a simple photo-polymerization technique. The highest ionic conductivity was found at 0.41 mS cm^{-1} at $80 \text{ }^\circ\text{C}$. Cells were prepared by two different cathodes: NVP and $\text{Na}_{0.67}\text{Ni}_{0.33}\text{Mn}_{0.67}\text{O}_2$ (NNM). While the NNM-based cells had a specific capacity of around 70 mAh g^{-1} after 30 cycles at 0.2 C , the NVP-based cells had a specific capacity of around 80 mAh g^{-1} after 530 cycles at 0.2 C . It was also reported that NVP/SE cells showed similar performance compared to the cells with liquid electrolyte [159].

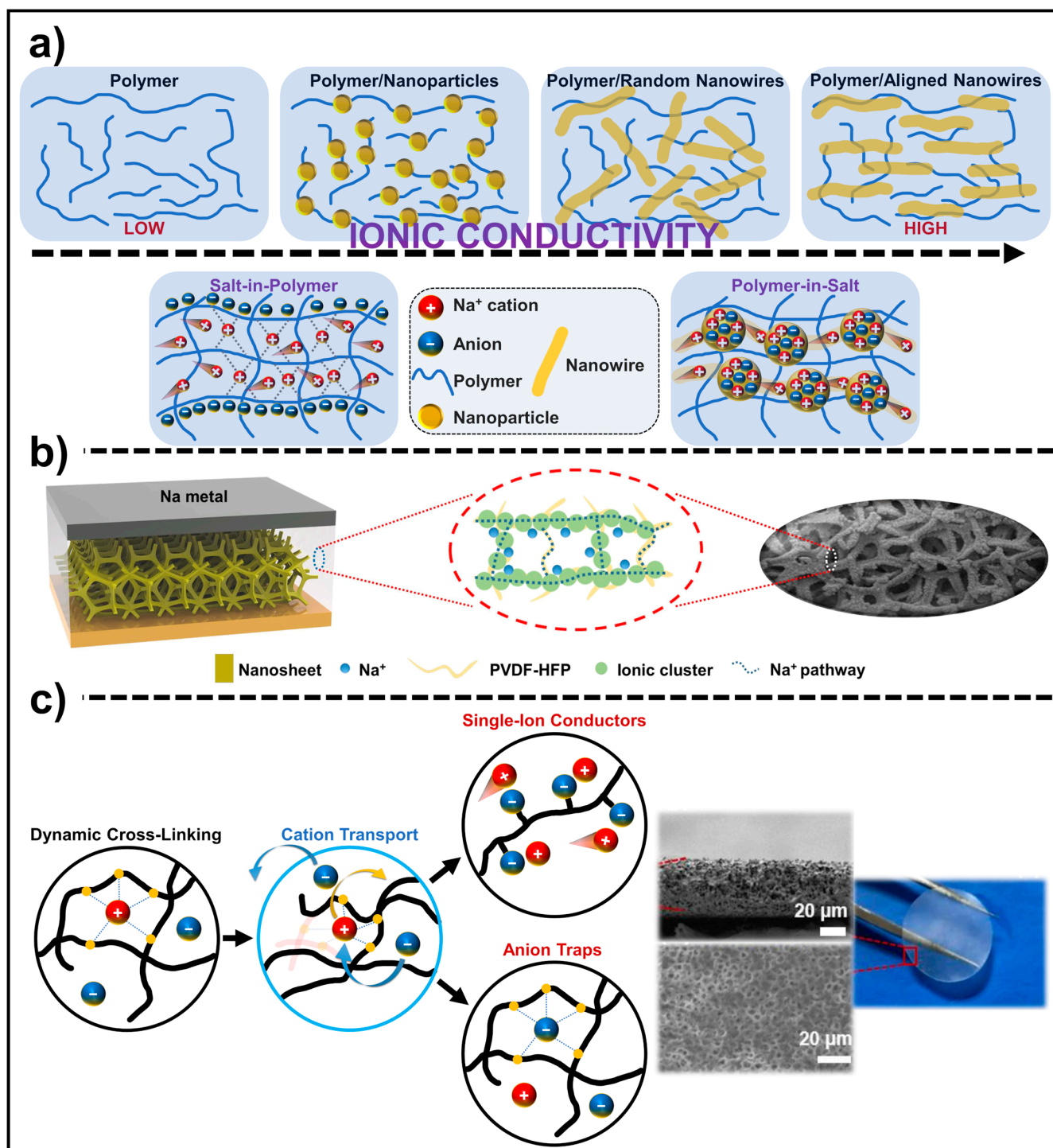


Figure 7. (a) Schematic diagram of Na⁺ transportation kinetics in different solid-polymer electrolyte architectures. Reproduced with the permission of references [29,160]. (b) Illustrations of Na/SPE/Cu₂MoS₄/Cu cell assembly and corresponding Na⁺ transport pathways in polymer electrolyte. Reproduced with the permission of references [155]. (c) SEM and optical images of surface and cross-section of single-ion conductor polymer membrane and corresponding ion transportation mechanism through metal-ligand coordination in single-ion conductor polymer electrolytes. Reproduced with the permission of references [161,162].

Additionally, TiO₂ nanofillers can also be incorporated into a PEO/NaClO₄ mixture. As reported by Ni'mah et al., a 5 wt.% nanofiller addition resulted in an ionic conduc-

tivity of 0.262 mS cm^{-1} at $60 \text{ }^\circ\text{C}$. The specific capacity of the SE was determined by Na/SE/Na_{2/3}Co_{2/3}Mn_{1/3}O₂ cells and compared with the cells prepared by liquid electrolytes. The discharge capacity for the SE and the LE were determined as 49.2 and 107.6 mAh g⁻¹, respectively [158]. Zhang et al. used the NASICON phase for the development of polymer composite electrodes (CPE) with PEO, and NaFSI with two different ceramics (Na₃Zr₂Si₂PO₁₂/Na_{3.4}Zr_{1.8}Mg_{0.2}Si₂PO₁₂). The cathode was prepared by using Na₃V₂(PO₄)₃ and Na_{3.4}Zr_{1.8}Mg_{0.2}Si₂PO₁₂. Na₃V₂(PO₄)₃/CPE/Na and Na₃V₂(PO₄)₃/SPE/Na cells were prepared. The ionic conductivity was found higher for Na_{3.4}Zr_{1.8}Mg_{0.2}Si₂PO₁₂ filler as 2.4 mS cm^{-1} at $80 \text{ }^\circ\text{C}$ at 40 wt.% filler loading. The electrochemical performance of the same SE was determined around 100 mAh g⁻¹ for 120 cycles at 0.1 C. This performance was attributed to the active NASICON fillers and their ability to form a Na⁺ conducting network throughout the electrolyte [154].

PEO blends can also be used for SEs. Colo et al. prepared SEs based on polyethylene oxide (PEO), sodium carboxymethyl cellulose (Na-CMC), and sodium perchlorate. Na-CMC was proposed to be promising in terms of improving the ion-conducting network structure and mechanical properties. In the first step, the optimum ratio of the components was determined as (wt.%) 82:9:9 for PEO:NaClO₄:Na-CMC based on various factors, including processing, the solubility of salt, ionic conductivity, and so on. The electrolyte film was prepared by casting. Half cells were prepared by using a Na/HPE/TiO₂-based anode and a Na/HPE/NaFePO₄-based cathode, and the specific capacities of half cells were ~80 mAh g⁻¹ at 0.05 C and ~80 mAh g⁻¹ at 0.2 C, respectively [156]. A PEO:PEI = 80:20 blend was prepared and various amounts of NaPF₆ were added into the polymer solution and SEs were prepared by casting. The highest ionic conductivity was obtained at O/Na = 10 ratio (NaPF₆) as $5.12 \times 10^{-3} \text{ mS cm}^{-1}$ at $40 \text{ }^\circ\text{C}$ with good thermal stability [163]. Devi et al. prepared polymer SEs by using PEO, poly(vinylpyrrolidone) (PVP), and NaPF₆ blends. Various levels of indium arsenide nanowires were incorporated into the blend and the highest ionic conductivity and ESW were measured as 0.150 mS cm^{-1} and 4.10 V, respectively, at $40 \text{ }^\circ\text{C}$ for 1 wt.% nanowire filling rate. In this work, a Na⁺-ion percolating network was achieved at 1D with relatively light materials, and it was found that Na⁺ ion transfer was improved by the hopping of ions throughout that ion-conducting network [153].

In addition to composites and blends, polymeric structures with various properties can be designed for SEs. Xiao et al. designed, and synthesized star polymers that have polymeric pseudocrown ether cavities with PEO arms. The aim of the work was to provide molecular-level interaction and size-fit with the metal cation to increase the electrochemical performance. The cavities were reported to coordinate with the cation, function as the diffusion channels, and lead to an increase in ionic conductivity. As reported in the study, tunable and custom-made star polymers can be synthesized by selecting proper monomers and templates. Three different monomers and NaI templates were used for polymerization. Star polymers were blended with PEO and SEs were prepared. The ionic conductivity of star polymer synthesized by Na-SPE750-Na resulted in the highest value at $2.37 \times 10^{-2} \text{ mS cm}^{-1}$ [151]. Hyperbranched copolymers can also be used for SEs in addition to star polymers. They also have ion-conducting functional groups with higher flexibility and lower mechanical properties. Chen et al. developed polymer composites for SEs from polyether-based hyperbranched copolymers by using 3-[2-[2-(2-methoxyethoxy) ethoxy]-ethoxy] methyl-3'-methyloxetane (MEMO) and 3-hydroxymethyl-3'-methyloxetane (HMO) monomers. MEMO was the ionic conductive phase and HMO functioned as the formation of the cross-linked phase. SEs were prepared by blending PVDF-HFP, copolymer, and NaClO₄ at different ratios, and solutions were cast. The highest ionic conductivity was reported as 0.57 mS cm^{-1} . The cell performance of SE was determined with a cell consisting of Na metal/NVP. The discharge capacity was measured as 98 mAh g⁻¹ at 0.2 C, and capacity retention was around 92% after 300 cycles [157]. Various solid-state electrolytes used in SIBs and their ionic conductivity values under certain temperature can be seen from Table 3.

Table 3. Different types of solid-state electrolytes used in SIBs.

Type	Content	IC (mS cm ⁻¹)	T (°C)	Ref.
Inorganic Solid Electrolyte	Na _{3.256} Mg _{0.128} Zr _{1.872} Si ₂ PO ₁₂	2.7	25	[108]
	Na _{3.2} Zr _{1.9} Ca _{0.1} Si ₂ PO ₁₂	10 ⁻³	25	[119]
	Na _{3.3} Zr _{1.85} Mg _{0.15} Si ₂ PO ₁₂	3.54	25	[118]
	Na _{3.4} Zr _{1.9} Zn _{0.1} Si _{2.2} P _{0.8} O ₁₂	5.27	25	[125]
	0.1 Co-Na ₃ Zr ₂ Si ₂ PO ₁₂	5.03 × 10 ⁻³	25	[126]
	Na _{3.3} Zr _{1.7} La _{0.3} Si ₂ PO ₁₂	3.4	25	[127]
	Na _{3.3} Zr _{1.7} Eu _{0.3} Si ₂ PO ₁₂	1.08	25	[121]
	Na ₃ Zr _{1.8} Zn _{0.2} Si ₂ PO _{11.8}	1.44	25	[122]
	Na _{3.3} Zr _{1.9} Nb _{0.1} Si _{2.4} P _{0.6} O ₁₂	5.51	25	[123]
	Na ₃ Zr ₂ Si ₂ PO ₁₂	0.61	25	[113]
	Na _{3.33} Zr _{1.67} Sc _{0.33} Si ₂ PO ₁₂	0.96	25	[113]
	Na _{3.33} Zr _{1.67} Sc _{0.29} Yb _{0.04} Si ₂ PO ₁₂	1.62	25	[113]
	Na ₃ Zr ₂ Si ₂ PO ₁₂	0.61	25	[131]
	Na _{3.33} Sc _{0.33} Zr _{1.67} Si ₂ PO ₁₂	0.96	25	[131]
	1 mol% Ce ⁴⁺ + Na _{3.33} Sc _{0.33} Zr _{1.67} Si ₂ PO ₁₂	2.44	25	[131]
	Na ₃ Zr ₂ Si ₂ PO ₁₂	0.39	30	[132]
	Na _{3.125} Zr _{1.75} Sc _{0.125} Ge _{0.125} Si ₂ PO ₁₂	4.64	30	[132]
	1 wt.% Bi ₂ O ₃ -Na _{3.1} Y _{0.1} Zr _{1.9} Si ₂ PO ₁₂	1.21	25	[114]
	5 wt.% Na ₂ SiO ₃ -Na ₃ Zr ₂ Si ₂ PO ₁₂	1.45	25	[139]
	4.8 wt.% Na ₃ BO ₃ -Na ₃ Zr ₂ Si ₂ PO ₁₂	1	25	[134]
1 wt.% MgF ₂ -Na _{3.4} Zr ₂ Si _{2.4} P _{0.6} O ₁₂	2.03	25	[138]	
Na ₃ Zr ₂ Si ₂ PO ₁₂	0.262	25	[115]	
La doped Na ₃ Zr ₂ Si ₂ PO ₁₂	1.017	25	[146]	
Na ₃ Zr ₂ Si ₂ PO ₁₂	2.12	25	[116]	
Polymer Solid Electrolyte	NaTFSI/PEO	4.5 × 10 ⁻³	20	[152]
	NaFSI/PEO	0.41	80	[159]
	TiO ₂ nanofillers/NaClO ₄ /PEO	0.262	60	[158]
	Na _{3.4} Zr _{1.8} Mg _{0.2} Si ₂ PO ₁₂ /NaFSI/PEO	2.4	80	[154]
	Na-CMC/NaClO ₄ /PEO	10 ⁻⁴	60	[156]
	PEO:PEI blend/NaPF ₆	5.12 × 10 ⁻³	40	[163]
	Indium arsenide nanowires/PVP/PEO/NaPF ₆	0.15	40	[153]
	Star polymer:PEO blend	2.37 × 10 ⁻²	25	[151]
	Hyperbranched copolymer:PVDF-HFP blend/NaClO ₄	0.57	30	[157]
	PVDF-HFP/1-(4-cyanophenyl) guanidine/NaPF ₆	1.76 × 10 ⁻²	30	[155]

IC: Ionic conductivity; T: temperature.

PVDF and its derivatives are other polymers used for the preparation of SEs due to high thermal and dimensional stability, good mechanical properties, high ionic conductivity, easy processing, safety, and compatibility with different types of active materials. As shown, PVDF and its derivatives are mostly used for the development of QSEs. There is a limited number of studies regarding solid-state electrolytes based on PVDF derivatives. Some of the electrolytes studied were categorized as solid electrolytes, while some of them were hybrid electrolytes [164], and some of them required LEs [165] for activation. As previously mentioned, the electrode/electrolyte interface is critical and current efforts have focused on that point. One recent approach was to embed the 3D anode into the polymer solid electrolyte to improve physical contact and restrict the volume expansion (Figure 7b). Zhao et al. used copper foam as a template and Cu₂MoS₄ was grown on the 3D scaffold. Subsequently, a PVDF-HFP/1-(4-cyanophenyl) guanidine/NaPF₆/acetone mixture was infiltrated, and an integrated anode/polymer solid electrolyte was prepared. The ionic conductivity of the anode/electrolyte integrated system was reported to be 1.76 × 10⁻² mS cm⁻¹ at 30 °C and 0.454 mS cm⁻¹ at 70 °C. The integrated 3D PVDF-HFP-based network increased the Na⁺ transfer. In addition, 1-(4-cyanophenyl) guanidine and NaPF₆ were useful in terms of providing shorter channels for ion transfer. Based on these results, the Na⁺-ion transfer number and the activation energy were determined as

0.45 and 63.9 kJ mol⁻¹, respectively. The specific capacity of the system was measured as 620 mAh g⁻¹ and 508 mAh g⁻¹ for 100 and 500 mA g⁻¹, respectively [155].

5. Hybrid Electrolytes

The hybrid electrolyte (HE) is one of the recent approaches for improving the performance of SIBs. The term “hybrid” defines any system consisting of at least two different species. As explained in the previous sections, each electrolyte has advantages and limitations. Hybrid SIBs are important alternatives that combine the benefits of each system and minimize their limitations. In other words, they are promising systems in terms of offering high energy density, long life, improved safety, and reduced risks. In this review, HEs are classified into binary and ternary electrolytes based on the number of components, as shown in Figure 8. Since most of the polymer electrolytes require salt, “polymer + salt” are considered as one material and evaluated as a polymer component of the hybrid electrolyte.

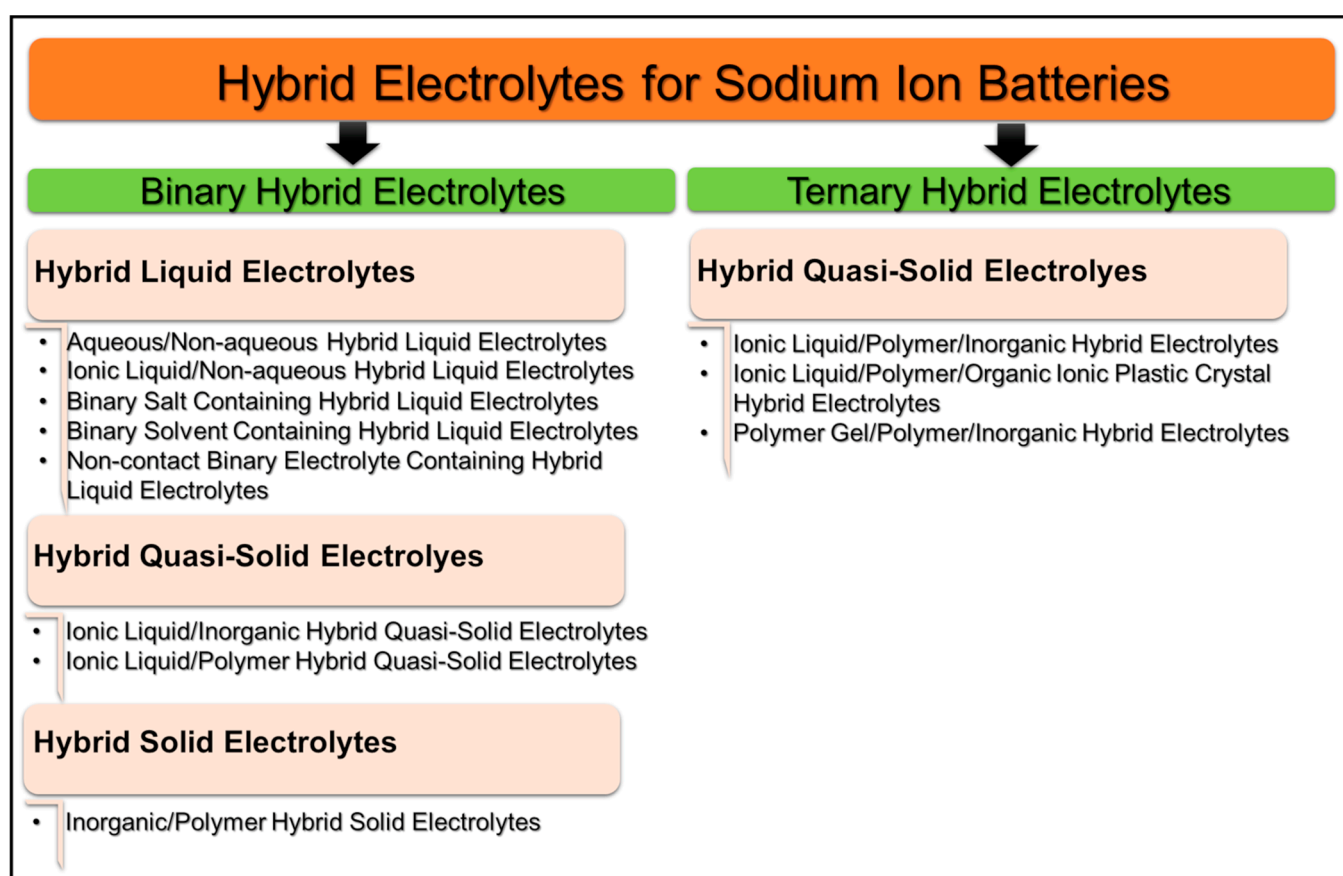


Figure 8. Classification of hybrid electrolytes used for SIBs.

5.1. Binary Hybrid Electrolytes

5.1.1. Hybrid Liquid Electrodes

Aqueous/Non-Aqueous Hybrid Liquid Electrolytes

Aqueous/non-aqueous hybrid liquid electrolytes (ANHLEs) consist of at least one aqueous and one non-aqueous phase. As mentioned previously, aqueous electrolytes are water-based and non-aqueous electrolytes are organic solvent-based systems. While aqueous electrolytes contribute to the hybrid system with their high ionic conductivity, safety, and low cost, non-aqueous electrolytes contribute with their high chemical and electrochemical stability and wide ESW. ANHLEs can be prepared by mixing aqueous and non-aqueous electrolytes at different ratios to increase the ESW and provide stable and reversible cyclic performance, improved cell voltage, and energy density [166,167].

Zhang et al. developed an aqueous/nonaqueous hybrid electrolyte from concentrated NaOTf/water and NaOTf/PC mixtures. The ionic conductivity of the ANHLE was reported to be directly affected by temperature change, and the values were given as ~ 60 , ~ 25 , and ~ 5.0 mS cm⁻¹ for 55, 20, and -15 °C, respectively. Na₃V₂(PO₄)₃ and NaTi₂(PO₄)₃ (NTP) were prepared as the positive and negative electrodes because of their high-rate performance. The initial charge and discharge capacities were determined as 115 and 91 mAh g⁻¹, respectively, at 0.2 C with 79% initial Coulombic efficiency and an energy density of 45 Wh kg⁻¹. In the case of the higher current rate (from 1 C to 10 C), the capacity changed from 65 to 22 mAh g⁻¹ [166]. In another study, Shen et al. prepared an ANHLE by using water, acetonitrile (AN), and NaClO₄. AN was preferred because of its wide ESW and its contribution to wettability and increased interaction throughout the electrolyte/electrode interface. NTP and Na_{2.85}K_{0.15}V₂(PO₄)₃ were used as an anode and cathode with ANHLE. The discharge capacity was 52 mA h g⁻¹, and the energy density was 51 Wh kg⁻¹ at 1 A g⁻¹ [167].

Ionic Liquid/Non-Aqueous Hybrid Liquid Electrolytes

Ionic liquid/non-aqueous hybrid liquid electrolytes (INHLEs) consist of at least ionic liquid and one non-aqueous phase. As mentioned previously ionic liquids are organic salts with low melting points and non-aqueous electrolytes are organic solvent-based systems. While ionic liquid electrolytes improve the system performance in terms of ionic conductivity, chemical and thermal stability, flame-ignition suppressibility, safety, and evaporation resistance, non-aqueous electrolytes contribute with their high chemical and electrochemical stability and wide ESW. However, excess amounts of ionic liquids may lead to lower ionic conductivity due to their higher viscosity. With these properties, INHLEs can be generally prepared by mixing at optimum ratios to increase the ESW and provide stable and reversible cyclic performance, improved cell voltage, and energy density [63,168,169]. One of the first studies about INHLEs was conducted by Monti et al. In the study, BMImTFSI, EMImTFSI, and Pyr₁₃TFSI were the ionic liquid components, and EC:PC was the non-aqueous components of the hybrid system. Additionally, NaTFSI salt was also incorporated. Different hybrid electrolytes were combined to investigate the compatibility between the two phases. In the case of an addition, ionic liquid in the range of 10–20% was found almost the same as the non-aqueous electrolyte in terms of ionic conductivity and higher flame resistance. Hard carbon-based half cells showed a specific capacity of 182 mAhg⁻¹ at 0.1 C with a hybrid electrolyte that consisted of 0.8 m NaTFSI in EC:PC:Pyr₁₃TFSI = 0.45:0.45:0.10 [169]. Hwang et al. prepared various INHLEs by using [C₃C₁pyrr][FSA] as the ionic liquid and PC as the organic liquid electrolyte with NaFSA and NaClO₄ salts to investigate the electrochemical performance, cost, and flammability of the system. For that aim, thermal stability, ionic conductivity, viscosity, and the electrochemical properties of the electrolytes were investigated. The flammability was prevented by using the electrolyte with the highest IL content, and the inhibition of flammability was obtained for the IL content higher than 40%. These results were similar for thermal stability. In the case of a higher IL ratio, the thermal stability of the system increased in the same manner as the results from thermal gravimetric analysis graphs. The highest ionic conductivity was obtained at 50% IL content as 9.7 mS cm⁻¹ and decreased to 6.6 and 4.9 mS cm⁻¹ for higher concentrations of 80 and 100%, respectively. A Higher IL ratio led to an increase in viscosity and density; however, the increase in temperature resulted in lower viscosity and density. Full cells were prepared by using hard carbon and NaCrO₂ as the anode and cathode, respectively, to determine the electrolyte performance. The energy densities of the electrolytes were determined as 158.4, 125.5, and 125.4 Wh kg⁻¹ for IL contents of 100, 50, and 20%, respectively. The initial capacity of 50% IL containing NIHE was determined around 70 and 79.5 mAh g⁻¹ at 278 and 363 K, respectively, and these values are relatively higher than those for the sample without any ILs (~ 62 mAh g⁻¹) [168].

Binary Salt Containing Hybrid Liquid Electrolytes

Another approach for the preparation of hybrid liquid electrolytes is using binary salts. Karlsmo et al. added Na_2SO_4 and MgSO_4 salts in aqueous electrolytes to reduce the dissolution of b-Perylene-3,4,9,10-tetracarboxylic dianhydride (PTCDA). For this aim, PTCDA was used as the anode of the half cell and electrochemical performance was determined with the Na_2SO_4 and $\text{Na}_2\text{SO}_4/\text{MgSO}_4$ hybrid electrolytes. The ionic conductivity of the Na_2SO_4 -based electrolytes was reported to increase alongside the increase in the concentration; however, the $\text{Na}_2\text{SO}_4/\text{MgSO}_4$ hybrid electrolyte showed lower ionic conductivity compared to the electrolyte that has the same amount of Na_2SO_4 due to the increase in viscosity. Additionally, the ESW was reported to be higher than 3 V and the hybrid electrolytes showed better cycling performance compared to Na_2SO_4 cells due to the dissolving of PTCDA in the electrolyte. Additionally, hybrid electrolytes showed a Coulombic efficiency of around 98%. The authors underlined that the hybrid electrolyte used in the study is important in terms of its relatively cheap price compared to other aqueous electrolytes [170].

Binary Solvent Containing Hybrid Liquid Electrolytes

In addition to the binary salt hybrid electrode, the binary solvent hybrid electrode approach can be applied to improve the performance of the electrolytes. The reasons for using cosolvents can be to widen the ESW; increase the concentration, oxidation stability, and service temperature range; minimize the dissolution of SEI and electrodes; decrease the freezing point; and improve the cycling performance [158]. Wang et al. used adiponitrile (ADN) as a cosolvent to prepare super-concentrated aqueous hybrid electrolytes. ADN is advantageous due to its high-voltage range and suppression of the dissolution of NaF-rich SEI and vanadium-based electrodes, lowering the freezing point. The hybrid electrolyte was prepared by dissolving NaTFSI salt into ADN/ H_2O . The electrolytes were coded as $1\text{Na}-1\text{H}_2\text{O}-x\text{ADN}$ and x was the molar ratio of ADN, 1:1: x ($x = 1, 1.8, 2.5, 3.5, 5$). The highest ionic conductivity was achieved for $x = 2.5$ (AWE) as 3.39 mS cm^{-1} at RT and 1.19 mS cm^{-1} at -20°C . $\text{Na}_3\text{V}_2(\text{PO}_4)_3/\text{NaTi}_2(\text{PO}_4)_3$ full cells were prepared and cycled 1000 times at 5 C and the initial capacity was determined as more than 100 mAh g^{-1} with 71% capacity retention [171].

Non-Contact Binary Electrolyte Containing Hybrid Liquid Electrolytes

In the studies reviewed above, components of the liquid electrolytes contact each other via mixing. However, non-contact hybrid electrolytes can also be used for SIBs. Although that concept cannot be applied to all energy storage applications, it can be feasible for stationary systems. In these systems, two different non-contact electrolytes are used for the anode and cathode. Sentilkumar et al. developed a sodium-ion battery system by using a hybrid electrolyte system. The positive electrode nickel hexacyanoferrate (NiHCF) was placed in seawater, $\text{Na}_3\text{Zr}_2\text{Si}_2\text{PO}_{12}$ was used as the separator, and a Na metal/hard carbon anode was placed in a NaCF_3SO_3 /tetra ethylene glycol dimethyl ether (TEGDME) organic electrolyte. As shown in Figure 9a, the uniqueness of the system is based on an easily replaceable cathode when required. Additionally, seawater is proposed as the Na-ion source and is a sustainable and cheap alternative. Since seawater flow is continuous, no cooling system is required. In this hybrid cell, the deintercalation of Na^+ from the NiHCF is followed by their transport through the inorganic solid electrolyte. The oxidation of Fe^{2+} to Fe^{3+} led to electron flow throughout the external circuit. Na^+ ions that reach the anode are deposited by the reduction of Fe^{3+} . The discharging process is the reverse of this mechanism. The hybrid electrolyte system showed the capacity of 56.58 and 19.8 mAh g^{-1} for 20 and 100 mA g^{-1} , respectively [172].

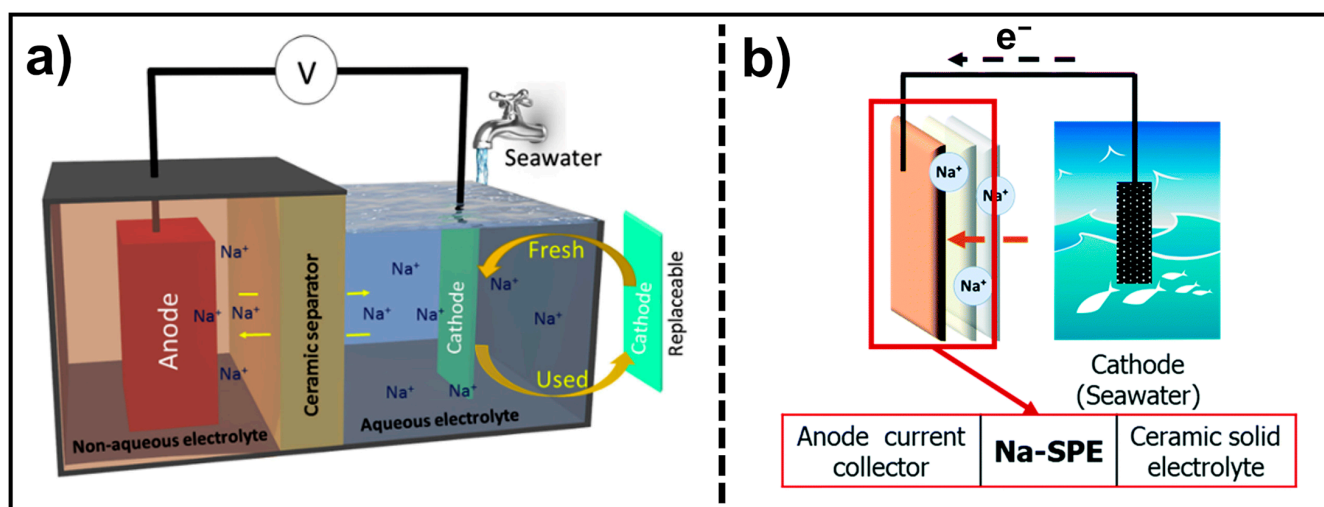


Figure 9. (a) Schematic illustration of sodium-ion hybrid electrolyte battery system with a replaceable cathode. Reproduced with the permission of reference [172]. (b) Illustration of anodeless Na seawater battery, formed using Na^+ conducting SPE. Reproduced with the permission of reference [173].

5.1.2. Hybrid Quasi-Solid Electrolytes

Ionic Liquid/Inorganic Hybrid Quasi-Solid Electrolytes

Ionic liquid/inorganic hybrid quasi-solid electrolytes (IIHQSEs) consist of at least one ionic liquid and one inorganic phase. As mentioned previously, ionic liquid electrolytes improve the system performance in terms of ionic conductivity and chemical stability, and inorganic electrolytes contribute their high chemical and electrochemical stability and wide ESW. Additionally, ionic liquids compensate for the grain boundary resistance by enhancing the Na^+ transfer and malleability, and increasing the wettability. For IIHES, ionic conductivity and electrochemical performance can be tailored by the ratio, morphology, and electrochemical properties of each system and their synergistic interaction [127,174–177].

Martínez-Cisneros et al. developed IIHQSEs by using NASICON and ionic liquids. In the first place, the effects of the Na precursor ratio on the structure of $\text{Na}_3\text{Zr}_{1.84}\text{Y}_{0.16}\text{Si}_2\text{PO}_{12}$ were investigated and porous layered electrolytes were prepared. The porous morphology was obtained by using various pore-formers or by freeze casting and 10% NaTFSI containing 1-Butyl-1-Methylpyrrolidinium (trifluoromethane sulfonyl) imide-Pyr0408a solution was infiltrated through the porous samples as the ionic liquid for the preparation of the HQSEs. The method and material used for the porous morphology were found to be significant in terms of the ionic conductivity of the hybrid system based on their capacity to host the ionic liquid inside. Additionally, porosity% and orientation of pores were also found significant for ionic conductivity. In all hybrid electrolytes, the highest ionic conductivity was obtained for the PMMA-based porous sample (20 vol.% PMMA) as 5.8 mS cm^{-1} at 90°C . The ionic liquid was reported to reduce the grain boundary resistance by filling the pores, and the porous morphology functioned as a Na ion reservoir. The cells were prepared by Na metal and $\text{Na}_3\text{V}_2(\text{PO}_4)_3$ as the cathode. The capacity values were determined as 61.5, 42, and 24 mA h g^{-1} for 0.1, 0.2, and 0.5 C, respectively [174].

Zhang et al. prepared hybrid electrolytes by using NASICON-type ceramic and ionic liquid. In the study, the optimum rate of La was determined and $\text{Na}_{3.3}\text{Zr}_{1.7}\text{La}_{0.3}\text{Si}_2\text{PO}_{12}$ was found as the optimum NASICON structure. $\text{Na}_3\text{V}_2(\text{PO}_4)_3/\text{SE}/\text{Na}$ and $\text{Na}_3\text{V}_2(\text{PO}_4)_3/\text{IL}/\text{SE}/\text{Na}$ cells were prepared to investigate the effect of PP₁₃FSI ionic liquid on electrochemical performance. The cell with a bare SE showed a relatively low capacity of 44 mA h g^{-1} after 10 cycles. On the other hand, the cell with a hybrid electrolyte showed better performance. The specific discharge capacities were reported as 113, 112, 109, 91, and 86 mA h g^{-1} at 0.2, 0.5, 1, 4, and 10 C rates, respectively. Additionally, capacity almost did not change at 10 C, even after 10,000 cycles [127].

One of the most comprehensive studies about IHQSEs was performed by Johari et al. In the study, hybrid electrolytes were prepared by halloysite clay-derived $\text{Na}_2\text{ZnSiO}_4$ (NZS) and ionic liquids. In the study, 22 substituents were used to consider the structure of $\text{Na}_2\text{Zn}_{1-x}\text{Si}_{1-x}\text{A}_{2x}\text{O}_4$ at $x = 0.05$ and $x = 0.1$, including $A = \text{Mg, Al, Ca, Sc, Ti, V, Cr, Mn, Fe, Co, Ni, Cu, Ga, Sr, Y, Zr, Nb, Mo, Rh, Ag, Cd, and In}$. Ionic conductivity values were determined between 0.003 and 0.453 mS cm^{-1} based on the dopant. The optimum results were obtained for $x = 0.1$. As shown in the results, IL/bare NZS hybrid electrolyte showed a fivefold higher ionic conductivity of 0.166 mS cm^{-1} at RT compared to bare NZS. It was reported that Ca, Al, Sr, Fe, Co, and In led to an enhancement in ionic conductivity without an important decrease in electronic conductivity. Since the substitution of In, Fe, and Co led to higher improvement in ionic conductivity, these materials were further investigated. The inorganic pellets were immersed and soaked into the heated $\text{Py}_{14}\text{TFSI}/\text{NaTFSI}$ mixture and dried before conducting electrochemical analysis. An $x = 0.1/\text{Co}$ -containing hybrid electrolyte was not found to be a good candidate for SIBs because of its narrow ESW. An $x = 0.1/\text{In}$ -containing hybrid electrolyte was reported to be compatible with some anodes due to its wider ESW. An $x = 0.1/\text{Fe}$ containing hybrid electrolyte was reported to be a promising material for almost all recent cathodes used for SIBs. Additionally, it was also reported that dendrite growth was not a problem for hybrid electrolytes [178].

Ionic Liquid/Polymer Hybrid Quasi-Solid Electrolytes

Ionic liquid/polymer hybrid quasi-solid electrolytes (IPHQSEs) consist of at least one ionic liquid and one polymer phase. While ionic liquid electrolytes improve the system performance in terms of ionic conductivity, and chemical stability, polymer electrolytes contribute their flexibility, easy processing, and good mechanical interface properties. Additionally, ionic liquids compensate for the grain boundary resistance by enhancing the Na-ion transfer. For IPHQSEs, ionic conductivity and electrochemical performance can be tailored by the ratio, morphology, and electrochemical properties of each system and their synergistic interaction. Boschini et al. developed IPHQSEs by using PEO, NaFSI, NaTFSI, $\text{Pyr}_{13}\text{FSI}$, and $\text{Pyr}_{13}\text{TFSI}$ with different ratios. $\text{NaTFSI}(\text{PEO})_n\text{—Pyr}_{13}\text{TFSI}$ and $\text{NaFSI}(\text{PEO})_n\text{—Pyr}_{13}\text{FSI}$ were designed based on the wt.% of IL (5, 10, and 20), O:Na molar ratios (n) of 6, 9, and 20, and O: Pyr_{13} ratios in the range of ca. 16–131. PEO was reported to coordinate with Na^+ ions and PEO–IL interaction was found to be relatively low. While TFSI containing electrolytes was not affected by IL content, FSI showed variations based on the IL content. IL was found to decrease the crystallization of PEO by the plasticization effect. Although the addition of IL resulted in higher ionic conductivity, none of the ionic conductivity of hybrid electrolytes showed less than 1 mS cm^{-1} at RT [179].

5.1.3. Hybrid Solid Electrodes

Inorganic/Polymer Hybrid Solid Electrolytes

Inorganic/polymer hybrid solid electrolytes (IPHSEs) consist of at least one polymer and one inorganic phase. They are composite systems. The flexibility (bending, twisting, rolling, etc.) of the system and a higher level of physical contact between the electrode/electrolyte are provided by the polymer, and rigidity, mechanical stability, ionic conductivity, and safety are mostly provided by the inorganic component. Furthermore, the addition of polymer leads can lower costs due to their cheaper price compared to high-energy-consuming ceramics [13,180]. IPHSEs provide better physical contact that enables a higher level of interaction with cathode active materials and extra pathways for ion transfer. They also provide the formation of a physical barrier to prevent Na dendrite growth. Their relatively flexible structure helps to compensate the volumetric change in the cell [180]. Cheng et al. prepared a hybrid solid electrode by using PVDF-HFP as the polymer phase and $\text{Na}_3\text{Zr}_2\text{Si}_2\text{PO}_{12}$ as the inorganic ceramic phase. The ionic conductivity of the IPHSE was reported as 0.25 mS cm^{-1} at RT. The NASICON: PVDF-HFP ratio was 1:9 and 5 wt.% polyethylene glycol (PEG) was added for better film formation. Solid-state cells were prepared by using NASICON and HSE electrolytes. $\text{Na}_3\text{V}_2(\text{PO}_4)_3/\text{C}|\text{HSE}|\text{Na}$

showed a reversible capacity of $98 \text{ mAh}\cdot\text{g}^{-1}$ at 0.2 C and 85% capacity retention after 175 cycles with low polarization [180].

5.2. Ternary Hybrid Electrolytes

In addition to binary hybrid electrodes, tertiary hybrid systems were also reported in the literature. Tertiary hybrid electrolytes are a type of electrolyte system that combines three different components to achieve optimal electrochemical performance. These three components might be any type of liquid electrolyte, quasi-solid electrolyte, or solid electrolyte. As in binary hybrid electrolytes, each component provides necessary requirements that were mentioned previously.

5.2.1. Ionic Liquid/Polymer/Inorganic Hybrid Electrolytes

Shen et al. developed a three-component flexible hybrid electrolyte. In the first step $\text{Na}_{3.4}\text{Zr}_{1.9}\text{Zn}_{0.1}\text{Si}_{2.2}\text{P}_{0.8}\text{O}_{12}$ and ionic liquid, $[\text{Py}_{13}] + [\text{NTf}_2]$ were mixed, and, following that, PEO and NaClO_4 were incorporated. The hybrid electrolyte was solution-cast and the dried film thickness was $95 \mu\text{m}$. Various hybrid electrolytes were prepared to compare the effect of each component on the electrochemical performance. The ionic conductivity of polymer and inorganic/polymer dual hybrid and IPIHE was determined as 1.79×10^{-4} , 3.48×10^{-3} , and 0.148 mS cm^{-1} , respectively. IPIHEs with 70 wt.% and 90 wt.% $\text{Na}_{3.4}\text{Zr}_{1.9}\text{Zn}_{0.1}\text{Si}_{2.2}\text{P}_{0.8}\text{O}_{12}$ contents were prepared and the best performance was achieved as 0.148 mS cm^{-1} for 80 wt.% NASICON content. Additionally, $\text{Na}_3\text{V}_2(\text{PO}_4)_3$ /IPIHE/Na solid-state cell had an initial discharge capacity of 109.4 mAh g^{-1} at 0.2 C and after 150 cycles capacity retention was calculated at around 85% [175].

Another example of IPIHEs was used for sodium-seawater batteries (Na-SWBs), developed by Kim et al. using PEO, Na-ion salt (NaFSI), and ionic liquid (Pyr14FSI). In the study, an anodeless energy storage system was developed using seawater and a hybrid solid electrolyte with higher safety and lower cost. The components (molar ratio) of the hybrid polymer electrolyte were 10(PEO)-NaFSI-4(Pyr₁₄FSI). The ionic conductivity of the flexible and transparent polymer electrolyte was 1.43 mS cm^{-1} (20°C). As shown in Figure 9b, a solid polymer electrolyte was placed between the NASICON electrolyte and the anode current collector. The charging process is based on the unlimited amount of Na^+ extraction from seawater. The ions pass through the electrolyte and electrodeposit on the current collector. The charge capacity values were reported at around 7.2 and 10 mAh cm^{-2} under the current rate of 0.1 mA cm^{-2} for copper and aluminum collectors, respectively. These results are promising for future applications [173].

5.2.2. Ionic Liquid/Polymer/Organic Ionic Plastic Crystal Hybrid Electrolytes

In addition to ionic liquids, liquid electrolytes, ceramics, polymers, polymer gels, and organic ionic plastic crystals (OIPCs) are promising materials for SEs due to their inherent properties, such as ionic conductivity and plasticity. Since OIPCs consist of organic cations and inorganic anions, the structure of anions and cations directly affects the electrochemical performance of the electrolyte. They can be used as the only phase for SEs or can be combined with other materials for hybrid electrolytes [164,181]. Makhlooghiyazad et al. prepared hybrid solid electrolytes based on PVDF electrospun fibers, triisobutyl(methyl)phosphonium bis(fluorosulfonyl)imide $[\text{P1i}_{444}][\text{FSI}]$, NaFSI, and NaTFSI. Ionic conductive mixtures were prepared as $[\text{P1i}_{444}][\text{FSI}]/\text{NaFSI}$ and $[\text{P1i}_{444}][\text{FSI}]/\text{NaTFSI}$. They were subsequently mixed with electrospun PVDF with a wt.% of 15/85. The ionic conductivity and Na^+ transference number at 50°C for 20 mol% $\text{NaFSI}/[\text{P1i}_{444}][\text{FSI}]/\text{PVDF}$ and 20 mol% $\text{NaTFSI}/[\text{P1i}_{444}][\text{FSI}]/\text{PVDF}$ were measured as $0.21/2.1 \text{ mS cm}^{-1}$ and $0.22/2.5 \text{ mS cm}^{-1}$, respectively. The difference was attributed to interactions between FSI and PVDF and TFSI and PVDF. Higher dipole–dipole interactions between TFSI and PVDF led to the formation of an interface with a higher ion flow. Na|NVP/C cells were prepared and the capacities of $\text{NaFSI}/[\text{P1i}_{444}][\text{FSI}]/\text{PVDF}$ and $\text{NaTFSI}/[\text{P1i}_{444}][\text{FSI}]/\text{PVDF}$ were

determined as 94 and 95 mAh g⁻¹ at 0.2 C/50 °C, respectively. At 1 C/50 °C, capacity was around 90 mAh g⁻¹ [164].

5.2.3. Polymer Gel/Polymer/Inorganic Hybrid Electrolytes

Electrospun Na₃Zr₂Si₂PO₁₂/PVDF-HFP composite porous mats were prepared, and a composite PVDF-HFP-in situ polymerized-PMMA gel electrolyte was synthesized by in situ polymerization on electrospun composite. The discharge capacity was determined as 94.6 mA h g⁻¹ after 100 cycles. It was reported that PMMA-based gel electrolytes led to the formation of an interface with electrodes that have good physical contact and lower interfacial resistance, and were successful in compensating for the volumetric changes during electrochemical reactions. In the study, electrochemical performance was evaluated for NNMM|GHSE|Na/C cells. A Na/C-anode-containing cell showed an initial discharge capacity of 96 mAh g⁻¹ at a current rate of 192 mA g⁻¹ [182]. Various hybrid electrolytes used in SIBs and their ionic conductivities at certain temperatures are shown in Table 4.

Table 4. Different hybrid electrolytes used in SIBs.

Content	IC (mS cm ⁻¹)	T (°C)	Ref.
NaClO ₄ , acetonitrile, water	~67	25	[167]
[C3C1pyrr][FSA]/PC/NaFSA/NaClO ₄	8.4	25	[168]
Na ₂ SO ₄ /MgSO ₄ /water	55	30	[170]
NaTFSI, adiponitrile, H ₂ O	3.39	25	[171]
Na ₃ Zr _{1.84} Y _{0.16} Si ₂ PO ₁₂ /NaTFSI/Pyr0408a	0.9	30	[174]
Halloysite clay-derived Na ₂ ZnSiO, ionic liquids	0.166	25	[178]
PEO/NaTFSI/NaFSI/Pyr ₁₃ TFSI/Pyr ₁₃ FSI	10 ⁻³	70	[179]
Na ₃ Zr ₂ Si ₂ PO ₁₂ /PVDF-HFP/NaClO ₄ /EC:DMC	2.25	25	[180]
PEO/NaFSI/Pyr ₁₄ FSI	1.43	20	[173]
Na _{3.4} Zr _{1.9} Zn _{0.1} Si _{2.2} P _{0.8} O ₁₂ /[Py ₁₃] + [NTf ₂]/PEO/NaClO ₄	0.148	25	[175]
[P1i ₄₄₄][FSI] organic ionic plastic crystal, NaFSI/NaTFSI/PVDF	2.1, 2.5	50	[164,182]
NZSPO-PVDF-HFP composite	2.78	30	[182]

IC: Ionic conductivity; T: temperature.

6. Impact of New Generation Electrolytes on SIBs

New generation electrolytes for SIBs are being developed to improve their performance in terms of capacity, stability, and rate-capability because of their relatively higher ionic conductivity, better stability, wider ESW, and higher thermal and chemical stability. They are either brand-new electrolytes with unique chemistry and morphology or modified/hybridized version of traditional electrolytes.

Liquid electrolytes: Glyme-based LEs can be considered advanced new-generation liquid electrolytes. Full cells prepared by glyme-based electrolyte showed a capacity of around 125 mAh g⁻¹ at 0.2 C and a capacity retention of around 25% at the end of 1000 cycles at 2 C [52]. Tetraglyme-based electrolyte resulted in 110 mAh g⁻¹ after 1000 cycles at 1 A g⁻¹ [53]. In addition to glymes, ionic liquid electrolytes have been another focused material group for SIBs. An amount of 320 mAh g⁻¹ at 0.5 A g⁻¹ was reported for 3500 cycles [71]. Aqueous electrolytes were also reported to show good performance even after 17,000 cycles, and SIBs in the low-concentration aqueous electrolyte could maintain a capacity of 65.5 mAh g⁻¹ at 2 A g⁻¹ with 65.1% capacity retention [68]. An amount of 80 mAh g⁻¹ capacity at 4 C at -50 °C, after 8000 cycles, is considered a good result in this category [60].

Quasi-solid electrolytes: Since they combine properties of both liquid and solid electrolytes, quasi-solid electrolytes seem to be one of the dominant electrolytes in the near future. Some promising results for this group include a capacity of 78.1 mAh g⁻¹ at 10 C with >90% capacity retention after 500 cycles [77]; 71.4 mAh g⁻¹ at 10 C [89]; 90.7 mA h⁻¹ at 2 C with 85.6% capacity retention rate after 5000 cycles [97]; 104.4 mAh g⁻¹ at 2 C with 90.6% capacity retention after 1250 cycles [99]; 100 mAh g⁻¹ at 1 C (~165 Wh kg⁻¹ energy density) [79]; and 120 mAh g⁻¹ at 1 C with 96.1% capacity retention after 1100 cycles [86].

Solid electrolytes: Recent trends in NASICON research can be summarized as structural and grain boundary-modified NASICONs. Following the conducted research, the capacity, stability, and rate capability of the cells were reported to increase; however, most of the satisfying results were reported for the samples that had an interfacial modification. Some promising capacity results include 236.5 mAh g^{-1} (100 cycles, 0.1 C rate); 133.1 mAh g^{-1} (300 cycles, 0.5 C) [125]; 160 mAh g^{-1} at 6 C [143]; and 99.2, 98.7, and 95.8 mAh g^{-1} at 1.5, 2, and 3 C, respectively [102]. Similar results were also reported for PSEs. PSEs have some important contributions in the area because of the design of special polymers or morphologies with unique structures. Although molecular level design for Na^+ transfer was enabled, the capacity values need to be increased for feasible production. An amount of 98 mAh g^{-1} at 0.2 C, with capacity retention around 92% after 300 cycles [157], and 620 mAh g^{-1} and 508 mAh g^{-1} for 100 and 500 mA g^{-1} , respectively [155], can be given as average results for this group.

Hybrid electrolytes can be evaluated as binary or ternary based on the number of components. Further classification can be given as hybrid liquid, hybrid quasi-solid, or hybrid solid electrolytes. In advanced hybrid electrolytes, the main goal is to maximize performance by compensating for the limitations of each system with another. Hybrid electrolytes seem to be one of the promising groups due to their tunable structure, form, and performance. Some of the promising results were reported as 100 mAh g^{-1} with 71% capacity retention for 1000 cycles at 5 C [171]. The results reported as 113, 112, 109, 91, and 86 mA h g^{-1} at 0.2, 0.5, 1, 4, and 10 C rates, respectively, even after 10,000 cycles [127].

7. Conclusions and Future Perspectives

Electrolytes are one of the most important units of SIBs. To obtain high performance, the basic requirements for electrolytes include high ionic conductivity, high ion transference number; low electrical conductivity; a wide ESW; high electrochemical, thermal, dimensional, and mechanical stability; good electrode/electrolyte interaction; low electrode/electrolyte interfacial resistance; inertness; safety; low raw material; and low processing costs. However, one type of electrolyte cannot show sufficient performance for all of these requirements. Liquid electrolytes are the most common type of electrolytes used in SIBs due to the knowledge transferred from LIBs. Since they are liquid-based mixtures, preparation and material cost is relatively lower compared to other electrolytes. Although they show superior performance in terms of ionic conductivity, they require a separator and have the same leakage and safety problems. Quasi-solid-state electrolytes have lower ionic conductivity than liquid electrolytes. On the other hand, they are advantageous due to the lower risk of electrolyte leaking and evaporation; however, they also have lower mechanical properties compared to solid electrolytes. QSEs can be given as one of the potential groups of electrolytes for future applications because of their tunable structure. Hundreds of different combinations can be designed easily, and their assembly is not a significant challenge as in ISEs. Solid electrolytes function as separators and ion-conducting electrolytes. The most prominent features of solid electrolytes include the lack of leakage, low explosion risk, and nonflammability. They show good thermal, dimensional, and mechanical properties. However, their ionic conductivity is not as high as that of liquid electrolytes, the electrode/electrolyte interface can be challenging, and battery assembly might be difficult compared to other electrolytes. To increase the performance of an ISE, divalent, trivalent, tetravalent, and pentavalent dopants can be used for structural modification with the primary aim of increasing ionic conductivity by the formation of a new 3D Na^+ -conductive network with optimum bottleneck structure and density. Additionally, grain boundary modification using special additives can be used to increase ionic conductivity. Even if these two methods are useful for increasing the ionic conductivity, the electrolyte/electrode interface can still be challenging, and some special modifications can be required to increase Na^+ transfers between different phases. Another point that should be considered is the high energy consumption. Recent trends have focused on the synthesis of ISOs with lower energy consumption that can be performed by ultrafast,

low-temperature reaction sintering methods. One other challenge is the assembly of ISEs because of their rigid structure and high dimensional robustness. Unlike ISEs, PSEs have various advantages due to their tunable structures. Since they are bendable and flexible, their assembly is less problematic compared to ISEs. However, their ionic conductivity is not very high. Recent trends on PSEs include polymer composites and the design of special structures that can enable Na^+ transfer at the molecular level. Although these are promising studies, they do not seem to be industrially applicable in the near future. To provide all the requirements mentioned above, recent research has focused on hybrid electrolyte systems. Hybrid electrolytes are systems that consist of binary combinations of liquid, quasi-solid, and solid electrolytes. They are significant in terms of maximizing the benefits and minimizing the restrictions of each component. When evaluated from a future perspective and considering the commercialization of SIBs, hybrid electrolytes can be counted as one of the most promising systems for obtaining high energy density, long life, improved safety, and reduced risks, because they can be prepared based on the application and requirements of the energy storage systems. SIBs can be used for stationary applications and the size/weight effect can be ignored by using the hybrid approach. Various types of liquid, quasi-solid, and solid electrolytes can be combined to increase the performance of the battery. To conclude, ionic conductivity, ion transference number, interface properties, stability, and rate capability of the advanced electrolytes for SIBs need to be improved regardless of the type of the electrolytes, and more research is needed to optimize the performance and improve commercial applications.

Author Contributions: Conceptualization, O.T. and H.A.K.T.; resources, O.T. and H.A.K.T.; writing—original draft preparation, O.T. and H.A.K.T.; writing—review and editing, O.T. and H.A.K.T.; supervision, O.T. and H.A.K.T.; project administration, H.A.K.T. All authors have read and agreed to the published version of the manuscript.

Funding: This research was funded by Yalova University, grant number 2022/AP/0007.

Data Availability Statement: Not applicable.

Conflicts of Interest: The authors declare no conflict of interest.

References

1. Palomares, V.; Casas-Cabanas, M.; Castillo-Martínez, E.; Han, M.H.; Rojo, T. Update on Na-Based Battery Materials. A Growing Research Path. *Energy Environ. Sci.* **2013**, *6*, 2312–2337. [[CrossRef](#)]
2. Hong, S.Y.; Kim, Y.; Park, Y.; Choi, A.; Choi, N.S.; Lee, K.T. Charge Carriers in Rechargeable Batteries: Na Ions vs. Li Ions. *Energy Environ. Sci.* **2013**, *6*, 2067–2081. [[CrossRef](#)]
3. Palomares, V.; Serras, P.; Villaluenga, I.; Hueso, K.B.; Carretero-González, J.; Rojo, T. Na-Ion Batteries, Recent Advances and Present Challenges to Become Low Cost Energy Storage Systems. *Energy Environ. Sci.* **2012**, *5*, 5884–5901. [[CrossRef](#)]
4. Pan, H.; Hu, Y.S.; Chen, L. Room-Temperature Stationary Sodium-Ion Batteries for Large-Scale Electric Energy Storage. *Energy Environ. Sci.* **2013**, *6*, 2338–2360. [[CrossRef](#)]
5. Yabuuchi, N.; Kubota, K.; Dahbi, M.; Komaba, S. Research Development on Sodium-Ion Batteries. *Chem. Rev.* **2014**, *114*, 11636–11682. [[CrossRef](#)]
6. Peters, J.; Buchholz, D.; Passerini, S.; Weil, M. Life Cycle Assessment of Sodium-Ion Batteries. *Energy Environ. Sci.* **2016**, *9*, 1744–1751. [[CrossRef](#)]
7. Slater, M.D.; Kim, D.; Lee, E.; Johnson, C.S. Sodium-Ion Batteries. *Adv. Funct. Mater.* **2013**, *23*, 947–958. [[CrossRef](#)]
8. Che, H.; Chen, S.; Xie, Y.; Wang, H.; Amine, K.; Liao, X.Z.; Ma, Z.F. Electrolyte Design Strategies and Research Progress for Room-Temperature Sodium-Ion Batteries. *Energy Environ. Sci.* **2017**, *10*, 1075–1101. [[CrossRef](#)]
9. Vignarooban, K.; Kushagra, R.; Elango, A.; Badami, P.; Mellander, B.E.; Xu, X.; Tucker, T.G.; Nam, C.; Kannan, A.M. Current Trends and Future Challenges of Electrolytes for Sodium-Ion Batteries. *Int. J. Hydrog. Energy* **2016**, *41*, 2829–2846. [[CrossRef](#)]
10. Ponrouch, A.; Monti, D.; Boschin, A.; Steen, B.; Johansson, P.; Palacín, M.R. Non-aqueous electrolytes for sodium-ion batteries. *J. Mater. Chem. A* **2015**, *3*, 22–42. [[CrossRef](#)]
11. Xu, X.; Wang, Y.; Yi, Q.; Wang, X.; Camacho, R.A.P.; Kungl, H.; Eichel, R.; Lu, L.; Zhang, H. Ion Conduction in Composite Polymer Electrolytes—Potential Electrolytes for Sodium-Ion Batteries. *ChemSusChem* **2023**, e202202152. [[CrossRef](#)] [[PubMed](#)]
12. Nurohmah, A.R.; Nisa, S.S.; Stulasti, K.N.R.; Yudha, C.S.; Suci, W.G.; Aliwarga, K.; Widiyandari, H.; Purwanto, A. Sodium-Ion Battery from Sea Salt: A Review. *Mater. Renew. Sustain. Energy* **2022**, *11*, 71–89. [[CrossRef](#)]

13. Maurya, D.K.; Dhanusuraman, R.; Guo, Z.; Angaiah, S. Composite Polymer Electrolytes: Progress, Challenges, and Future Outlook for Sodium-Ion Batteries. *Adv. Compos. Hybrid Mater.* **2022**, *5*, 2651–2674. [[CrossRef](#)]
14. Li, P.; Hu, N.; Wang, J.; Wang, S.; Deng, W. Recent Progress and Perspective: Na Ion Batteries Used at Low Temperatures. *Nanomaterials* **2022**, *12*, 3529. [[CrossRef](#)]
15. Peljo, P.; Girault, H.H. Electrochemical Potential Window of Battery Electrolytes: The HOMO–LUMO Misconception. *Energy Environ. Sci.* **2018**, *11*, 2306–2309. [[CrossRef](#)]
16. Gering, K.L. Prediction of Electrolyte Conductivity: Results from a Generalized Molecular Model Based on Ion Solvation and a Chemical Physics Framework. *Electrochim. Acta* **2017**, *225*, 175–189. [[CrossRef](#)]
17. Hayamizu, K.; Chiba, Y.; Haishi, T. Dynamic Ionic Radius of Alkali Metal Ions in Aqueous Solution: A Pulsed-Field Gradient NMR Study. *RSC Adv.* **2021**, *11*, 20252–20257. [[CrossRef](#)]
18. Ye, L.; Feng, Z. Polymer Electrolytes as Solid Solvents and Their Applications. In *Polymer Electrolytes: Fundamentals and Applications*; Woodhead Publishing Limited: Cambridge, UK, 2010.
19. Wang, Y.; Song, S.; Xu, C.; Hu, N.; Molenda, J.; Lu, L. Development of Solid-State Electrolytes for Sodium-Ion Battery—A Short Review. *Nano Mater. Sci.* **2019**, *1*, 91–100. [[CrossRef](#)]
20. Okamoto, Y.; Tsuzuki, S.; Tataru, R.; Ueno, K.; Dokko, K.; Watanabe, M. High Transference Number of Na Ion in Liquid-State Sulfolane Solvates of Sodium Bis(Fluorosulfonyl)Amide. *J. Phys. Chem. C* **2020**, *124*, 4459–4469. [[CrossRef](#)]
21. Watanabe, Y.; Ugata, Y.; Ueno, K.; Watanabe, M.; Dokko, K. Does Li-Ion Transport Occur Rapidly in Localized High-Concentration Electrolytes? *Phys. Chem. Chem. Phys.* **2023**, *25*, 3092–3099. [[CrossRef](#)] [[PubMed](#)]
22. Fu, H.; Yin, Q.; Huang, Y.; Sun, H.; Chen, Y.; Zhang, R.; Yu, Q.; Gu, L.; Duan, J.; Luo, W. Reducing Interfacial Resistance by Na-SiO₂ Composite Anode for NASICON-Based Solid-State Sodium Battery. *ACS Mater. Lett.* **2020**, *2*, 127–132. [[CrossRef](#)]
23. Deng, T.; Ji, X.; Zou, L.; Chiekezi, O.; Cao, L.; Fan, X.; Adebisi, T.R.; Chang, H.J.; Wang, H.; Li, B.; et al. Interfacial-Engineering-Enabled Practical Low-Temperature Sodium Metal Battery. *Nat. Nanotechnol.* **2022**, *17*, 269–277. [[CrossRef](#)] [[PubMed](#)]
24. Chen, L.; Venkatram, S.; Kim, C.; Batra, R.; Chandrasekaran, A.; Ramprasad, R. Electrochemical Stability Window of Polymeric Electrolytes. *Chem. Mater.* **2019**, *31*, 4598–4604. [[CrossRef](#)]
25. Takenaka, N.; Bouibes, A.; Yamada, Y.; Nagaoka, M.; Yamada, A. Frontiers in Theoretical Analysis of Solid Electrolyte Interphase Formation Mechanism. *Adv. Mater.* **2021**, *33*, 2100574. [[CrossRef](#)] [[PubMed](#)]
26. Kulova, T.L.; Skundin, A.M. Electrode/Electrolyte Interphases of Sodium-Ion Batteries. *Energy* **2022**, *15*, 8615. [[CrossRef](#)]
27. Song, J.; Xiao, B.; Lin, Y.; Xu, K.; Li, X. Interphases in Sodium-Ion Batteries. *Adv. Energy Mater.* **2018**, *8*, 1703082. [[CrossRef](#)]
28. Zhang, J.; Gai, J.; Song, K.; Chen, W. Advances in Electrode/Electrolyte Interphase for Sodium-Ion Batteries from Half Cells to Full Cells. *Cell Rep. Phys. Sci.* **2022**, *3*, 100868. [[CrossRef](#)]
29. Yao, P.; Yu, H.; Ding, Z.; Liu, Y.; Lu, J.; Lavorgna, M.; Wu, J.; Liu, X. Review on Polymer-Based Composite Electrolytes for Lithium Batteries. *Front. Chem.* **2019**, *7*, 522. [[CrossRef](#)]
30. Hou, W.; Guo, X.; Shen, X.; Amine, K.; Yu, H.; Lu, J. Solid Electrolytes and Interfaces in All-Solid-State Sodium Batteries: Progress and Perspective. *Nano Energy* **2018**, *52*, 279–291. [[CrossRef](#)]
31. Li, Z.-Y.; Li, Z.; Fu, J.-L.; Guo, X. Sodium-Ion Conducting Polymer Electrolytes. *Rare Met.* **2023**, *42*, 1–16. [[CrossRef](#)]
32. Li, Y.; Wu, F.; Li, Y.; Liu, M.; Feng, X.; Bai, Y.; Wu, C. Ether-Based Electrolytes for Sodium Ion Batteries. *Chem. Soc. Rev.* **2022**, *51*, 4484–4536. [[CrossRef](#)]
33. Suharto, Y.; Lee, Y.; Yu, J.S.; Choi, W.; Kim, K.J. Microporous Ceramic Coated Separators with Superior Wettability for Enhancing the Electrochemical Performance of Sodium-Ion Batteries. *J. Power Sources* **2018**, *376*, 184–190. [[CrossRef](#)]
34. Kim, H.; Hong, J.; Park, Y.-U.; Kim, J.; Hwang, I.; Kang, K. Sodium Storage Behavior in Natural Graphite Using Ether-Based Electrolyte Systems. *Adv. Funct. Mater.* **2015**, *25*, 534–541. [[CrossRef](#)]
35. Lei, S.; Zeng, Z.; Liu, M.; Zhang, H.; Cheng, S.; Xie, J. Balanced Solvation/de-Solvation of Electrolyte Facilitates Li-Ion Intercalation for Fast Charging and Low-Temperature Li-Ion Batteries. *Nano Energy* **2022**, *98*, 107265. [[CrossRef](#)]
36. Huang, Y.; Zhao, L.; Li, L.; Xie, M.; Wu, F.; Chen, R. Electrolytes and Electrolyte/Electrode Interfaces in Sodium-Ion Batteries: From Scientific Research to Practical Application. *Adv. Mater.* **2019**, *31*, 1808393. [[CrossRef](#)] [[PubMed](#)]
37. Eshetu, G.G.; Elia, G.A.; Armand, M.; Forsyth, M.; Komaba, S.; Rojo, T.; Passerini, S. Electrolytes and Interphases in Sodium-Based Rechargeable Batteries: Recent Advances and Perspectives. *Adv. Energy Mater.* **2020**, *10*, 2000093. [[CrossRef](#)]
38. Eshetu, G.G.; Grugeon, S.; Kim, H.; Jeong, S.; Wu, L.; Gachot, G.; Laruelle, S.; Armand, M.; Passerini, S. Comprehensive Insights into the Reactivity of Electrolytes Based on Sodium Ions. *ChemSusChem* **2016**, *9*, 462–471. [[CrossRef](#)]
39. Meng, J.; Jia, G.; Yang, H.; Wang, M. Recent Advances for SEI of Hard Carbon Anode in Sodium-Ion Batteries: A Mini Review. *Front. Chem.* **2022**, *10*, 1–7. [[CrossRef](#)]
40. Kamath, G.; Cutler, R.W.; Deshmukh, S.A.; Shakourian-Fard, M.; Parrish, R.; Huether, J.; Butt, D.P.; Xiong, H.; Sankaranarayanan, S.K.R.S. In Silico Based Rank-Order Determination and Experiments on Nonaqueous Electrolytes for Sodium Ion Battery Applications. *J. Phys. Chem. C* **2014**, *118*, 13406–13416. [[CrossRef](#)]
41. Komaba, S.; Murata, W.; Ishikawa, T.; Yabuuchi, N.; Ozeki, T.; Nakayama, T.; Ogata, A.; Gotoh, K.; Fujiwara, K. Electrochemical Na Insertion and Solid Electrolyte Interphase for Hard-Carbon Electrodes and Application to Na-Ion Batteries. *Adv. Funct. Mater.* **2011**, *21*, 3859–3867. [[CrossRef](#)]
42. Lu, H.; Wu, L.; Xiao, L.; Ai, X.; Yang, H.; Cao, Y. Investigation of the Effect of Fluoroethylene Carbonate Additive on Electrochemical Performance of Sb-Based Anode for Sodium-Ion Batteries. *Electrochim. Acta* **2016**, *190*, 402–408. [[CrossRef](#)]

43. Huang, J.; Guo, X.; Du, X.; Lin, X.; Huang, J.Q.; Tan, H.; Zhu, Y.; Zhang, B. Nanostructures of Solid Electrolyte Interphases and Their Consequences for Microsized Sn Anodes in Sodium Ion Batteries. *Energy Environ. Sci.* **2019**, *12*, 1550–1557. [[CrossRef](#)]
44. Zhang, J.; Wang, D.W.; Lv, W.; Zhang, S.; Liang, Q.; Zheng, D.; Kang, F.; Yang, Q.H. Achieving Superb Sodium Storage Performance on Carbon Anodes through an Ether-Derived Solid Electrolyte Interphase. *Energy Environ. Sci.* **2017**, *10*, 370–376. [[CrossRef](#)]
45. Sun, J.; Gunathilaka, I.E.; O'Dell, L.A.; Howlett, P.C.; Forsyth, M. High-Rate Formation Protocol Enables a High Ionic Conductivity SEI for Sodium-Ion Batteries. *J. Power Sources* **2023**, *554*, 232298. [[CrossRef](#)]
46. Dugas, R.; Ponrouch, A.; Gachot, G.; David, R.; Palacin, M.R.; Tarascon, J.M. Na Reactivity toward Carbonate-Based Electrolytes: The Effect of FEC as Additive. *J. Electrochem Soc.* **2016**, *163*, A2333. [[CrossRef](#)]
47. Hou, X.; Li, T.; Qiu, Y.; Jiang, M.; Zheng, Q.; Li, X. Weak Coulomb Interaction between Anions and Na⁺ during Solvation Enabling Desirable Solid Electrolyte Interphase and Superior Kinetics for HC-Based Sodium Ion Batteries. *Chem. Eng. J.* **2023**, *453*, 139932. [[CrossRef](#)]
48. Eshetu, G.G.; Martinez-Ibañez, M.; Sánchez-Diez, E.; Gracia, I.; Li, C.; Rodriguez-Martinez, L.M.; Rojo, T.; Zhang, H.; Armand, M. Electrolyte Additives for Room-Temperature, Sodium-Based, Rechargeable Batteries. *Chem. Asian J.* **2018**, *13*, 2770–2780. [[CrossRef](#)]
49. Eshetu, G.G.; Diemant, T.; Hekmatfar, M.; Grugeon, S.; Behm, R.J.; Laruelle, S.; Armand, M.; Passerini, S. Impact of the Electrolyte Salt Anion on the Solid Electrolyte Interphase Formation in Sodium Ion Batteries. *Nano Energy* **2019**, *55*, 327–340. [[CrossRef](#)]
50. Sun, Z.; Fu, W.; Liu, M.Z.; Lu, P.; Zhao, E.; Magasinski, A.; Liu, M.; Luo, S.; McDaniel, J.; Yushin, G. A Nanoconfined Iron(III) Fluoride Cathode in a NaDFOB Electrolyte: Towards High-Performance Sodium-Ion Batteries. *J. Mater. Chem. A Mater.* **2020**, *8*, 4091–4098. [[CrossRef](#)]
51. Tao, W.; Chen, J.; Xu, C.; Liu, S.; Fakudze, S.; Wang, J.; Wang, C. Nanostructured MoS₂ with Interlayer Controllably Regulated by Ionic Liquids/Cellulose for High-Capacity and Durable Sodium Storage Properties. *Small* **2023**, 2207397. [[CrossRef](#)]
52. Liu, Y.; Yao, Z.; Vanaphuti, P.; Yang, X.; Mei, L.; Zhu, X.; Liu, S.; Wang, Y. Stable Fast-Charging Sodium-Ion Batteries Achieved by a Carbomethoxy-Modified Disodium Organic Material. *Cell Rep. Phys. Sci.* **2023**, *4*, 101240. [[CrossRef](#)]
53. Yang, R.; Sun, L.; Liu, W.; Zhang, Y.; Cui, Y.; Du, Y.; Liu, S.; Wang, H.; Huang, M. Bio-Derived 3D TiO₂ Hollow Spheres with a Mesocrystal Nanostructure to Achieve Improved Electrochemical Performance of Na-Ion Batteries in Ether-Based Electrolytes. *J. Mater. Chem. A Mater.* **2019**, *7*, 3399–3407. [[CrossRef](#)]
54. Nacimiento, F.; Cabello, M.; Ortiz, G.F.; Alcántara, R.; Lavela, P.; Tirado, J.L. Morphological Adaptability of Graphitic Carbon Nanofibers to Enhance Sodium Insertion in a Diglyme-Based Electrolyte. *Dalton Trans.* **2019**, *48*, 5417–5424. [[CrossRef](#)] [[PubMed](#)]
55. Wang, S.; Chen, Y.; Jie, Y.; Lang, S.; Song, J.; Lei, Z.; Wang, S.; Ren, X.; Wang, D.; Li, X.; et al. Stable Sodium Metal Batteries via Manipulation of Electrolyte Solvation Structure. *Small Methods* **2020**, *4*, 1900856. [[CrossRef](#)]
56. Zhang, K.; Yoon, G.; Zhang, J.; Park, M.; Yang, J.; Kang, K.; Kang, Y.-M. Pseudocapacitive Behavior and Ultrafast Kinetics from Solvated Ion Cointercalation into MoS₂ for Its Alkali Ion Storage. *ACS Appl. Energy Mater.* **2019**, *2*, 3726–3735. [[CrossRef](#)]
57. Kim, H.; Hong, J.; Yoon, G.; Kim, H.; Park, K.-Y.; Park, M.-S.; Yoon, W.-S.; Kang, K. Sodium Intercalation Chemistry in Graphite. *Energy Environ. Sci.* **2015**, *8*, 2963–2969. [[CrossRef](#)]
58. Song, K.; Wang, X.; Xie, Z.; Zhao, Z.; Fang, Z.; Zhang, Z.; Luo, J.; Yan, P.; Peng, Z.; Chen, W. Ultrathin CuF₂-Rich Solid-Electrolyte Interphase Induced by Cation-Tailored Double Electrical Layer toward Durable Sodium Storage. *Angew. Chem. Int. Ed.* **2023**, *62*, e202216450. [[CrossRef](#)]
59. Yu, X.; Lu, T.; Li, X.; Qi, J.; Yuan, L.; Man, Z.; Zhuo, H. Realizing Outstanding Electrochemical Performance with Na₃V₂(PO₄)₂F₃ Modified with an Ionic Liquid for Sodium-Ion Batteries. *RSC Adv.* **2022**, *12*, 14007–14017. [[CrossRef](#)]
60. Yu, X.; Lu, T.; Li, X.; Qi, J.; Yuan, L.; Man, Z.; Zhuo, H. Ionic Liquid–Acrylic Acid Copolymer Derived Nitrogen–Boron Codoped Carbon-Covered Na₃V₂(PO₄)₂F₃ as Cathode Material of High-Performance Sodium-Ion Batteries. *Langmuir* **2022**, *38*, 7815–7824. [[CrossRef](#)]
61. Xu, X.; Si, L.; Zhou, X.; Tu, F.; Zhu, X.; Bao, J. Chemical bonding between antimony and ionic liquid derived nitrogen-doped carbon for sodium-ion battery. *J. Power Sources* **2017**, *349*, 37–44. [[CrossRef](#)]
62. Maça, R.R.; Etacheri, V. Effect of Vinylene Carbonate Electrolyte Additive on the Surface Chemistry and Pseudocapacitive Sodium-Ion Storage of TiO₂ Nanosheet Anodes. *Batteries* **2021**, *7*, 1. [[CrossRef](#)]
63. Zhang, X.; Ma, T.; Fang, T.; Gao, Y.; Gao, S.; Wang, W.; Liao, L. A Novel MoS₂@C Framework Architecture Composites with Three-Dimensional Cross-Linked Porous Carbon Supporting MoS₂ Nanosheets for Sodium Storage. *J. Alloys Compd.* **2020**, *818*, 152821. [[CrossRef](#)]
64. Dahbi, M.; Fukunishi, M.; Horiba, T.; Yabuuchi, N.; Yasuno, S.; Komaba, S. High Performance Red Phosphorus Electrode in Ionic Liquid-Based Electrolyte for Na-Ion Batteries. *J. Power Sources* **2017**, *363*, 404–412. [[CrossRef](#)]
65. Santamaría, C.; Morales, E.; del Rio, C.; Herradón, B.; Amarilla, J.M. Studies on Sodium-Ion Batteries: Searching for the Proper Combination of the Cathode Material, the Electrolyte and the Working Voltage. The Role of Magnesium Substitution in Layered Manganese-Rich Oxides, and Pyrrolidinium Ionic Liquid. *Electrochim. Acta* **2023**, *439*, 141654. [[CrossRef](#)]
66. Sun, Z.; Wang, B.; Boebinger, M.G.; Magasinski, A.; Jhulki, S.; Zhang, Y.; Fu, W.; McDowell, M.T.; Yushin, G. Stability of FeF₃-Based Sodium-Ion Batteries in Nonflammable Ionic Liquid Electrolytes at Room and Elevated Temperatures. *ACS Appl. Mater. Interfaces* **2022**, *14*, 33447–33456. [[CrossRef](#)]

67. Reber, D.; Grissa, R.; Becker, M.; Kühnel, R.S.; Battaglia, C. Anion Selection Criteria for Water-in-Salt Electrolytes. *Adv Energy Mater.* **2021**, *11*, 2002913. [[CrossRef](#)]
68. Bi, H.; Luo, Y.; Zhao, C.; Ma, L.; Huang, H. Graphene Oxide Suspension-Based Electrolyte Promotes the Cycling Performance of Aqueous Sodium-Ion Batteries through the Interaction between Metal Ions, Free Water Molecules and Functional Groups. *J. Power Sources* **2023**, *555*, 232380. [[CrossRef](#)]
69. Yang, W.; Wang, X.; Lu, S.; Gao, Y.; Gao, T.; Guo, T.; Xie, Q.; Ruan, Y. Bimetallic Synergies Help the Application of Sodium Vanadyl Phosphate in Aqueous Sodium-Ion Batteries Possible. *ChemSusChem* **2023**, e202202257. [[CrossRef](#)]
70. Nakamoto, K.; Sakamoto, R.; Nishimura, Y.; Xia, J.; Ito, M.; Okada, S. A Trifluoroacetate-Based Concentrated Electrolyte for Symmetrical Aqueous Sodium-Ion Battery with NASICON-Type $\text{Na}_2\text{VTi}(\text{PO}_4)_3$ Electrodes. *Electrochemistry* **2021**, *89*, 415–419. [[CrossRef](#)]
71. Sun, J.; O'Dell, L.A.; Armand, M.; Howlett, P.C.; Forsyth, M. Anion-Derived Solid-Electrolyte Interphase Enables Long Life Na-Ion Batteries Using Superconcentrated Ionic Liquid Electrolytes. *ACS Energy Lett.* **2021**, *6*, 2481–2490. [[CrossRef](#)]
72. Fiates, J.; Ratochinski, R.H.; Lourenço, T.C.; da Silva, J.L.F.; Dias, L.G. Fluoroalkoxyaluminate-Based Ionic Liquids as Electrolytes for Sodium-Ion Batteries. *J. Mol. Liq.* **2023**, *369*, 120919. [[CrossRef](#)]
73. Yang, M.; Luo, J.; Guo, X.; Chen, J.; Cao, Y.; Chen, W. Aqueous Rechargeable Sodium-Ion Batteries: From Liquid to Hydrogel. *Batteries* **2022**, *8*, 180. [[CrossRef](#)]
74. Kühnel, R.S.; Reber, D.; Battaglia, C. A High-Voltage Aqueous Electrolyte for Sodium-Ion Batteries. *ACS Energy Lett.* **2017**, *2*, 2005–2006. [[CrossRef](#)]
75. Ge, J.; Fan, L.; Rao, A.M.; Zhou, J.; Lu, B. Surface-Substituted Prussian Blue Analogue Cathode for Sustainable Potassium-Ion Batteries. *Nat. Sustain.* **2022**, *5*, 225–234. [[CrossRef](#)]
76. Ge, J.; Zhang, Y.; Xie, Z.; Xie, H.; Chen, W.; Lu, B. Tailored ZnF_2/ZnS -Rich Interphase for Reversible Aqueous Zn Batteries. *Nano Res.* **2023**. [[CrossRef](#)]
77. Guo, J.Z.; Yang, A.B.; Gu, Z.Y.; Wu, X.L.; Pang, W.L.; Ning, Q.L.; Li, W.H.; Zhang, J.P.; Su, Z.M. Quasi-Solid-State Sodium-Ion Full Battery with High-Power/Energy Densities. *ACS Appl. Mater. Interfaces* **2018**, *10*, 17903–17910. [[CrossRef](#)] [[PubMed](#)]
78. Janakiraman, S.; Surendran, A.; Ghosh, S.; Anandhan, S.; Venimadhav, A. Electroactive Poly(Vinylidene Fluoride) Fluoride Separator for Sodium Ion Battery with High Coulombic Efficiency. *Solid State Ion.* **2016**, *292*, 130–135. [[CrossRef](#)]
79. DeBlock, R.H.; Lai, C.-H.; Butts, D.M.; Dunn, B.S. Sodium-Ion Conducting Pseudosolid Electrolyte for Energy-Dense, Sodium-Metal Batteries. *J. Power Sources* **2023**, *554*, 232305. [[CrossRef](#)]
80. Zhang, Y.; Bakenov, Z.; Tan, T.; Huang, J. Polyacrylonitrile-Nanofiber-Based Gel Polymer Electrolyte for Novel Aqueous Sodium-Ion Battery Based on a $\text{Na}_4\text{Mn}_9\text{O}_{18}$ Cathode and Zn Metal Anode. *Polymers* **2018**, *10*, 853. [[CrossRef](#)]
81. Rani, M.A.A.; Hwang, J.; Matsumoto, K.; Hagiwara, R. Poly(Vinyl Chloride) Ionic Liquid Polymer Electrolyte Based on Bis(Fluorosulfonyl)Amide for Sodium Secondary Batteries. *J. Electrochem Soc.* **2017**, *164*, H5031. [[CrossRef](#)]
82. Chen, S.; Che, H.; Feng, F.; Liao, J.; Wang, H.; Yin, Y.; Ma, Z.F. Poly(Vinylene Carbonate)-Based Composite Polymer Electrolyte with Enhanced Interfacial Stability to Realize High-Performance Room-Temperature Solid-State Sodium Batteries. *ACS Appl. Mater. Interfaces* **2019**, *11*, 43056–43065. [[CrossRef](#)] [[PubMed](#)]
83. Wang, X.; Liu, Z.; Tang, Y.; Chen, J.; Mao, Z.; Wang, D. PVDF-HFP/PMMA/TPU-Based Gel Polymer Electrolytes Composed of Conductive $\text{Na}_3\text{Zr}_2\text{Si}_2\text{PO}_{12}$ Filler for Application in Sodium Ions Batteries. *Solid State Ion.* **2021**, *359*, 115532. [[CrossRef](#)]
84. Gebert, F.; Knott, J.; Gorkin, R.; Chou, S.L.; Dou, S.X. Polymer Electrolytes for Sodium-Ion Batteries. *Energy Storage Mater.* **2021**, *36*, 10–30. [[CrossRef](#)]
85. Ma, J.; Feng, X.; Wu, Y.; Wang, Y.; Liu, P.; Shang, K.; Jiang, H.; Hou, X.; Mitlin, D.; Xiang, H. Stable Sodium Anodes for Sodium Metal Batteries (SMBs) Enabled by in-Situ Formed Quasi Solid-State Polymer Electrolyte. *J. Energy Chem.* **2023**, *77*, 290–299. [[CrossRef](#)]
86. Yang, M.; Feng, F.; Shi, Z.; Guo, J.; Wang, R.; Xu, Z.; Liu, Z.; Cai, T.; Wang, Z.; Wang, C.; et al. Facile Design of Asymmetric Flame-Retardant Gel Polymer Electrolyte with Excellent Interfacial Stability for Sodium Metal Batteries. *Energy Storage Mater.* **2023**, *56*, 611–620. [[CrossRef](#)]
87. Colò, F.; Bella, F.; Nair, J.R.; Gerbaldi, C. Light-Cured Polymer Electrolytes for Safe, Low-Cost and Sustainable Sodium-Ion Batteries. *J. Power Sources* **2017**, *365*, 293–302. [[CrossRef](#)]
88. Parveen, S.; Sehrawat, P.; Hashmi, S.A. Triglyme-Based Solvate Ionic Liquid Gelled in a Polymer: A Novel Electrolyte Composition for Sodium Ion Battery. *Mater. Today Commun.* **2022**, *31*, 103392. [[CrossRef](#)]
89. Zhao, C.d.; Guo, J.Z.; Gu, Z.Y.; Wang, X.T.; Zhao, X.X.; Li, W.H.; Yu, H.Y.; Wu, X.L. Flexible Quasi-Solid-State Sodium-Ion Full Battery with Ultralong Cycle Life, High Energy Density and High-Rate Capability. *Nano Res.* **2022**, *15*, 925–932. [[CrossRef](#)]
90. Zhu, Y.; Yang, Y.; Fu, L.; Wu, Y. A Porous Gel-Type Composite Membrane Reinforced by Nonwoven: Promising Polymer Electrolyte with High Performance for Sodium Ion Batteries. *Electrochim. Acta* **2017**, *224*, 405–411. [[CrossRef](#)]
91. Zheng, Z.; Zhang, X.; Shi, W.; Liang, S.; Cao, H.; Fu, Y.; Wang, H.; Zhu, Y. A P(VDF-HFP) and Nonwoven-Fabric Based Composite as High-Performance Gel Polymer Electrolyte for Fast-Charging Sodium Metal Batteries. *Polymers* **2023**, *269*, 125751. [[CrossRef](#)]
92. Lei, D.; He, Y.B.; Huang, H.; Yuan, Y.; Zhong, G.; Zhao, Q.; Hao, X.; Zhang, D.; Lai, C.; Zhang, S.; et al. Cross-Linked Beta Alumina Nanowires with Compact Gel Polymer Electrolyte Coating for Ultra-Stable Sodium Metal Battery. *Nat. Commun.* **2019**, *10*, 4244. [[CrossRef](#)] [[PubMed](#)]

93. Zhao, Y.; Liu, H.; Meng, X.; Liu, A.; Chen, Y.; Ma, T. A Cross-Linked Tin Oxide/Polymer Composite Gel Electrolyte with Adjustable Porosity for Enhanced Sodium Ion Batteries. *Chem. Eng. J.* **2022**, *431*, 133922. [[CrossRef](#)]
94. Saroja, A.P.V.K.; Kumar, A.; Moharana, B.C.; Kamaraj, M.; Ramaprabhu, S. Design of Porous Calcium Phosphate Based Gel Polymer Electrolyte for Quasi-Solid State Sodium Ion Battery. *J. Electroanal. Chem.* **2020**, *859*, 113864. [[CrossRef](#)]
95. Lai, H.; Lu, Y.; Zha, W.; Hu, Y.; Zhang, Y.; Wu, X.; Wen, Z. In Situ Generated Composite Gel Polymer Electrolyte with Crosslinking Structure for Dendrite-Free and High-Performance Sodium Metal Batteries. *Energy Storage Mater.* **2023**, *54*, 478–487. [[CrossRef](#)]
96. Chen, G.; Zhang, K.; Liu, Y.; Ye, L.; Gao, Y.; Lin, W.; Xu, H.; Wang, X.; Bai, Y.; Wu, C. Flame-Retardant Gel Polymer Electrolyte and Interface for Quasi-Solid-State Sodium Ion Batteries. *Chem. Eng. J.* **2020**, *401*, 126065. [[CrossRef](#)]
97. Zheng, J.; Li, W.; Zhang, J.; Sun, Y.; Chen, W. Effects of Flexible Group Length of Phosphonate Monomers on the Performance of Gel Polymer Electrolytes for Sodium-Ion Batteries with Ultralong Cycling Life. *ACS Sustain. Chem. Eng.* **2022**, *10*, 7158–7168. [[CrossRef](#)]
98. Sehrawat, P.; Parveen, S.; Hashmi, S.A. High-Performance Sodium Ion Conducting Gel Polymer Electrolyte Based on a Biodegradable Polymer Polycaprolactone. *Energy Storage* **2022**, e375. [[CrossRef](#)]
99. Liu, D.; Du, G.; Qi, Y.; Niu, Y.; Bao, S.; Xu, M. Bacterial Cellulose Network Based Gel Polymer Electrolyte for Quasi-Solid-State Sodium-Ion Battery. *J. Mater. Sci. Mater. Electron.* **2022**, *33*, 15313–15322. [[CrossRef](#)]
100. Mittal, N.; Tien, S.; Lizundia, E.; Niederberger, M. Hierarchical Nanocellulose-Based Gel Polymer Electrolytes for Stable Na Electrodeposition in Sodium Ion Batteries. *Small* **2022**, *18*, 2107183. [[CrossRef](#)]
101. Chen, J.; Luo, C.; Huang, Y.; Liu, J.; Li, C.; Zhao, Z.; Xu, X.; Zheng, H.; Tang, Z.; Li, X.; et al. Hydroxypropyl Methyl Cellulose-Based Gel Polymer Electrolyte Provides a Fast Migration Channel for Sodium-Ion Batteries. *J. Mater. Sci.* **2022**, *57*, 4311–4322. [[CrossRef](#)]
102. Cai, S.; Meng, W.; Tian, H.; Luo, T.; Wang, L.; Li, M.; Luo, J.; Liu, S. Artificial Porous Heterogeneous Interface for All-Solid-State Sodium Ion Battery. *J. Colloid Interface Sci.* **2023**, *632*, 179–185. [[CrossRef](#)] [[PubMed](#)]
103. Ma, Q.; Tietz, F. Solid-State Electrolyte Materials for Sodium Batteries: Towards Practical Applications. *ChemElectroChem* **2020**, *7*, 2691–2713. [[CrossRef](#)]
104. Zhao, C.; Liu, L.; Qi, X.; Lu, Y.; Wu, F.; Zhao, J.; Yu, Y.; Hu, Y.S.; Chen, L. Solid-State Sodium Batteries. *Adv. Energy Mater.* **2018**, *8*, 1703012. [[CrossRef](#)]
105. Delmas, C. Sodium and Sodium-Ion Batteries: 50 Years of Research. *Adv. Energy Mater.* **2018**, *8*, 1703137. [[CrossRef](#)]
106. Goodenough, J.B.; Hong, H.Y.P.; Kafalas, J.A. Fast Na⁺-Ion Transport in Skeleton Structures. *Mater. Res. Bull.* **1976**, *11*, 203–220. [[CrossRef](#)]
107. Li, C.; Li, R.; Liu, K.; Si, R.; Zhang, Z.; Hu, Y.-S. NaSICON: A Promising Solid Electrolyte for Solid-State Sodium Batteries. *Interdiscip. Mater.* **2022**, *1*, 396–416. [[CrossRef](#)]
108. Samiee, M.; Radhakrishnan, B.; Rice, Z.; Deng, Z.; Meng, Y.S.; Ong, S.P.; Luo, J. Divalent-Doped Na₃Zr₂Si₂PO₁₂ Natrium Superionic Conductor: Improving the Ionic Conductivity via Simultaneously Optimizing the Phase and Chemistry of the Primary and Secondary Phases. *J. Power Sources* **2017**, *347*, 229–237. [[CrossRef](#)]
109. Zhang, Z.; Zou, Z.; Kaup, K.; Xiao, R.; Shi, S.; Avdeev, M.; Hu, Y.S.; Wang, D.; He, B.; Li, H.; et al. Correlated Migration Invokes Higher Na⁺-Ion Conductivity in NaSICON-Type Solid Electrolytes. *Adv. Energy Mater.* **2019**, *9*, 1902373. [[CrossRef](#)]
110. Zhang, L.; Liu, Y.; You, Y.; Vinu, A.; Mai, L. NASICONs-Type Solid-State Electrolytes: The History, Physicochemical Properties, and Challenges. *Interdiscip. Mater.* **2023**, *2*, 91–110. [[CrossRef](#)]
111. Singh, K.; Chakraborty, A.; Thirupathi, R.; Omar, S. Recent Advances in NASICON-Type Oxide Electrolytes for Solid-State Sodium-Ion Rechargeable Batteries. *Ionics* **2022**, *28*, 5289–5319. [[CrossRef](#)]
112. Yang, Z.; Tang, B.; Xie, Z.; Zhou, Z. NASICON-Type Na₃Zr₂Si₂PO₁₂ Solid-State Electrolytes for Sodium Batteries. *ChemElectroChem* **2021**, *8*, 1035–1047. [[CrossRef](#)]
113. Pal, S.K.; Saha, R.; Kumar, G.V.; Omar, S. Designing High Ionic Conducting NASICON-Type Na₃Zr₂Si₂PO₁₂ Solid-Electrolytes for Na-Ion Batteries. *J. Phys. Chem. C* **2020**, *124*, 9161–9169. [[CrossRef](#)]
114. Miao, R.J.; Cao, X.G.; Wang, W.G.; Zhang, H.Y. Influence of Bi₂O₃ Additive on the Electrochemical Performance of Na₃Y_{0.1}Zr_{1.9}Si₂PO₁₂ Inorganic Solid Electrolyte. *Ceram Int.* **2021**, *47*, 17455–17462. [[CrossRef](#)]
115. Jiang, P.; Du, G.; Shi, Y.; She, F.; Guo, P.; Qian, G.; Lu, X.; Xie, F.; Lu, X. Ultrafast Sintering of Na₃Zr₂Si₂PO₁₂ Solid Electrolyte for Long Lifespan Solid-State Sodium Ion Batteries. *Chem. Eng. J.* **2023**, *451*, 138771. [[CrossRef](#)]
116. Shindrov, A.A. Increasing Sinterability and Ionic Conductivity of Na₃Zr₂Si₂PO₁₂ Ceramics by High Energy Ball-Milling. *Solid State Ion.* **2023**, *391*, 116139. [[CrossRef](#)]
117. Noguchi, Y.; Kobayashi, E.; Plashnitsa, L.S.; Okada, S.; Yamaki, J.I. Fabrication and Performances of All Solid-State Symmetric Sodium Battery Based on NASICON-Related Compounds. *Electrochim. Acta* **2013**, *101*, 59–65. [[CrossRef](#)]
118. Zhang, Q.; Zhou, Q.; Lu, Y.; Shao, Y.; Qi, Y.; Qi, X.; Zhong, G.; Yang, Y.; Chen, L.; Hu, Y.S. Modification of NASICON Electrolyte and Its Application in Real Na-Ion Cells. *Engineering* **2022**, *8*, 170–180. [[CrossRef](#)]
119. Lu, Y.; Alonso, J.A.; Yi, Q.; Lu, L.; Wang, Z.L.; Sun, C. A High-Performance Monolithic Solid-State Sodium Battery with Ca²⁺-Doped Na₃Zr₂Si₂PO₁₂ Electrolyte. *Adv. Energy Mater.* **2019**, *9*, 1901205. [[CrossRef](#)]
120. Jolley, A.G.; Cohn, G.; Hitz, G.T.; Wachsman, E.D. Improving the Ionic Conductivity of NASICON through Aliovalent Cation Substitution of Na₃Zr₂Si₂PO₁₂. *Ionics* **2015**, *21*, 3031–3038. [[CrossRef](#)]

121. Wang, X.; Chen, J.; Mao, Z.; Wang, D. Effective Resistance to Dendrite Growth of NASICON Solid Electrolyte with Lower Electronic Conductivity. *Chem. Eng. J.* **2022**, *427*, 130899. [[CrossRef](#)]
122. Chen, D.; Luo, F.; Zhou, W.; Zhu, D. Influence of Nb⁵⁺, Ti⁴⁺, Y³⁺ and Zn²⁺ Doped Na₃Zr₂Si₂PO₁₂ Solid Electrolyte on Its Conductivity. *J. Alloys Compd.* **2018**, *757*, 348–355. [[CrossRef](#)]
123. Liu, Y.; Liu, L.; Peng, J.; Zhou, X.; Liang, D.; Zhao, L.; Su, J.; Zhang, B.; Li, S.; Zhang, N.; et al. A Niobium-Substituted Sodium Superionic Conductor with Conductivity Higher than 5.5 MS Cm^{−1} Prepared by Solution-Assisted Solid-State Reaction Method. *J. Power Sources* **2022**, *518*, 230765. [[CrossRef](#)]
124. Li, D.; Sun, C.; Wang, C.; Li, J.; Wang, Z.; Jin, H. Regulating Na/NASICON Electrolyte Interface Chemistry for Stable Solid-State Na Metal Batteries at Room Temperature. *Energy Storage Mater.* **2023**, *54*, 403–409. [[CrossRef](#)]
125. Yang, J.; Liu, G.; Avdeev, M.; Wan, H.; Han, F.; Shen, L.; Zou, Z.; Shi, S.; Hu, Y.S.; Wang, C.; et al. Ultrastable All-Solid-State Sodium Rechargeable Batteries. *ACS Energy Lett.* **2020**, *5*, 2835–2841. [[CrossRef](#)]
126. Luo, J.; Zhao, G.; Qiang, W.; Huang, B. Synthesis of Na Ion-Electron Mixed Conductor Na₃Zr₂Si₂PO₁₂ by Doping with Transition Metal Elements (Co, Fe, Ni). *J. Am. Ceram. Soc.* **2022**, *105*, 3428–3437. [[CrossRef](#)]
127. Zhang, Z.; Zhang, Q.; Shi, J.; Chu, Y.S.; Yu, X.; Xu, K.; Ge, M.; Yan, H.; Li, W.; Gu, L.; et al. A Self-Forming Composite Electrolyte for Solid-State Sodium Battery with Ultralong Cycle Life. *Adv. Energy Mater.* **2017**, *7*, 1601196. [[CrossRef](#)]
128. Ruan, Y.; Song, S.; Liu, J.; Liu, P.; Cheng, B.; Song, X.; Battaglia, V. Improved Structural Stability and Ionic Conductivity of Na₃Zr₂Si₂PO₁₂ Solid Electrolyte by Rare Earth Metal Substitutions. *Ceram. Int.* **2017**, *43*, 7810–7815. [[CrossRef](#)]
129. Sun, F.; Xiang, Y.; Sun, Q.; Zhong, G.; Banis, M.N.; Liu, Y.; Li, R.; Fu, R.; Zheng, M.; Sham, T.K.; et al. Origin of High Ionic Conductivity of Sc-Doped Sodium-Rich NASICON Solid-State Electrolytes. *Adv. Funct. Mater.* **2021**, *31*, 2102129. [[CrossRef](#)]
130. Wang, Q.; Yu, C.; Li, L.; Liu, X.; Zhang, X.; Gao, G.; Wang, Y.; Li, G. Sc-Doping in Na₃Zr₂Si₂PO₁₂ Electrolytes Enables Preeminent Performance of Solid-State Sodium Batteries in a Wide Temperature Range. *Energy Storage Mater.* **2023**, *54*, 135–145. [[CrossRef](#)]
131. Thirupathi, R.; Omar, S. A Strategic Co-Doping Approach Using Sc³⁺ and Ce⁴⁺ toward Enhanced Conductivity in NASICON-Type Na₃Zr₂Si₂PO₁₂. *J. Phys. Chem. C* **2021**, *125*, 27723–27735. [[CrossRef](#)]
132. Ran, L.; Baktash, A.; Li, M.; Yin, Y.; Demir, B.; Lin, T.; Li, M.; Rana, M.; Gentle, I.; Wang, L.; et al. Sc, Ge Co-Doping NASICON Boosts Solid-State Sodium Ion Batteries' Performance. *Energy Storage Mater.* **2021**, *40*, 282–291. [[CrossRef](#)]
133. Zhao, Y.; Wang, C.; Dai, Y.; Jin, H. Homogeneous Na⁺ Transfer Dynamic at Na/Na₃Zr₂Si₂PO₁₂ Interface for All Solid-State Sodium Metal Batteries. *Nano Energy* **2021**, *88*, 106293. [[CrossRef](#)]
134. Noi, K.; Suzuki, K.; Tanibata, N.; Hayashi, A.; Tatsumisago, M. Liquid-Phase Sintering of Highly Na⁺ Ion Conducting Na₃Zr₂Si₂PO₁₂ Ceramics Using Na₃BO₃ Additive. *J. Am. Ceram. Soc.* **2018**, *101*, 1255–1265. [[CrossRef](#)]
135. He, S.; Xu, Y.; Ma, X.; Chen, Y.; Lin, J.; Wang, C. Mg²⁺/F[−] Synergy to Enhance the Ionic Conductivity of Na₃Zr₂Si₂PO₁₂ Solid Electrolyte for Solid-State Sodium Batteries. *ChemElectroChem* **2020**, *7*, 2087–2094. [[CrossRef](#)]
136. Cao, X.G.; Zhang, X.H.; Tao, T.; Zhang, H.Y. Effects of Antimony Tin Oxide (ATO) Additive on the Properties of Na₃Zr₂Si₂PO₁₂ Ceramic Electrolytes. *Ceram. Int.* **2020**, *46*, 8405–8412. [[CrossRef](#)]
137. Wang, C.; Sun, C.; Sun, Z.; Wang, B.; Song, T.; Zhao, Y.; Li, J.; Jin, H. Optimizing the Na Metal/Solid Electrolyte Interface through a Grain Boundary Design. *J. Mater. Chem. A Mater.* **2022**, *10*, 5280–5286. [[CrossRef](#)]
138. Zhou, P.; Sun, K.; Ji, S.; Zhao, Z.; Fu, Y.; Xia, J.; Wu, S.; Zhu, Y.; Hui, K.N.; Li, H.-F. MgF₂ as an Effective Additive for Improving Ionic Conductivity of Ceramic Solid Electrolytes. *Mater. Today Energy* **2023**, *32*, 101248. [[CrossRef](#)]
139. Oh, J.A.S.; He, L.; Plewa, A.; Morita, M.; Zhao, Y.; Sakamoto, T.; Song, X.; Zhai, W.; Zeng, K.; Lu, L. Composite NASICON (Na₃Zr₂Si₂PO₁₂) Solid-State Electrolyte with Enhanced Na⁺ Ionic Conductivity: Effect of Liquid Phase Sintering. *ACS Appl. Mater. Interfaces* **2019**, *11*, 40125–40133. [[CrossRef](#)]
140. Lou, S.; Zhang, F.; Fu, C.; Chen, M.; Ma, Y.; Yin, G.; Wang, J. Interface Issues and Challenges in All-Solid-State Batteries: Lithium, Sodium, and Beyond. *Adv. Mater.* **2021**, *33*, 2000721. [[CrossRef](#)]
141. Yang, J.; Wan, H.L.; Zhang, Z.H.; Liu, G.Z.; Xu, X.X.; Hu, Y.S.; Yao, X.Y. NASICON-Structured Na_{3.1}Zr_{1.95}Mg_{0.05}Si₂PO₁₂ Solid Electrolyte for Solid-State Sodium Batteries. *Rare Met.* **2018**, *37*, 480–487. [[CrossRef](#)]
142. Sampathkumar, R.; Echeverría, M.; Zhang, Y.; Armand, M.; Galceran, M. Interface Stability between Na₃Zr₂Si₂PO₁₂ Solid Electrolyte and Sodium Metal Anode for Quasi-Solid-State Sodium Battery. *Batteries* **2023**, *9*, 8. [[CrossRef](#)]
143. Kehne, P.; Guhl, C.; Ma, Q.; Tietz, F.; Alff, L.; Hausbrand, R.; Komissinskiy, P. Sc-Substituted Nasicon Solid Electrolyte for an All-Solid-State Na_xCoO₂/Nasicon/Na Sodium Model Battery with Stable Electrochemical Performance. *J. Power Sources* **2019**, *409*, 86–93. [[CrossRef](#)]
144. Uchida, Y.; Hasegawa, G.; Shima, K.; Inada, M.; Enomoto, N.; Akamatsu, H.; Hayashi, K. Insights into Sodium Ion Transfer at the Na/NASICON Interface Improved by Uniaxial Compression. *ACS Appl. Energy Mater.* **2019**, *2*, 2913–2920. [[CrossRef](#)]
145. Miao, X.; Di, H.; Ge, X.; Zhao, D.; Wang, P.; Wang, R.; Wang, C.; Yin, L. AlF₃-Modified Anode-Electrolyte Interface for Effective Na Dendrites Restriction in NASICON-Based Solid-State Electrolyte. *Energy Storage Mater.* **2020**, *30*, 170–178. [[CrossRef](#)]
146. Jung, S.W.; Wang, J.E.; Kim, D.G.; Ma, H.J.; Kim, D.K.; Kim, D.J. Rare-Earth Element Substitution of Na_{1+x}Zr₂Si₂P₃-XO₁₂ (x = 2) Solid Electrolyte: Implications for All-Solid-State Na Ion Batteries. *ACS Appl. Nano Mater.* **2022**, *5*, 13894–13902. [[CrossRef](#)]
147. Grady, Z.M.; Tsuji, K.; Ndayishimiye, A.; Hwan-Seo, J.; Randall, C.A. Densification of a Solid-State NASICON Sodium-Ion Electrolyte below 400 °C by Cold Sintering with a Fused Hydroxide Solvent. *ACS Appl. Energy Mater.* **2020**, *3*, 4356–4366. [[CrossRef](#)]

148. Okubo, K.; Wang, H.; Hayashi, K.; Inada, M.; Enomoto, N.; Hasegawa, G.; Osawa, T.; Takamura, H. A Dense NASICON Sheet Prepared by Tape-Casting and Low Temperature Sintering. *Electrochim. Acta* **2018**, *278*, 176–181. [[CrossRef](#)]
149. Suzuki, K.; Noi, K.; Hayashi, A.; Tatsumisago, M. Low Temperature Sintering of Na⁺ + XZr₂Si₆P₃ – XO₁₂ by the Addition of Na₃BO₃. *Scr. Mater.* **2018**, *145*, 67–70. [[CrossRef](#)]
150. Gadjourova, Z.; Andreev, Y.G.; Tunstall, D.P.; Bruce, P.G. Ionic Conductivity in Crystalline Polymer Electrolytes. *Nature* **2001**, *412*, 520–523. [[CrossRef](#)]
151. Xiao, Z.; Zhou, B.; Wang, J.; Zuo, C.; He, D.; Xie, X.; Xue, Z. PEO-Based Electrolytes Blended with Star Polymers with Precisely Imprinted Polymeric Pseudo-Crown Ether Cavities for Alkali Metal Ion Batteries. *J. Memb. Sci.* **2019**, *576*, 182–189. [[CrossRef](#)]
152. Boschin, A.; Johansson, P. Characterization of NaX (X: TFSI, FSI)—PEO Based Solid Polymer Electrolytes for Sodium Batteries. *Electrochim. Acta* **2015**, *175*, 124–133. [[CrossRef](#)]
153. Devi, C.; Gellanki, J.; Pettersson, H.; Kumar, S. High Sodium Ionic Conductivity in PEO/PVP Solid Polymer Electrolytes with InAs Nanowire Fillers. *Sci. Rep.* **2021**, *11*, 20180. [[CrossRef](#)] [[PubMed](#)]
154. Zhang, Z.; Zhang, Q.; Ren, C.; Luo, F.; Ma, Q.; Hu, Y.-S.; Zhou, Z.; Li, H.; Huang, X.; Chen, L. A Ceramic/Polymer Composite Solid Electrolyte for Sodium Batteries. *J. Mater. Chem. A Mater.* **2016**, *4*, 15823–15828. [[CrossRef](#)]
155. Zhao, Y.; Meng, X.; Kang, Q.; Yan, L.; Ye, X.; Zhang, J.; Liu, H.; Han, Q.; Chen, Y.; Ma, T. Integrating a Three-Dimensional Cu₂MoS₄ Electrode and Solid-State Polymer Electrolyte for Sodium-Ion Batteries. *Chem. Eng. J.* **2022**, *450*, 137903. [[CrossRef](#)]
156. Colò, F.; Bella, F.; Nair, J.R.; Destro, M.; Gerbaldi, C. Cellulose-Based Novel Hybrid Polymer Electrolytes for Green and Efficient Na-Ion Batteries. *Electrochim. Acta* **2015**, *174*, 185–190. [[CrossRef](#)]
157. Chen, G.; Ye, L.; Zhang, K.; Gao, M.; Lu, H.; Xu, H.; Bai, Y.; Wu, C. Hyperbranched Polyether Boosting Ionic Conductivity of Polymer Electrolytes for All-Solid-State Sodium Ion Batteries. *Chem. Eng. J.* **2020**, *394*, 124885. [[CrossRef](#)]
158. Ni'Mah, Y.L.; Cheng, M.Y.; Cheng, J.H.; Rick, J.; Hwang, B.J. Solid-State Polymer Nanocomposite Electrolyte of TiO₂/PEO/NaClO₄ for Sodium Ion Batteries. *J. Power Sources* **2015**, *278*, 375–381. [[CrossRef](#)]
159. Qi, X.; Ma, Q.; Liu, L.; Hu, Y.-S.; Li, H.; Zhou, Z.; Huang, X.; Chen, L. Sodium Bis(Fluorosulfonyl)Imide/Poly(Ethylene Oxide) Polymer Electrolytes for Sodium-Ion Batteries. *ChemElectroChem* **2016**, *3*, 1741–1745. [[CrossRef](#)]
160. Zhou, Z.; Tao, Z.; Zhang, L.; Zheng, X.; Xiao, X.; Liu, Z.; Li, X.; Liu, G.; Zhao, P.; Zhang, P. Scalable Manufacturing of Solid Polymer Electrolytes with Superior Room-Temperature Ionic Conductivity. *ACS Appl. Mater. Interfaces* **2022**, *14*, 32994–33003. [[CrossRef](#)]
161. Schauser, N.S.; Seshadri, R.; Segalman, R.A. Multivalent Ion Conduction in Solid Polymer Systems. *Mol. Syst. Des. Eng.* **2019**, *4*. [[CrossRef](#)]
162. Liang, X.; Liu, Z.; Cao, Y.; Yang, L.; Jiang, Y.; Lei, Y.; Yuan, T.; Lu, H.; Feng, J. Novel Sodium–poly(Tartaric Acid)Borate-Based Single-Ion Conducting Polymer Electrolyte for Sodium–metal Batteries. *ACS Appl. Energy Mater.* **2020**, *3*, 10053–10060. [[CrossRef](#)]
163. Pritam; Arya, A.; Sharma, A.L. Selection of Best Composition of Na⁺ Ion Conducting PEO-PEI Blend Solid Polymer Electrolyte Based on Structural, Electrical, and Dielectric Spectroscopic Analysis. *Ionics* **2020**, *26*, 745–766. [[CrossRef](#)]
164. Makhlooghiyazad, F.; Nti, F.; Sun, J.; Mendes, T.C.; Malunavar, S.S.; Pringle, J.M.; Forsyth, M. Composite Electrolytes Based on Electrospun PVDF and Ionic Plastic Crystal Matrices for Na-Metal Battery Applications. *J. Phys. Mater.* **2021**, *4*, 034003. [[CrossRef](#)]
165. Kim, J.-K.; Lim, Y.J.; Kim, H.; Cho, G.-B.; Kim, Y. A Hybrid Solid Electrolyte for Flexible Solid-State Sodium Batteries. *Energy Environ. Sci.* **2015**, *8*, 3589–3596. [[CrossRef](#)]
166. Zhang, H.; Qin, B.; Han, J.; Passerini, S. Aqueous/Nonaqueous Hybrid Electrolyte for Sodium-Ion Batteries. *ACS Energy Lett.* **2018**, *3*, 1769–1770. [[CrossRef](#)]
167. Shen, Y.; Han, X.; Cai, T.; Hu, H.; Li, Y.; Zhao, L.; Hu, H.; Xue, Q.; Zhao, Y.; Zhou, J.; et al. High-Performance Aqueous Sodium-Ion Battery Using a Hybrid Electrolyte with a Wide Electrochemical Stability Window. *RSC Adv.* **2020**, *10*, 25496–25499. [[CrossRef](#)] [[PubMed](#)]
168. Hwang, J.; Yang, H.; Matsumoto, K.; Hagiwara, R. Benefits of the Mixtures of Ionic Liquid and Organic Electrolytes for Sodium-Ion Batteries. *J. Electrochem. Soc.* **2021**, *168*, 030508. [[CrossRef](#)]
169. Monti, D.; Ponrouch, A.; Palacín, M.R.; Johansson, P. Towards Safer Sodium-Ion Batteries via Organic Solvent/Ionic Liquid Based Hybrid Electrolytes. *J. Power Sources* **2016**, *324*, 712–721. [[CrossRef](#)]
170. Karlsmo, M.; Bouchal, R.; Johansson, P. High-Performant All-Organic Aqueous Sodium-Ion Batteries Enabled by PTCDA Electrodes and a Hybrid Na/Mg Electrolyte. *Angew. Chem. Int. Ed.* **2021**, *60*, 24709–24715. [[CrossRef](#)]
171. Wang, H.; Liu, T.; Du, X.; Wang, J.; Yang, Y.; Qiu, H.; Lu, G.; Li, H.; Chen, Z.; Zhao, J.; et al. Hybrid Electrolytes Enabling In-Situ Interphase Protection and Suppressed Electrode Dissolution for Aqueous Sodium-Ion Batteries. *Batter Supercaps* **2022**, *5*, e202200246. [[CrossRef](#)]
172. Senthilkumar, S.T.; Abirami, M.; Kim, J.; Go, W.; Hwang, S.M.; Kim, Y. Sodium-Ion Hybrid Electrolyte Battery for Sustainable Energy Storage Applications. *J. Power Sources* **2017**, *341*, 404–410. [[CrossRef](#)]
173. Kim, Y.; Künzel, M.; Steinle, D.; Dong, X.; Kim, G.-T.; Varzi, A.; Passerini, S. Anode-Less Seawater Batteries with a Na-Ion Conducting Solid-Polymer Electrolyte for Power to Metal and Metal to Power Energy Storage. *Energy Environ. Sci.* **2022**, *15*, 2610–2618. [[CrossRef](#)]
174. Martínez-Cisneros, C.S.; Pandit, B.; Antonelli, C.; Sanchez, J.Y.; Levenfeld, B.; Varez, A. Development of Sodium Hybrid Quasi-Solid Electrolytes Based on Porous NASICON and Ionic Liquids. *J. Eur. Ceram Soc.* **2021**, *41*, 7723–7733. [[CrossRef](#)]

175. Shen, L.; Deng, S.; Jiang, R.; Liu, G.; Yang, J.; Yao, X. Flexible Composite Solid Electrolyte with 80 Wt% Na_{3.4}Zr_{1.9}Zn_{0.1}Si_{2.2}P_{0.8}O₁₂ for Solid-State Sodium Batteries. *Energy Storage Mater.* **2022**, *46*, 175–181. [[CrossRef](#)]
176. de la Torre-Gamarra, C.; Appetecchi, G.B.; Ulissi, U.; Varzi, A.; Varez, A.; Passerini, S. Na₃Si₂Y_{0.16}Zr_{1.84}PO₁₂-Ionic Liquid Hybrid Electrolytes: An Approach for Realizing Solid-State Sodium-Ion Batteries? *J. Power Sources* **2018**, *383*, 157–163. [[CrossRef](#)]
177. Johari, N.S.M.; Adnan, S.B.R.S.; Mohamed, N.S.; Ahmad, N. Structural and Electrical Properties of Na₂ZnSiO₄—Py₁₄TFSI Hybrid Solid Electrolyte. *Ceram. Int.* **2020**, *46*, 8039–8046. [[CrossRef](#)]
178. Johari, N.S.M.; Jonderian, A.; Jia, S.; Cozea, V.; Yao, E.; Adnan, S.B.R.S.; Ahmad, N.; McCalla, E. High-Throughput Development of Na₂ZnSiO₄-Based Hybrid Electrolytes for Sodium-Ion Batteries. *J. Power Sources* **2022**, *541*, 231706. [[CrossRef](#)]
179. Boschini, A.; Johansson, P. Plasticization of NaX-PEO Solid Polymer Electrolytes by Pyr₁₃X Ionic Liquids. *Electrochim. Acta* **2016**, *211*, 1006–1015. [[CrossRef](#)]
180. Cheng, M.; Qu, T.; Zi, J.; Yao, Y.; Liang, F.; Ma, W.; Yang, B.; Dai, Y.; Lei, Y. A Hybrid Solid Electrolyte for Solid-State Sodium Ion Batteries with Good Cycle Performance. *Nanotechnology* **2020**, *31*, 425401. [[CrossRef](#)]
181. Sirigiri, N.; Chen, F.; Forsyth, C.M.; Yunis, R.; O'Dell, L.; Pringle, J.M.; Forsyth, M. Factors Controlling the Physical Properties of an Organic Ionic Plastic Crystal. *Mater. Today Phys.* **2022**, *22*, 100603. [[CrossRef](#)]
182. Yi, Q.; Zhang, W.; Li, S.; Li, X.; Sun, C. Durable Sodium Battery with a Flexible Na₃Zr₂Si₂PO₁₂-PVDF-HFP Composite Electrolyte and Sodium/Carbon Cloth Anode. *ACS Appl. Mater. Interfaces* **2018**, *10*, 35039–35046. [[CrossRef](#)] [[PubMed](#)]

Disclaimer/Publisher's Note: The statements, opinions and data contained in all publications are solely those of the individual author(s) and contributor(s) and not of MDPI and/or the editor(s). MDPI and/or the editor(s) disclaim responsibility for any injury to people or property resulting from any ideas, methods, instructions or products referred to in the content.